Cand. Scient. thesis

Biophysical Chemistry

Quinolone-DNA interactions

Interactions and association between Ofloxacin and a DNA-oligomer studied by NMR methods

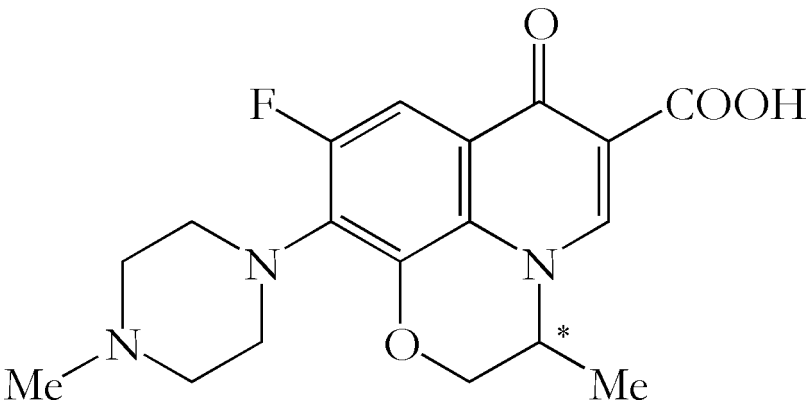

Department of Chemistry
University of Bergen
2003

Magnus Jensen

Contents

Acknowledgement

First and foremost I want to express my gratitude to Prof. Dr. Philos. Einar Sletten for this project. Thank you for a very interesting problem and guidance along the way!

Dr. Iztok Turel provided the quinolone and Dr. Nils Åge Frøystein has done much appreciated work on the pulse-sequences and other NMR related subjects. Their contributions have been vital.

Jo Vinje and Tormod Skauge have been indispensable during this project. Their knowledge as well as their company has been a support to me throughout this thesis. Especially Tormod and his knowledge on quinolones has been a great help and inspiration. Thank you.

Brit Aksnes is thanked for her proofreading. Your help is much appreciated.

There are so many others at the Department of Chemistry that should have been mentioned. Long lunches are important when inspiration runs dry; thank you all for being there.

Last, but definitely not least, I want to thank Brita Vangdal for help and support. Without you I would never have made it, your my inspiration. I know this is told to seldom; I´m grateful.

Summary

The first part of this thesis examines Ofloxacin (Oflo), a second-generation quinolone, by applying 1D ^{1}H NMR. Molecular dynamics, stacking conditions and the self-diffusion constant were investigated.

No certain conclusion could be drawn concerning molecular dynamics. It appears like hindering of the ring-rotation initiated by hydrogen bonding arising from the F9 and O1 is the reason for the coalescence observed in the ^{1}H NMR spectrum. Slow inversion of the methylpiperazine ring cannot be excluded.

It was confirmed that no stacking occurs in the concentration range 1 - 6 mM and the self-diffusion constant was determined to be 4.33 ($\pm$ 0.07) * 10^{-10} m^2s^{-1}. The self-diffusion constant appears to depend on concentration, but the dependency was within the limits of error in the concentration range used in this thesis, and it has therefore been regarded as independent of concentration.

In the second part of this thesis the 1D ^{1}H and 2D NOESY NMR spectra of a palindromic decamer $T_1A_2T_3G_4G_5C_6C_7A_8T_9A_{10}$ (named GGCC) were investigated and the self-diffusion constant calculated to be 1.33 ($\pm$0.07) * $10^{-10}m^2s^{-1}$.

The third part of this thesis combines GGCC and Oflo in a series of titrations. 1D ^{1}H NMR spectra and diffusion constants were obtained at 11 different Oflo:GGCC ration. A NOESY spectrum was obtained for the last titration.

A model for the interaction between Ofloxacin and GGCC has been proposed. This model postulates both minor/major groove and intercalation interactions. The minor/major groove interaction occurs at all concentration levels, the intercalation is initiated at a Oflo:GGCC ratio of 1. The minor/major groove interaction and the intercalation appear to be linked.

The results fail to exclude other models of interaction. The only certain conclusion may therefore be that intercalation takes place, but there appears to be more than one interaction mode.

1. Introduction

The first quinolone, Nalidixic acid (Nal), was synthesized in 1962 by Lesher et al. Since then quinolones have developed and are today regarded as an important group of antimicrobial agents.

Ofloxacin (Oflo) is a second-generation fluoroquinolone and has been in clinical use for more than a decade. Oflo is a racemic mixture as it containes a chiral centre (marked by * in figure 1.1). The pure (-)S isomer of Oflo is the most active enantiomer and in its pure form considered a third generation quinolone called Levofloxacin (Levo). Oflo is highly active against Gram-negative bacilli, less active against Gram-positive coccus and is not sufficiently active against anaerobic bacteria for medicinal purposes. For therapeutic purposes it is used in complicated urinary tract and catheter-related infections, prostatitis and some sexually transmitted diseases among others.

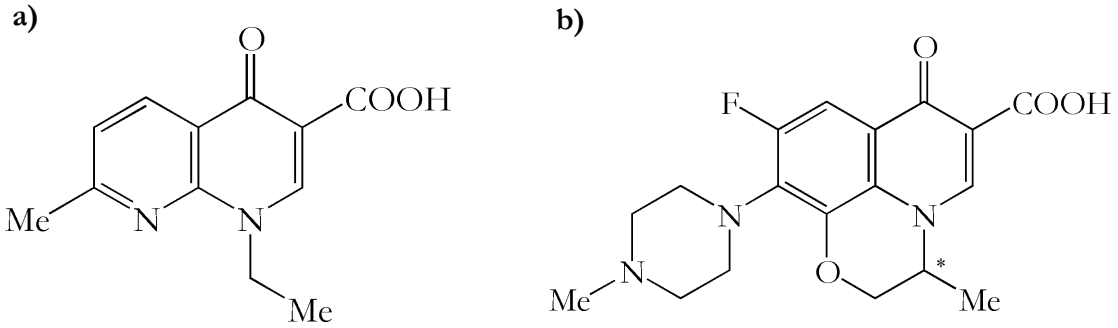

Figure 0.1 Nalidixic acid a) and Ofloxacin b)

Oflo, along with Ciprofloxacin (Cipro), are the most widely used second-generation quinolones. Oflo has been the centre of great interest both as a drug and as model system for quinolone investigations. 3.361 articles regarding Ofloxacin and 1.219 regarding Levofloxacin were found when searching the ISI Web of KNOWLEDGE indicating the immense interest in these compounds.

In Gram negative bacteria Oflo is active against the DNA gyrase enzyme that super coils DNA and removes knots by cleavage of the helix. The enzyme is essential for all bacteria and blocking the enzyme will eventually lead to cell death. In Gram-positive bacteria, however, the target for blocking is the topoisomerase IV enzyme. More information on quinolones and mechanisms of reaction is given in the theory, chapter 3.

Quinolones are the first man-made antimicrobials. Knowledge of how quinolones function will be important in the search for new antimicrobials. Resistancy against antimicrobial agents are of great concern and multidrug resistant bacteria may cause severe problems in the future. Leading

experts are concerned with the coming of a post-antibiotic area. This is the reason why it is immensely vital to investigate the molecular mechanisms of action for antimicrobials and find the pathways leading to antimicrobial resistance.

The aim of this project is to gain insight on how quinolones interact with DNA and to find the properties making Oflo one of the most efficient second-generation quinolones.
A model system of the interaction between a quinolone and DNA is employed consisting of Oflo and a model DNA oligomer. The self-complementary decamer oligonucleotide d(TATGGCCATA)*d(ATACCGGTAT) was used as a model for DNA. The oligomer will from hereon be referred to as GGCC.

Different mechanisms on how quinolones interact with DNA have been proposed. Several structures and theories on where the quionolone are most likely to interact with DNA have also been reported.
The project consists of three different parts where the following problems are investigated:

The first part concerns different properties of Oflo. The methylpiperazine ring, which is considered important to cell-penetration, has a hindered motion. Termodynamic parameters for this motion has been calculated using NMR techniques.

Some theories postulate stacking of the quinolones before interacting with the DNA or while interacting in DNA. Stacking conditions of Oflo at several concentrations were investigated using NMR diffusion measurements to monitor changes in the stacking conditions. This constitutes the second part of this thesis.

The third part investigates the interaction between the quinolone and DNA. Self-diffusion constants of Oflo and GGCC were measured separately and in a mixture of Oflo and GGCC applying NMR diffusion measurements techniques. The association constant of the Oflo-GGCC interaction was calculated using different techniques.

Theory - Part A:

2. Deoxyribonucleic acid

Deoxyribonucleic acid (DNA) was first discovered by Friedrich Meischer in 1868. As research proceeded DNA´s role in replication was discovered, but not until 1943. Solving the secondary structure of this macromolecule still proved difficult, and finally James D. Watson and Francis Crick suggested the double helix in 1953. For their work Watson and Crick was awarded the Nobel Prize in Chemistry together with Maurice Wilkins. Some say that the basis for Watson and Crick´s discovery was the ground-breaking x-ray diffraction work performed by Rosalind Franklin who worked at the same laboratory.

As the secondary structure was solved, the functional properties of DNA could finally be investigated. The current knowledge on DNA and how it functions is extensive. It is even a household term used in daily conversations and the media around the world. However there are still new applications for DNA to be discovered. The latest application of DNA (or other similar oligomers) is in the field of nanotechnology, giving rise to even smaller microprocessors and other miniature equipment.

2.1 DNA structure[1]

The primary structure of DNA is relatively simple. It is built up from only four different nucleic bases, a deoxyribose sugar ring and a phosphate group. The nucleic bases are: Guanine (G), Adenine (A), Cytosine (C) and Thymine (T).

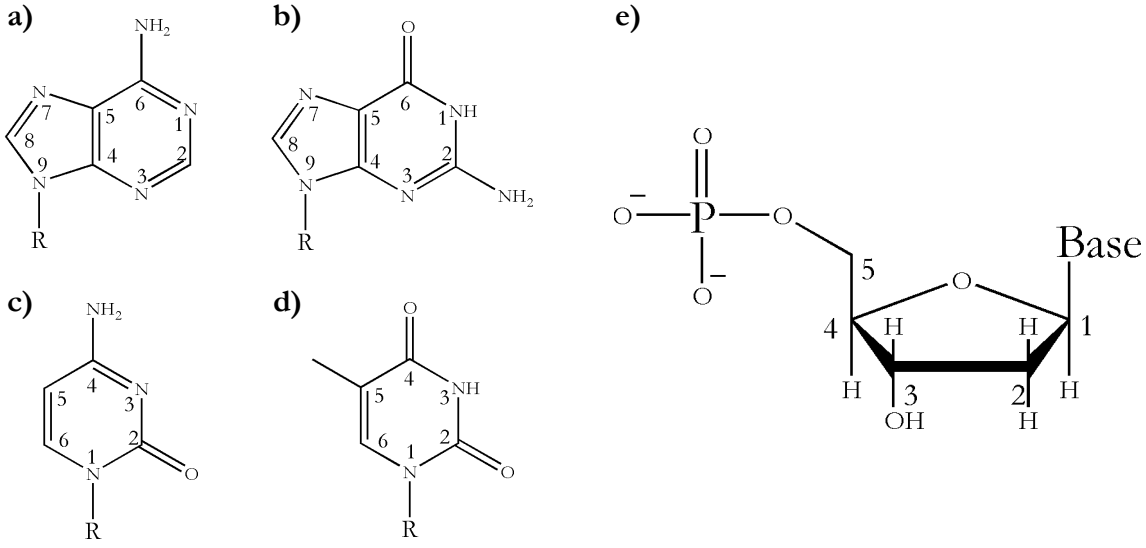

Figure 2.1 The nucleic bases a) Adenine, b) Guanine, c) Cytocine, d) Thymine and e) the sugar ring with a phosphate groupe attached in 5' position.

The bases are attached to the sugar ring and the sugar rings and phosphate group constitute the backbone in a strand of bases.

Each sugar ring has two phosphate groups attached, one in the 5´ position and the other in the 3´ position:

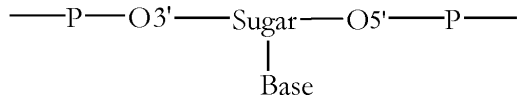

The order of the bases is important, hence we need to define the direction of the strand. By convention the strand is always read from the 5´ side to the 3´ side. However simple in its construction, the DNA single strand is remarkably flexible. The bonds between the sugar ring and the base and between the sugar ring and both the phosphates can rotate 360° though there are some retrictions in the helix conformation. The sugar ring is not perfectly planar, giving rise to 20 distinct conformations as a result of puckering.

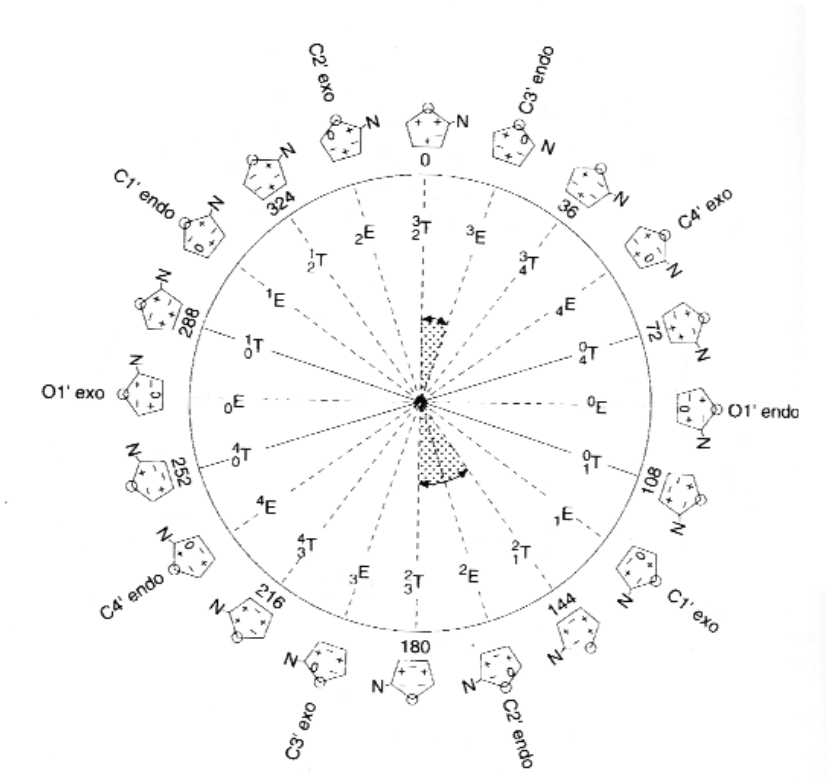

Figure 2.2 Possible configurations of the sugar ring due to puckering. The 2 and 3 carbon positions are used to define the conformation. The C3´-endo and C2´-endo are preferred conformations[1]p44.

Two DNA strands are needed to constitute a DNA helix. The base pairs in each strand are connected by hydrogen bonds to each other. If the sequence of one strand is known, the other is given since there are only two base pairs: GC and AT. The strands are complementary and antiparallel.

The GC base pair is stronger than the AT base pair since there are three H-bonds between G and

C and only two between A and T. This is especially important in small DNA fragments as AT base pairing at the end of the fragment results in less stable helixes.

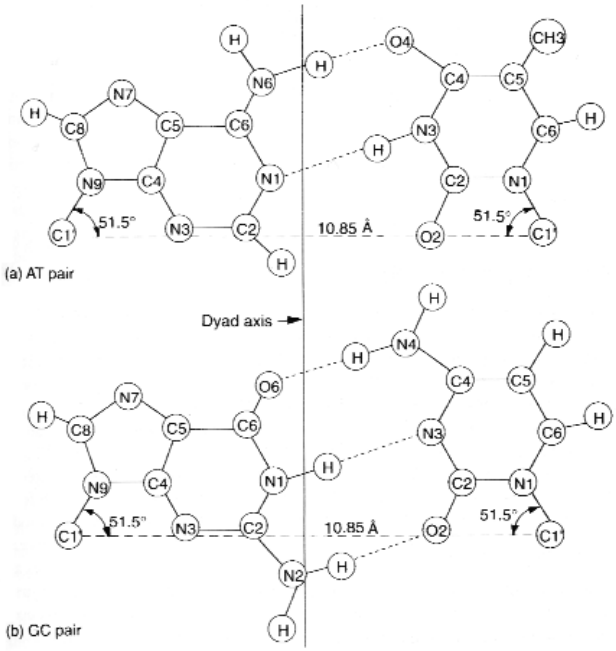

Figure 2.3 a) AT pairing and b) GC pairing. AT are connected by two hydrogen bonds and GT by three[1]p49.

In a double helix, the rotation around the bonds between the sugar ring and the base, and between the sugar ring and the phosphates are somewhat restrained. Still the molecule is remarkably flexible. This means that the helix can be twisted either to the right (right-handed DNA) or to the left (left-handed DNA) and that the base pairs could be twisted, rolled or tilted.

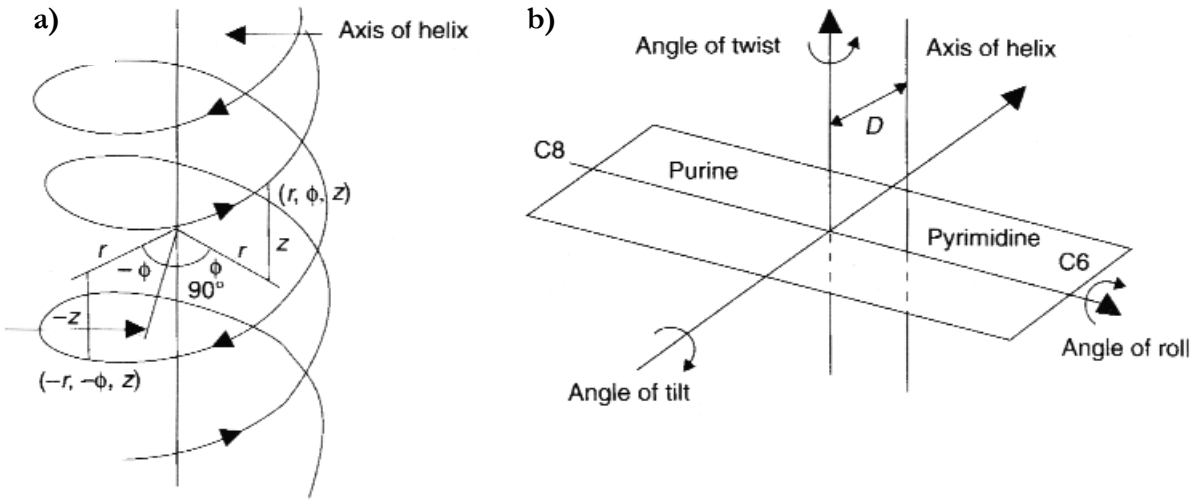

Figure 2.4 a) Illustration of the double helix construction and definition of angles in a helix conformation and b) definitions of twisting, rolling and tilting of the DNA bases[1]p51.

This flexibility leads to three different double helix conformations, or rather three different families with small variations in their geometrical parameters.

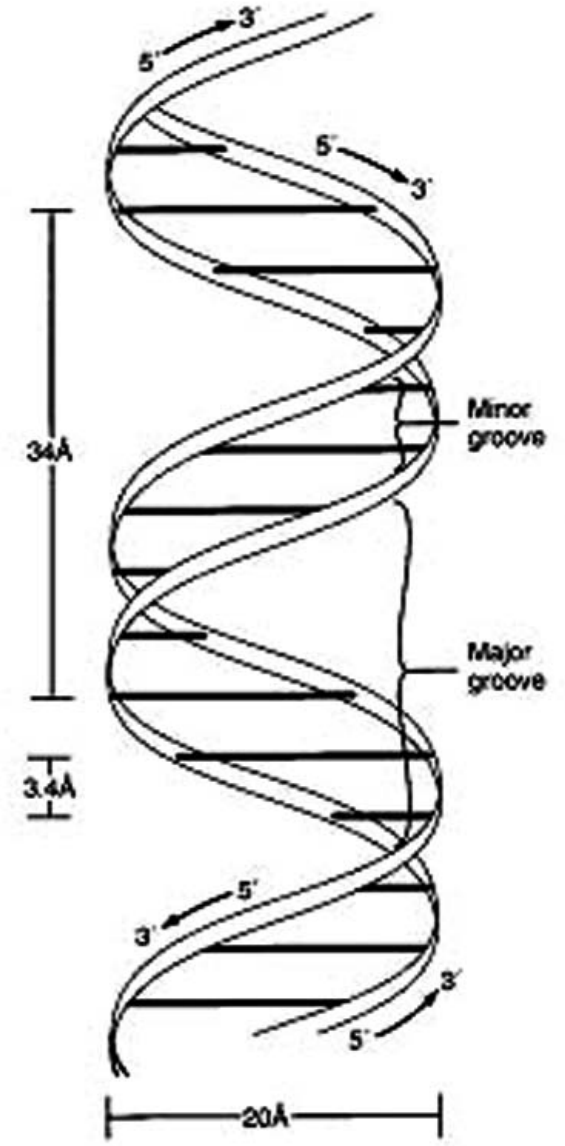

Figure 2.5 Major and Minor groove in the DNA double helix[2].

The two main DNA structures are A and B DNA. A third, Z DNA, is less common. The B form of the DNA double helix is known to be the typical conformation of in vivo DNA of eucariotes.

B DNA is a right-handed double helix with approximately 10 base pairs per turn and a 3.4 Å axial distance between the base pairs. The A form of the double helix is also right handed. It has approximately 11 base pairs per turn and a 2.6 Å axial distance between the base pairs. Z DNA is left-handed with 12 base pairs per turn and the phosphodiester chain has a zigzag shape, hence the name.

The base pairing and the helix shape give an uneven opening towards the middle of the chain. These openings are defined as the minor- and major groove (*see figure 2.1.5*). Normally the major groove is larger than the minor groove, though not without exeptions.

Since the bases pair, the sugar phosphate backbone is located outwards. This part of the DNA is negatively charged and hydrophilic, while the inside of the helix, the bases, are hydrophobic. This results in a high solubility for DNA in water.

The Watson-Crick base pairing and the ideal base pairs are basically described in the section above. In reality things are more complicated. There are several ways for the base pairs to interact, and there are also the possibilities of mismatching pairs and even chemical altering of the bases, allowing other kinds of pairing. The oligomer GGCC used in this thesis contains "ordinary" bases in Watson-Crick pairing.

The organisation of DNA *in vivo* is rather complicated. The double helix is supercoiled around histones, which again is coiled up in telomeres that constitutes chromosomes.

Different proteins at different levels stabilize the structure.

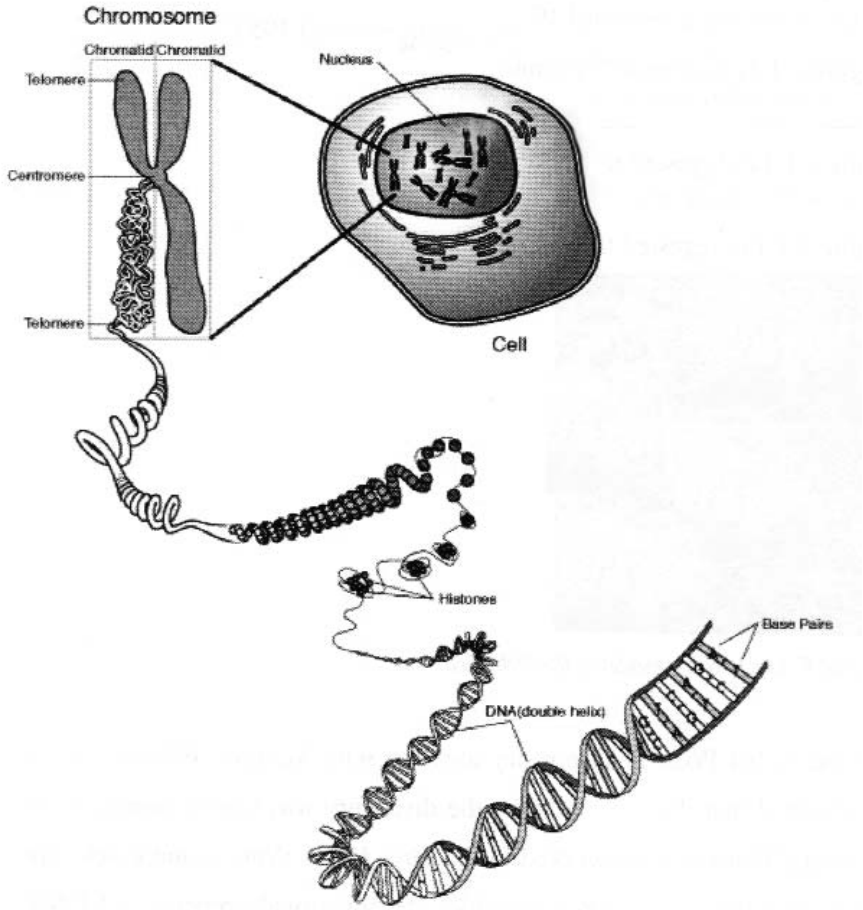

Figure 2.6 Illustration of the organisation of DNA in the cell (in vivo)[3]p58.

2.2 Ligands interacting with DNA

Drugs bind to DNA through one of four possible interactions: intercalation, groove binding, covalent attachment, cross-linking or a combination of these modalities.

Intercalation is insertion of a drug or part of a drug between two adjacent base pairs. Intercalators often contain an aromatic ring system with the aromatic ring being flat enough to fit between the bases. The intercalation results in an increased distance between the bases and a local unwinding of the helix. Still, because of the flexibility, the rest of the DNA helix is practically uninfluenced by the process. The intercalation is stabilized by stacking interactions between the aromatic rings or substituents in the grooves or on the DNA surface. An example of intercalating drug is actinomycin.

Both minor and major groove bindings may also occur. The geometry of the molecule is more important in minor groove bindings than in major groove bindings. A drug binding typically has

a structure that fits well in the minor groove. The flexibility of the helix is also playing an important part, as the groove may adjust to fit the molecule. Once inside the minor groove the molecule will be stabilized through hydrogen bonds and Van der Waals interactions. An example of minor groove-binding drug is neutropsin.

The major groove, on the other hand, is usually bigger and the geometry of less importance. The major groove is opening in towards the bases. This will give several possibilities for specific hydrogen bonds to donors and acceptors in the base pairs leading to complex stabilisation or sequence specificity. Proteins are often bound to DNA in the major groove.

Covalently bound drugs and cross linkers interact with the bases or the phosphate backbone. Certain drugs are base specific and bind covalently to for instance A or G sites. Cross linkers interact in the same way, but utilise both of the strands in the helix, forming a bridge between the two. An example of a bifunctional cross-linking agent is Bizelesin.

Theory - Part B:
3. The antimicrobial quinolones

The development of antimicrobial[1] chemotherapeutic agents started in the 19th century with the acceptance of the germ theory which linked micro-organisms to several diseases. To cure infections the scientists started the hunt for "the magic bullet".

In the late 1870s Louise Pasteur demonstrated that the bacterial disease anthrax could be cured in animals by injecting a soil bacteria. Late 1880s Rudolf Emmerich and Oscar Low conducted experiments proving that the same bacteria causing one disease could cure another, and from the bacteria bacillus pycyoneus they created the medicine pyocyanase to cure cholera, tyhpoid diphteria and anthrax. This was the first antibiotic in use in hospitals. Unfortunately, the medicine had some unexpected side-effects and after a short while the drug was no longer in use.

Alexander Fleming accidentially discovered penicillin in 1928, during an experiment that was contaminated by the mold bacteria Penicillium notatum. This proved to be a highly useful drug but it was not available commercially until 1943. Fleming, Florey and Chain was awarded the Nobel Price in medicine in 1945 for the discovery, structural assignment and synthesis of penicillin.

In 1932 another useful antimicrobial chemotherapeutic agent was discovered. Gerhard Domagk investigated a dye called Prontsil and demonstrated that it cured streptococcus when injected in animals. Later he discovered that the active part of Prontosil was a sulfonamide. This was the birth of a whole range of drugs called Sulfa-drugs and by 1945 pharmacologists had 5488 different sulfonamides. For his work with sulfonamide Domagk received the Nobel Price in medicine in 1939.

Other discoveries of importance are tetracyclines and quinolones. Tetracyclines were first found in 1948, the first quinolone (nalixic acid) in 1962. This thesis will focus on the interaction between DNA and the quinolone Ofloxacin (*see chapter 3.3)*. The quinolones will be discussed further in the following sections.

3.1 Quinolones

Quinolones are a class of antimicrobial agents developed from Nalidixic acid (Nal), discovered in 1962 by Lesher et al.[4]. They discovered Nal by chance while investigating by-products from the synthesis of the anti-malaria drug chloroquine. Lesher proved that Nal had significant antimicrobial abilities as a narrow spectrum drug effective mainly on Gram negative bacteria[2]. With Nal a

1 Antimicrobials are natural, semi-natural or synthetic chemicals that can interfer directly with the growth of microbes at a very low concentrations. Natural or semi-natural antimicrobials are often referred to as antibiotics.
2 Bacteria are mainly devided in Gram positive and Gram negative bacteria based on a colouring technique developed by Hans Christian Gram in 1884. Gram negative bacteria have an outer membrane that the Gram positive bacteria do without.

whole range of quinolones developed the following decade. Among the most important new quinolones were oxolinic (oxo), cinolaxic and pipemidic.

3.2 Structure and classification

All quinolones exhibit the same ground-structure (*see figure 3.1a*). They all contain a carboxylic group at the 4 position, thus the first generation quinolones are often referred to as 4-quinolones. In first generation quinolones the R_1 substituent is usually an ethyl group.

In the 1980s the introduction of fluorine, mainly at the 6-position, gave rise to a second generation of quinolones, the fluoroquinolones, possessing a broad spectrum activity against microbes[3]. Since the fluorine is attached to the 6-position, they are often referred to as 6-fluoroquinolones. Second generation quinolones usually have a piperazine- or methylpiperazine ring substituated at the R_7 position and the atom at postiton 8 is usually a carbon. Otherwise they essentially contain the same basic structure as first generation quinolones. Third generation quinolones exhibit second generation skeleton in addition to a variation in the substituent groups R_1, R_2 and R_3 and the atom X_8. There are no general requirements to take into consideration.

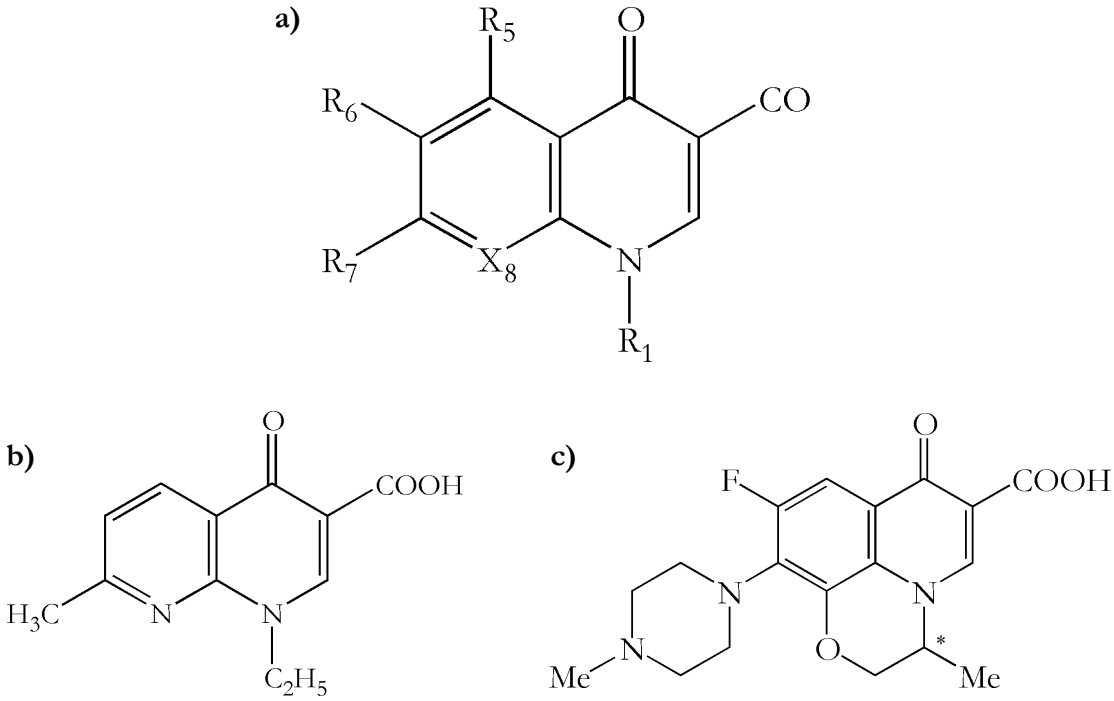

Figure 3.1 a) Quinolone-skeleton b) Nal c) Oflo

Ofloxacin (Oflo), used in this thesis, is a second generation fluoroquinolone and containes R_1 = CH(CH3)CH2O (with the oxygen attached to the carbon X_8), R_7 = methylpiperazine, R_6 = fluorine, R_5 = hydrogen and X_8 = carbon. The chiral centre in the R_1 substituent (marked by * in figure 3.1) gives rise to two distinct isomeres.

3 Antimicrobial chemotherapeutic agents are said to be broad when they act on a large range of both Gram negative and Gram positive microbes, narrow when they act on mostly Gram negative or Gram positive microbes and limited if they act on a single microbe.

Quinolones can be classified into four generations based on their antimicrobial activity. The term "generation" does not reflect the time of discovery. Levofloxacin, the most active isomer of Oflo, is considered a third generation quinolone whereas the rasemic mixture Oflo is classified as a second generation quinolone.

The development of new fluoroquinolones is a continuously growing field even today. Fluoroquinolones are highly active against both Gram negative and Gram positive bacteria and some other microbes as well. Their structures allow excellent tissue penetration and a great bioavailability.

3.3 Ofloxacin

(±)-9-Fluoro-2,3-dihydro-3-methyl-10-(4-methyl-1-piperazinyl)-7-oxo-7H-pyrido [1,2,3-de] [1, 4] benzoxazine-6-carboxylic acid is usually called Ofloxacin (Oflo) and has the molecular formula C18H20FN3O4. It acts as a zwitterion (as most quinolones) at physiological pH. The pKa values are 6.05 (pKa_1) and 8.22 (pKa_2)[5].

Oflo was first patented in Europe for medical use by Daiichi (Eur.pat. appl. 47,005) in 1982 and the first article focusing on the drug was published in 1983. In 1987 Levofloxacin (Levo), the most active isomer of Oflo, was patented for medical use by Daiichi (Eur.pat. 206,283). Oflo, together with Ciprofloxacin (cipro) are the only second generation quinolones still in medical use today.

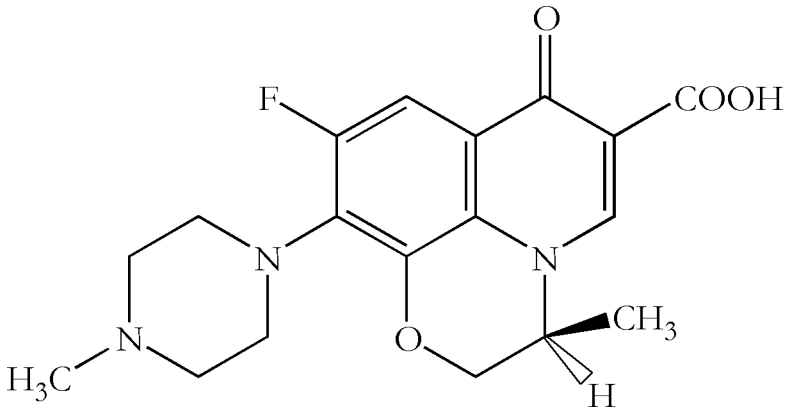

Figure 3.2 Levofloxacin (Levo) is the most active isomer of Oflo

Oflo is considered soluble in aqueous solutions at pH 2 - 5 and sparingly to slightly soluble at pH 7 (4mg/mL). In aqueous solutions above pH 9 it is regarded freely soluble as defined by USP nomenclature[6].

Both the methylpiperazine and carboxylic substituents are expected to have free rotations around the C7-N and C3-C11 bonds in solution. The rotation of methylpiperazine is investigated in this

thesis. Ab initio quantum mechanical calculations by Chidangil et al.[7] have proved that the carboxylic group does not exhibit free rotation in the protonated state due to hydrogen bonds between the hydroxyl group and O4.

In the deprotonated state Oflo forms chelates to several metal ions, following the order Fe^{3+} > Al^{3+} > Cu^{2+} > Ni^{2+} > Pb^{2+} > Zn^{2+} > Mg^{2+} > Ca^{2+} > Ba^{2+}[6]. The metal coordinates between the 6-carboxylic group and the 7-keto group[8].

Recently, work has been done on enantioselective binding modes of Oflo to B form DNA and to various synthetic polynucleotides by Seog K Kim et al[9,10]. These articles conclude that the R-enantiomer is insignificantly bound to DNA, inspite of the S-enantiomer being strongly binding. The association constant for Oflo-DNA complexation was calculated at 8.2 * $10^3 M^{-1}$ for the S-isomer and estimated to be 3 to 4 times higher than the R-isomer. They concluded that Oflo is propably interacting with DNA as described in the Nordén model (*see chapter 3.4.3)*, and that the binding geometry is similar for both enantiomers.

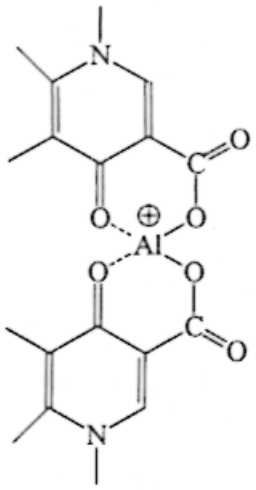

Figure 3.3 Oflo chelating with Al^{3+}[8]

When investigating binding of R- and S-Oflo to polynucleotides they discovered that the R-isomer is selective towards GC base pairs and confirmed that the S- and R- isomers exhibit similar binding geometry, namely possible partially intercalating in the minor groove.

Little work has been done on Oflo using NMR, but in 1996 Mucci et al. reported structural properties of Oflo applying both ^{1}H-NMR, NOE and ^{1}H, ^{13}C inverse detection NMR through heteronuclear multiple-quantum (HMQC) and multiple bond (HMBC) techniques[11]. The spectra were obtained at 300K using DMSO-d6 as solvent. Interestingly, they concluded that the fluorine has four and five bonds long-range coupling to the 2´ and 6´ protons mainly distributed through space.

3.4 Mechanisms of action

Fluoroquinolones display essentially two different mechanisms of action when interacting with DNA, either targeting the DNA gyrase enzyme or the topoisomerase IV enzyme. Mainly, the DNA gyrase is attached in Gram negative and topoisomerase IV in Gram positive bacteria. Both procedures prevent cell reproduction by stopping DNA replication which can lead to cell death. Since Oflo is a narrow range antimicrobial agen acting mainly on Gram negative microbes, the

focus will be on DNA gyrase inhibition.

The DNA gyrase enzyme is essential to all organisms with supercoiling of the DNA strand being essential for transcription. The gyrase enzyme is built up by two gyrA and two gyrB sub-units in a A_2B_2 tetramer. The Tyr-122 site in gyrA is considered the active site in DNA cleavage.

The enzyme cleaves the DNA helix, allows another part of the DNA to pass through a DNA-"gate" created by the enzyme and closes the gate again. In order for the DNA gyrase enzyme to function it recuires ATP as an energy source and Mg^{2+} ions for DNA cleavage.

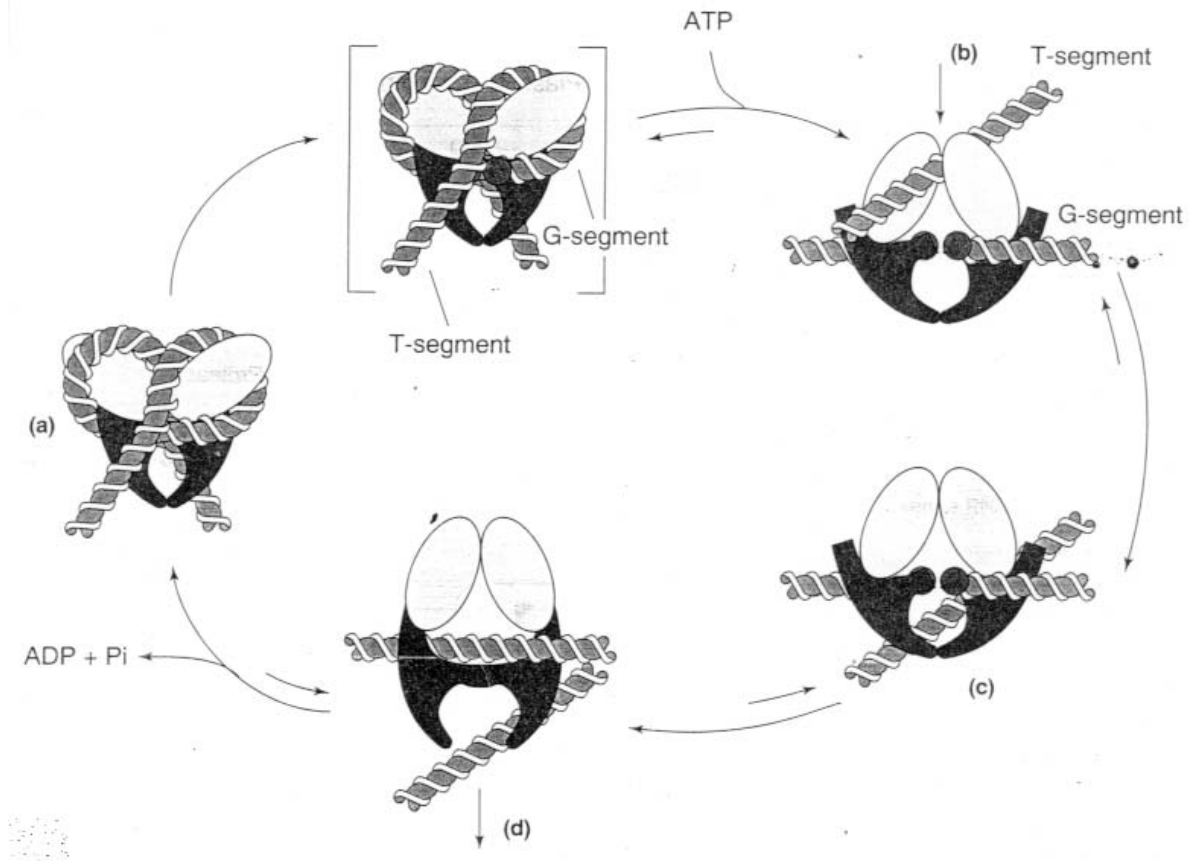

Figure 3.4 The DNA gyrase cyclus[12]
a) Gyrase binds to the DNA as a tetramer and wraps the segment as to induce a positive supercoil in the helix. This leads to a cleavage of the DNA strand and a "DNA gate" is produced (G-segment in figure).
b) When gyrase binds to DNA conformational changes are introduced. The gyrase traps another segment of the DNA (T-segment in figure)
c) The gyrase leads the T segment through the opening in the G segment
d) The "DNA gate" is closed in the G segment and the process is over. A supercoil has now been introduced in the DNA helix.

The cleavage of the helix has been proposed to be sequence specific. In 1979 Morrison and Cozzarelli[13] showed that the gyrase cleaves the DNA four bases appart, one strand in 5´ position and the other in 3´ position. The strand being cleaved in 5´ position is always attacked between a G and a T.

The DNA gyrase is considered the target for quinolone activity. The detailed mechanisms, however, are still discussed. It is known that DNA gyrase and the quinolone form a ternary complex., but it is not known in what order the complex is formed. Is quinolone interacting with DNA and then gyrase? Does the quinolone interacts first with gyrase? It is also a possibility that DNA and gyrase interact before quinolone and complex. Is the complex stable or does it dissolve?

Many questions are still to be answered and many theories have been proposed. Up to 1985, the general opinion was that quinolones are binding directly to the DNA gyrase, since the quinolones prevent the action of the enzyme.

In 1985 Linus L. Shen and Andre G. Pernet[14] reported that Norfloxacin (Nor) was binding to DNA and not gyrase as previously anticipated. Nor was even binding at a higher magnitude to singelstranded DNA (ss-DNA) than double stranded DNA (ds-DNA). A new paradigm was created in quinolone research. The view of Shen and Pernet dominated the reseach area for the next decade, and only in the past ten years has this model been challenged.

3.4.1 The Shen model

Shen et al.[15] presented a model in 1989 for the binding of quinolones to DNA, followed by a number of supporting articles[16,17,18]. On the basis of work done by Shen and Pernet in 1985 and a number of available evidence found by others they suggested what is now called the Shen model.

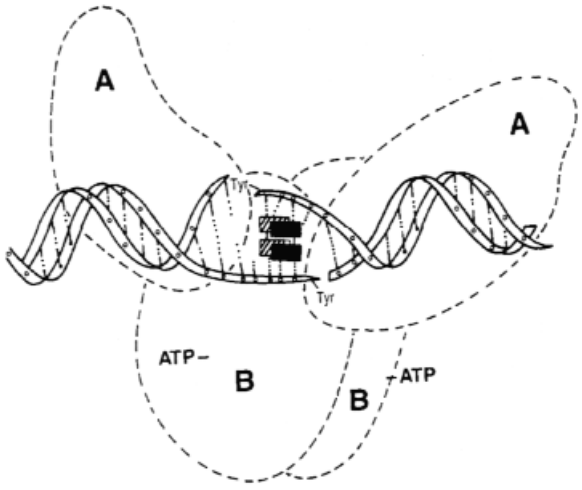

Figure 3.5 The interaction of quinolones in DNA gyrase. Four quinolones are binding in DNA (square boxes) on the four single stranded base pairs from each strand[15].

The gyrase interacts with DNA by cleaving one of the DNA strands and leaving four bases unpaired on each strand. Before the DNA supercoils and the bases pair again, quinolone will interact with one of the single-strand fragments. The first quinolone molecule interacts with DNA forming hydrogen bond (s). This allows the next quinolone to bond with both DNA and the first quinolone making it a cooperative process. A total of four quinolone molecules will interact in this way, stabilising the gyrase-DNA complex preventing the enzyme from moving further.

The four quinolones are interacting with each other resulting in further stabilisation of the complex. The two molecules bonding to the same DNA strand are oriented so that the 4-keto groups of both molecules point in the same direction. This allows for stacking. The two quinolone molecules at each DNA strand interact tail-to-tail with the other two molecule through hydrophobic interactions.

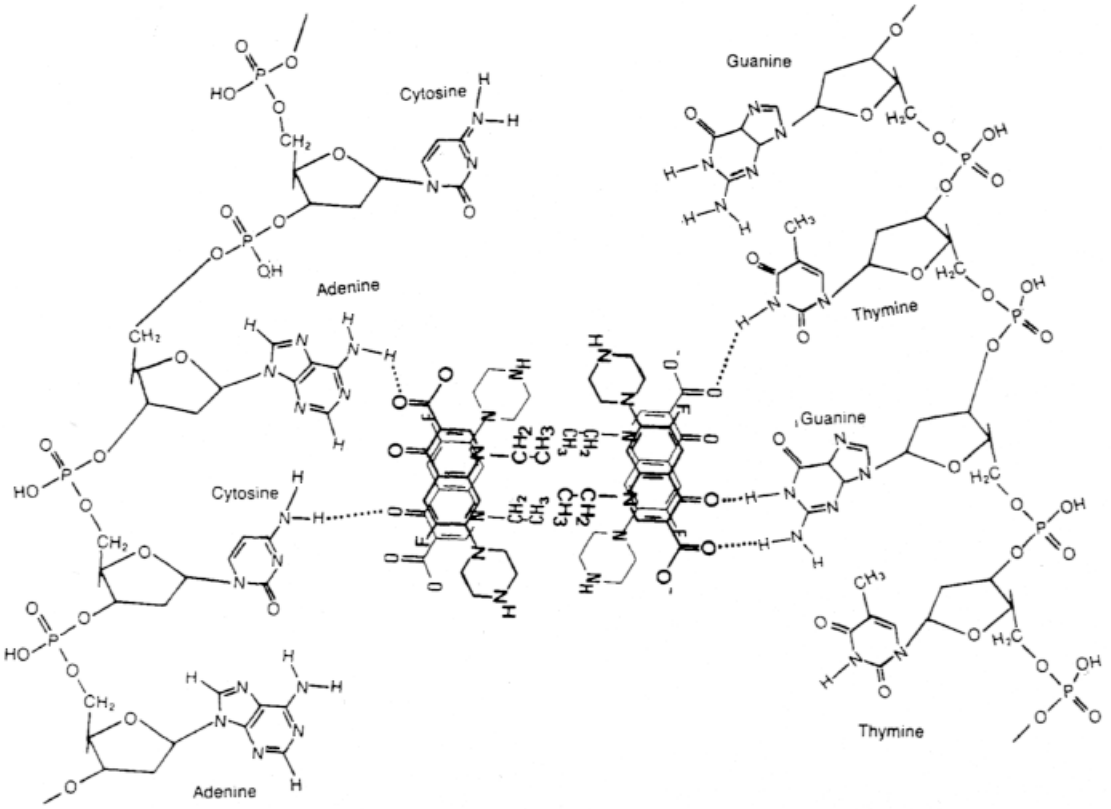

Figure 3.6 The quinolones stabilise the complex by stacking and tail-to-tail hydrophobic interactions[15]

Experimental results reported after the proposal of this model are usually either pro or contra the Shen model.

3.4.2 The Maxwell model

In 1993 Maxwell and Willmott[19] discovered that quinolones only bind to the gyrase-DNA complex and not to gyrase or DNA alone.

In 1996 Maxwell and Critchlow[20] showed that the single strand fragments, as generated by the

DNA cleavage, are not necessary for quinolones binding to the complex as Shen proposed. This led Maxwell and Kampranis two years later to propose a different mechanism for quinolone-DNA interaction[21].

When DNA interacts with gyrase a certain unwinding occurs. This generates a DNA-"bubble" where some of the base pairs in the DNA helix no longer pair (*see figure 3.7, lower part*). Quinolones then intercalate between the base pairs flanking this DNA-"bubble", making the DNA strand unstable, and will eventually lead to cleavage of the DNA strand at one side. The cleavage of one strand then makes the DNA more unstable, inducing even faster cleavage of the second strand. The Maxwell model clearly states that DNA cleavage is a result of, and not an essential requirement for, quinolone activity.

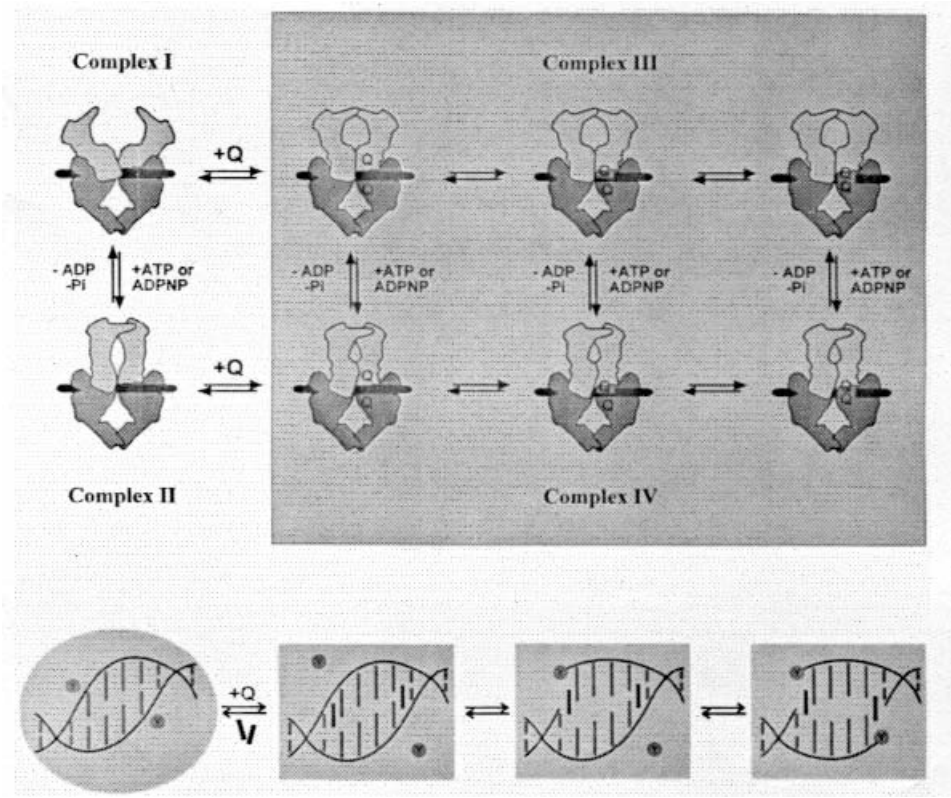

Figure 3.7 Quinolones interacting with DNA makes the DNA-gyrase complex unstable utilising cleavage of the DNA double helix[21].

Experiments with Ca^{2+} also suggested that drug-induced cleavage is only occuring when the appropriate DNA base sequence exists at the active site.

3.4.3 The Nordén model

Two other groups that have done substansial work on quinolone activity is one South Korean (Son et al.) and one Swedish group (Nordén et al.). Together they investigated the angles between quinolone and DNA in a quionolone-DNA complex at different temperatures[22]. They found that quinolone was interacting with DNA without the presence of gyrase or ATP. They also dis-

covered that the quinolone was complexating with DNA without the presence of metal ions and that it interacted both with DNA as single stranded and as a double helix. All this is contrary to earlier reports written by both Shen and Maxwell.

From their results they excluded both minor groove binding and surface binding and concluded with only one binding site. They also found that DNA is deformed at the binding site.

The classical intercalating mode would not deform DNA, so they proposed a intercalating mode of action followed by a deformation of the DNA, bending the helix near the binding site. The model proposed is not in coherence with the Shen model or the Maxwell model.

3.4.4 Metal ion based models

Many models take the stand that metal ion presence (preferably Ca^{2+} or Mg^{2+}) is necessary to explain the quinolone action.

Palú et al.[23] published in 1992 a paper where they found that Mg^{2+} played an important part in quinolone-DNA interactions. From experimental results they concluded that Mg^{2+} present at moderate concentrations was important to the reaction mechanism.

The model proposed that a Mg^{2+} ion act as a bridge between the phosphate groups of the nucleic acid and the carbonyl and carboxyl moieties of the quinolone. Additional stabilisation may originate from the stacking interactions between the condensed rings of the quinolone and DNA bases.

Another group, Kervin et al.[24], proposed a complexation of 4:4 of quinobenzoxazine:Mg^{2+}. Quinobenzoxacine (QB) is a quinolone related antitumour drug. This complex is formed when one drug molecule is intercalated into DNA and a second molecule is bound externally, held to the first molecule by two Mg^{2+} bridges. Two such heterodimers form the 4:4 complex in which the two externally bound molecules interact via pi-pi interactions.

Further experiments led to a proposal of a model for quinolone activity resembling the model by Palú et al., but they suggested that partly unwinded double helix must be the likely target action site rather than the unwinded single strands.

Kervin presented a model where a quinolone intercalated into DNA in the partially unwinded double helix (due to gyrase) and another quinolone molecule bound externally to the first with two Mg^{2+} form a bridge, as with QB. There is also the possibility of forming a 4:4 complex as with QB.

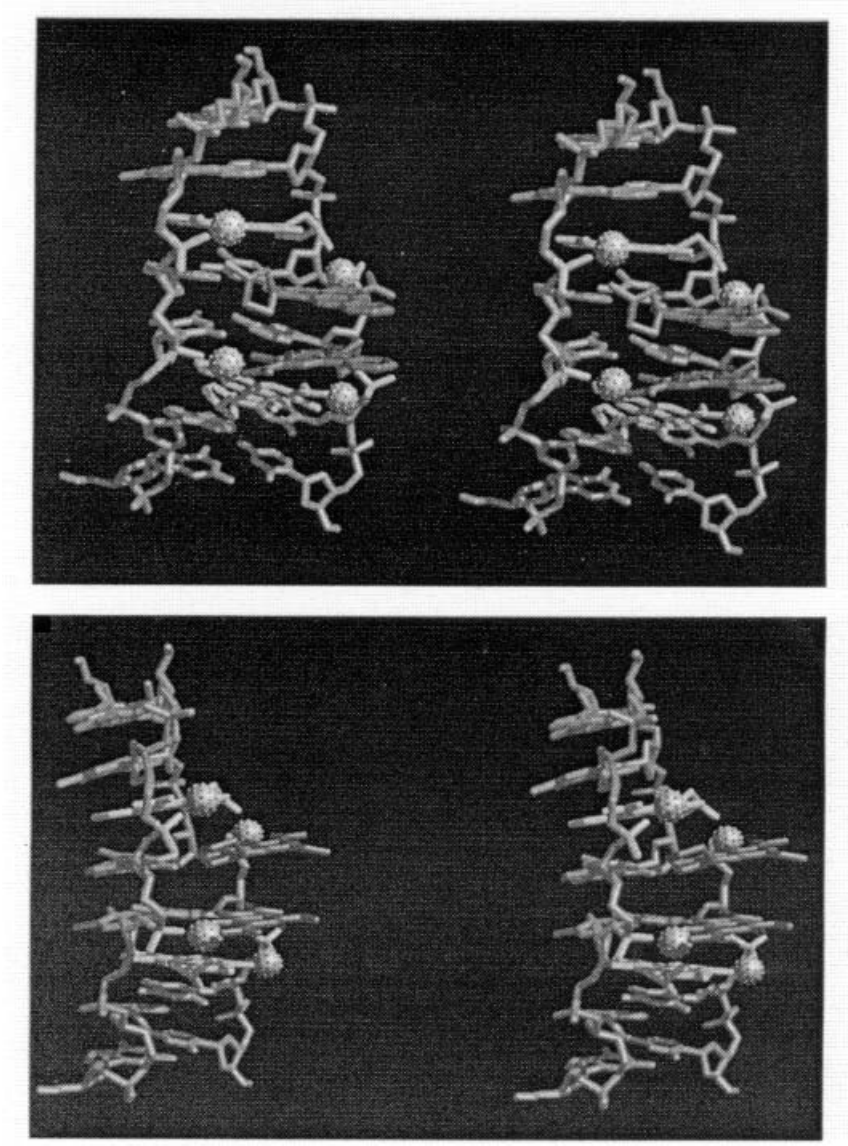

Figure 3.8 Stereoview of the model proposed by Kerwin et al. QB partially intercalating and partially binding to the surface complexating with Mg^{2+} in a 4:4 ratio[24].

3.4.5 Other models

In 1998 Bailly et al.[25] reported a sequence-dependent GC cleavage of DNA with interaction with quinolones. A quinolone was found to form intercalation complexes with DNA , preferably with GC sequences under low ionic strength conditions. No distinct conclusions were suggested what concerns binding mode, since substitutions in either the minor or major grooves of the double helix interfered with the binding reaction.

Theory - Part C:
4. Nuclear Magnetic Resonance

In the history of science, the Nuclear Magnetic Resonance (NMR) technique is fairly new. In 1946, two separate groups led by Felix Bloch and Edvard Purcell both discovered and developed the technique. For their work Bloch and Purcell shared the Nobel Prize in physics in 1952.

At first NMR was a method used solely by physicists. Later several other groups discovered the advantages of NMR, including chemists, biochemists and medicins. Today the NMR technique is an important tool for all of these groups and NMR experiments are carried out on a routine basis. Advancements in the utilization of instrument, software and techniques together with the constant improvement in computational power drive the knowledge on the field further onwards.

One of the milestones in the development of the NMR experiment was the introduction of the "Fourier Transform (FT) Spectroscopy" in 1970. Previously the only method available was the "Continuous Wave (CW) Spectroscopy". The FT-spectroscopy method shortened the experiment timespan, enhanced both sensitivity and resolution and made it possible to use small samples in the experiments. But the greatest advancement was perhaps the possibility of utilizing several dimensions.

The application of NMR-techniques makes it seemingly easy to study the magnetic properties of atomic nuclei and their relative position in the molecule. One of the greatest advantage of NMR compared to other methods, like x-ray crystallography, is that even large molecules will give high-resolution data in solution.

4.1 Basic theory

The physical basis of the Nuclear Magnetic Resonance (NMR) experiment is the nuclear angular momentum P. That is, most nuclei are assumed to be spherical and rotating about its own axis producing an angular momentum. According to quantum mechanical considerations, quantized:

$$P = (I(I+1))^{1/2} (h/2\pi) \qquad 4 - 1$$

where P is the nuclear angular momentum, I is the angular momentum quantum number (often called the nuclear spin) and h is Plankcs constant equal to $6.6256 * 10^{-34}$ J s

The nuclear spin I may have the values 0, 1/2, 1, 3/2, 2, …up to 6. The angular momentum is associated with a magnetic moment mu, both being vector quantities and proportional to each other (*see equation 4 - 2*).

$$\mu = \gamma \mathbf{P} \qquad 4-2$$

The proportionality factor gamma is a constant for the isotope of each element and is called the magnetogyric (or gyromagnetic) ratio. Nuclides with small gammas are said to be insensitive, meaning difficult to observe, whereas nuclides with large gammas are the opposite. By combining equations 4-1 and 4-2 we get another expression for mu:

$$\mu = \gamma (I(I+1))^{1/2} (h/2\pi) \qquad 4-3$$

Nuclides with I = 0 have no nuclear magnetic moment and cannot be observed in NMR experiments. Important examples are the main building blocks of organic compounds ^{12}C and ^{16}O. Nuclides with spins have a non-spherically shaped charge distribution making them behave simmilar to bar magnets in an external magnetic field. These bar magnets will then have 2I+1 possible orientations in the magnetic field. Nuclides with an odd mass number has I values 1/2, 3/2, 5/2, and so on.

Table 4.1: Spin (I) and natural abundance for some nuclides

Nuclide	**Spin**	**Natural abundance (%)**
^{1}H	1/2	99.985
^{2}H	1	0.015
^{12}C	0	98.9
^{13}C	1/2	1.108
^{14}N	1	99.63
^{15}N	1/2	0.37
^{16}O	0	99.96
^{17}O	5/2	0.037

Table content adapted from ref[25]p3.

For most nuclides the nuclear angular momentum vector P and the magnetic moment vector mu point in the same direction. However, in a few cases they are anti-parallel as in ^{15}N and ^{29}Si and even in the electron.

4.2 Energy levels

If a nucleus with I > 0 is placed in a static magnetic field B_0, the z-component of the angular momentum will take one of the orientations given by:

$$\mathbf{P}_z = m * h/2\pi \qquad 4-4$$

where m is the magnetic quantum number defined by I (m = I, I-1....-I+1, -I), hence the 2I+1 possible orientations. From equations 4 - 2 and 4 - 4 we get the z-component of mu in the field:

$$\mu_z = m \gamma h/2\pi \qquad 4 - 5$$

The energy of the magnetic momentum in the field is given by:

$$E = -\mu_z B_0 \qquad 4 - 6$$

where B_0 is the flux density of the applied magnetic field. For a nuclei with 2I+1 possible orientations there will be 2I+1 energy states called the nuclear Zeeman levels. From equation 4 - 5 we find that:

$$E = - (m \gamma h/2\pi) B_0 \qquad 4 - 7$$

For nuclei with I = 1/2 (i.e. ^{1}H and ^{13}C) two possible orientations exist (2I+1 = 2) and two nuclear Zeeman levels:

$$E_{m=+1/2} = -(1/2 \gamma h/2\pi) B_0 \qquad 4 - 8$$

and

$$E_{m=-1/2} = (1/2 \gamma h/2\pi) B_0 \qquad 4 - 9$$

In quantum mechanics the m = +1/2 state is described by the spin function alpha and the m = -1/2 state is described by the spin function betha, therefore it is common to use alpha and betha as labels instead of m = ±1/2.

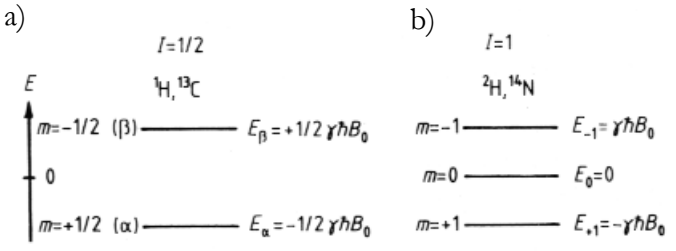

Figure 4.1 Energy levels for nuclei with a) I = 1/2 and b)I = 1 [25]p5.

The energy difference between two adjacent nuclear Zeeman levels is:

$$\Delta E = \gamma\ (h/2\pi)\ B_0 \qquad 4 - 10$$

4.3 Populations and precession

One never looks at single nuclei, but rather populations of a nuclei. There is always a distribution of the population along the energy levels and the lowest energy level is slightly more populated. In the case of investigating a nucleus with I = 1/2 there are two different energy levels, hence two populations N_{alpha} and N_{betha} (using the labelling described earlier). The distribution of nuclei between the energy levels follows the Boltzman distribution law, which gives the following relationship:

$$N_\beta/N_\alpha = e^{-\Delta E/k_b T} \qquad 4 - 11$$

which can be simplified to:

$$N_\beta/N_\alpha \approx 1-(\Delta E/k_b T) = 1 - (\gamma\ (h/2\pi)\ B_0/k_b T \qquad 4 - 12$$

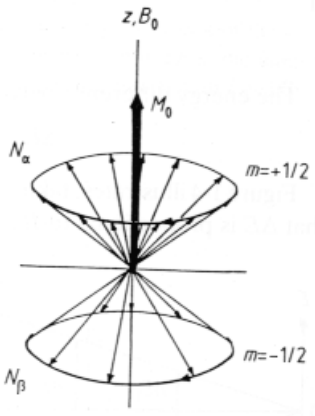

Figure 4.2 The cone distribution of magnetization vectors[25]p6.

where k_b is the Boltzman constant equal to $1.3805*10^{-23}JK^{-1}$ and T is the absolute temperature in Kevin. The population in the lowest energy level is N_{alpha}. Similar calculations can be outlined for nucleus with I other than 1/2.

For all nuclei the energy difference, delta E, will be small compared to the energy of the thermal conditions k_bT and the difference of populations in N_{alpha} and N_{betha} is in the region parts per million. This is one of the reasons why NMR is a rather insensitive method and the electronics and other equipment must be equally sensitive to get good results. One way to increase the sensitivity is to use a higher magnetic field to increase the difference between the energy levels.

The classical representation of a nuclear dipole precessing around a z-axis would resemble that of a spinning top. In contrast to the spinning top, however, the nuclear dipole must keep within the energy level such as only certain angles are allowed. For a nuclide with I = 1/2 this angle is 54°44'.

The precession frequency, also called the Larmor frequency, nu_L is proportional to the magnetic flux density B_0:

$$\nu_L = |\gamma/2\pi| \, B_0 \qquad 4 - 13$$

When populations precess at different energy levels there will be a resulting macroscopic magnetization vector M_0. Further discussions will be referring to the macroscopic magnetization vector.

4.4 Resonance, shielding and the internal scale

If a radio frequency signal is applied to the system the relationship between the populations will alter so long as the radio signal frequency matches the frequency the nuclear magnets naturally presess in the magnetic field. This is called resonance.

According to quantum mechanics only those energy level transitions in wich the magnetic quantum number m changes by a single quantum are allowed:

$$\Delta m = \pm 1 \qquad 4 - 14$$

Therefore the only transitions allowed are between adjacent energy levels. The energy of a radio signal can be given by:

$$E = h\nu \qquad 4 - 15$$

Equation 4-10 expressed the energy difference between two adjacent energy levels. Combining equations 4-15 and 4-10 will lead to the resonance condition:

$$\nu = \gamma B_0/2\pi \qquad 4 - 16$$

which also equals the Larmor frequency (equation 4-13). The resonance arising from each nuclide is influenced by the chemical environment of the nuclei allowing separate observations. The electrons surrounding the core will, because of the applied magnetic field B_0, induce a current, which sets up a magnetic field B in the opposite direction of the applied magnetic field thus reducing the field experienced by the nucleus. This is called shielding. The effective field experienced by the nucleus is given by:

$$B_{eff} = B_0 - B' = B \, (1 - \sigma) \qquad 4 - 17$$

where s is the shielding constant, a molecular, dimensionless constant independent of the magnetic field, determined solely by the electric and magnetic environment of the nuclei in question. The resonance condition now becomes:

$$\nu_1 = (\gamma/2\pi)(1-\sigma)B_0 \qquad 4-18$$

meaning that nuclei with different shielding constants, s, will resonate at different frequencies and thus are possible to separate.

But absolute frequencies are difficult to measure. To obtain such frequencies would demand extremely stable magnets. It would also mean that magnets of different strength would give different results and there would be a need for several frequency lists for every magnetic strength in order to compare results. An internal standard is introduced to avoid these problems. Most common as an internal standard is Tetramethylsilane (TMS). It is applied in most ^{1}H and ^{13}C NMR experiments today. To avoid the dependencies on the magnetic field strength, one introduced the chemical shift, little delta, defined as:

$$\delta = ((\nu_{sample} - \nu_{reference}) / \nu_{reference}) * 10^6 \qquad 4-19$$

The factor 10^6 is introduced to simplify the numerical values. The chemical shift is really a dimensionless value, but because of the factor 10^6 one commonly refers to chemical shift values as part per million (ppm). The definition of the chemical shift requires that the absolute frequency of TMS has to be measured every time. To avoid this, one introduced the observing frequency instead:

$$\delta = (\Delta\nu/\text{observing frequency})*10^6 \qquad 4-20$$

TMS, the internal standard, was chosen as a standard because it contained the least shielded protons known at that time. Today protons with less shielding are known, giving negative chemical shifts.

4.5 The pulse

There are in fact several ways to carry out an NMR experiment. In the early stages of NMR there were two ways to obtain an NMR spectrum; variating the field with radiation of a constant frequency pulse or variating the puls in a static magnetic field. Both these methods "screen" the sample and the result are written out as the experiments proceeds. This is the Continuous Wave (CW) Spectroscopy described earlier in this chapter. The method requires a sensitive nucleus and a high

concentration of the sample. The first method also requires a magnetic field that can be varied. It can only be obtained for low fields, thus the insensitivity of the method. The most common method today is the Pulsed Fourier Transform (PFT) Spectroscopy using a static magnetic field. This is the method described further on in this text.

All the nuclei of the species in question are simultaneously excited by a radio frequency pulse in the PFT method. Although, as seen in the earlier chapters, all of the nuclei do not reach the resonance condition at the same frequency the pulse is constant at a fixed frequency nu_1. What makes this possible is the time span. When the pulse is set on and shut of there is a short period where the frequency is not constant. When the pulse is switched on only briefly, tau_p being in the order of ms, this results in a pulse with a continuous band of frequencies symmetrical around the centre frequency nu_1 rather than just the set frequency. Approximately only tau_p^{-1} of the frequency band is effective in exciting transitions. The choice of the frequency nu_1 is determined by B_0 and the nuclide to be observed and the duration of the pulse is determined by the width of the spectrum.

Short pulses with high power, "hard pulses", are used to radiate all nuclei simultaneously. The duration of the pulse is then chosen so the frequency bandwidth exceeds the width of the spectrum by one or two powers of ten, typically several watts.

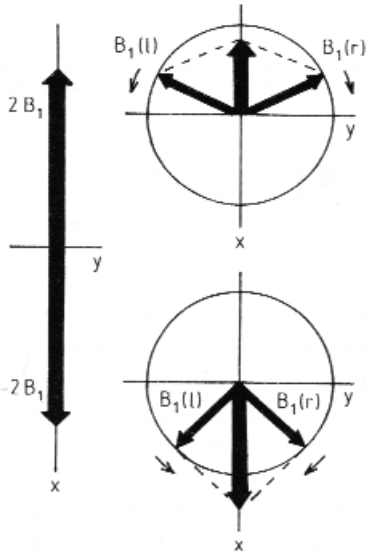

Figure 4.3 Illustration of the rotation of the two magnetizationvectors from the nuclides[25]p10.

4.6 The pulse angle

At equilibrium, the nuclear moments precess with the Larmor frequency on the surface of a cone (see figure 4.3) and as a result a magnetization vector M_0 occurs in the same direction as the field. To induce transition, the radio frequency pulse is sent in along the x-axis. The magnetic vector of the electromagnetic radiation can thus interact with the magnetic vectors of the nuclei, changing the magnetization vector M_0. The magnetic field from the radio frequency pulse is alternating: Picture two magnetization vectors with the same magnitude, $B_1(r)$ and $B_1(l)$, but in opposite directions. These two vectors both precess with the Larmor frequency giving a resultant vector along the x-axis direction that alternates between 0 and $2B_1$.

Only one of the two magnetization vectors from the pulse has the same direction of rotation as the precessing magnetization vectors from the nuclei. This is the only magnetization vector from the pulse able to interact with the nuclei. From now on this vector will be refered to as B_1.

Under the influence of B_1, M_0 rotates from the z-axis in a plane perpendicular to the direction of B_1. However, since B_1 rotates with the Larmor frequency, this is rather difficult to illustrate. A new coordinate system x´, y´ and z where x´ and y´ rotates with the same frequency as B_1 is defined to simplify this. The orientation and magnitude of B_1 in this system will now be fixed, and M_0 is tipped about the x´ axis by B_1. The magnetization vector M_0 is tipped by an angle, tetha, depending on the amplitude B_{1i} of the component of the radio frequency pulse at the frequency nu_i of the nuclear resonance transition, the nucleus in question and the length of time for which the pulse is applied:

$$\Theta = \gamma \mathbf{B}_{1i} \tau_p \qquad 4 - 21$$

Pulses are named after the angle of which they rotate M_0.

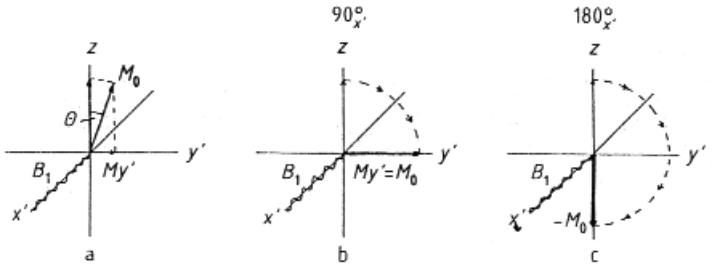

Figure 4.5 Flipping of a magnetization vector from an arbitrary angle pulse, 90-degree pulse and 180-degree pulse[25]p11.

As seen in the figure, the transverse magnetization vector $M_{y'}$ is at a maximum immediately after a $90_{x'}$° pulse and 0 immediately after an $180_{x'}$° pulse, hence the best signal is achieved using a $90_{x'}$° pulse.

4.7 Relaxation

The pulse rotates the magnetization vector away from equilibrium through an angle Q. M_0 now deflects around the z-axis described by its components Mx, My, and Mz, which vary with time, t. After the pulse is switched off the spin system will return to its original equilibrium through relaxation. This process may last from milliseconds to hours. There are two different relaxation processes: Spin-lattice relaxation along the direction of the applied magnetic field and spin-spin relaxation perpendicular to the applied magnetic field.

4.7.1 Spin-lattice relaxation

The rate of wich the relaxation along the direction of the applied magnetic field leads is determi-

ned by the spin-lattice relaxation time, given by the time constant T_1. Felix Bloch described this process with the Bloch equation for spin-lattice relaxation:

$$dM_z/dt = -(M_z-M_0)/T_1 \qquad 4 – 22$$

This is considered to be a first order process giving T_1^{-1} as the rate constant for the relaxation. The time constant T_1 is usually not recorded for ^1H under high-resolution NMR conditions, since in most cases they are of the order of milliseconds. ^{13}C on the other hand has greater variation of T_1, ranging from a few milliseconds in large molecules to several minutes in small molecules.

Spin-lattice relaxation is associated with an energy change in the spin system. The radio frequency pulse has excited the spin system which now will exchange energy with the surroundings through emmition in the relaxation process. The energy is transported to neighbouring molecules or even the wall of the vessel - the lattice in general, thereby increasing the thermal energy of the lattice. Different intra- and intermolecular interactions contribute to the spin-lattice relaxation and the mechanisms can be classified as:

- Dipole-dipole relaxation (dipolar relaxation)
- Spin-rotation relaxation
- Relaxation through chemical shift anisotropy
- Relaxation through scalar coupling
- Electric quadrupolar relaxation
- Relaxation through interaction with unpaired electrons in paramagnetic compounds.

The main source of spin-lattice relaxation for ^{13}C nucleus is dipole-dipole coupling, which can be measured directly through the Nuclear Overhauser Effect (NOE, chapter 4.9). Dipole-dipole relaxation is also the most important process studied and the only relaxation mechanism this text will concentrate on.

Interactions between nuclear dipoles arise from the fact that every nucleus is surrounded by moving magnetic nuclei in the same or neighbouring molecules. This motion sets up fluctuating magnetic fields around the nucleus in question. The frequency band is relatively broad and largely dependent on the viscosity of the solution. These fluctuating magnetic fields are able to induce nuclear spin transitions if they possess the right frequency.

The theoretical description of dipolar relaxation for an assembly of molecules leads to the proportional relationship between T_1 and tau_c formulated in the following rule: The faster a molecule moves, the greater is T_1. Here tau_c is the correlation time, corresponding roughly to the interval between two successive reorientations or positional changes of the molecule, by either vibration, rotation or translation. The dipole-dipole relaxation mechanism is especially effective when the

carbon nucleus in question is directly connected to one or more hydrogen atoms.

4.7.2 Spin-spin relaxation

Immediately after a $90_{x'}°$ there are components of the magnetization vector in the x´ and y´ planes, $M_{x'}$ and $M_{y'}$. These magnetization vectors are due to the fact that all the nuclei´s magnetization vectors are not uniformly distributed in the cone energy level. This is called phase coherence (*see figure 4.2*)

As these nuclear magnetization vectors fan out the resultant magnetization, vectors $M_{x'}$ and $M_{y'}$ are eliminated. This process is described by the Bloch equation for spin-spin relaxation:

$$d\mathbf{M}_{y'}/dt = \mathbf{M}_{y'}/T_2 \qquad 4-23$$

and

$$d\mathbf{M}_{x'}/dt = \mathbf{M}_{x'}/T_2 \qquad 4-24$$

The time constant T_2 is called the spin-spin or transverse relaxation time. No energy is lost during spin-spin relaxation, only the phase coherence between the precessing nuclear spins is lost, and the level populations will not change due to this relaxation, which is the reason why this type of relaxation sometimes is being referred to as an entropy process.

The main contribution to the spin-spin relaxation comes from B_0 not remaining homogeneous throughout the volume of the sample. These inhomogeneities even cause nucleus with the same chemical environment to precess with slightly different Larmor frequencies. When some nucleus precess slightly slower and some slightly faster than the Larmor frequency, it will result in the fanning out ending with the elimination of the macroscopic magnetization vectors.

T_2 is related to the line width of the observed NMR signal and this is the main practical significance of this time constant. The relationship is given by:

$$1/T_2 = \pi\Delta\nu_{1/2} \qquad 4-25$$

It is possible for the transverse magnetization $M_{y'}$ to decay completely before the longitudinal magnetization M_z has reached equilibrium, but it is not possible for the longitudinal magnetization to reach equilibrium before the transverse magnetization has completely disappeared. As a result of this, T_1 must always be larger or equal to T_2.

4.8 The Free Induction Decay (FID)

As mentioned earlier the signal registered in the apparatus arises from the magnetization in the x´y´-plane. The relaxation of these magnetization vectors induces a signal picked up by the receiver coil in the apparatus. This results in a decaying time dependent signal. This signal is called the Free Induction Decay (FID), it contains all the information from the sample but is rather hard to analyse directly. The FID is therefore Fouriere Transformed to obtain a frequency dependent spectrum which is possible to analyse.

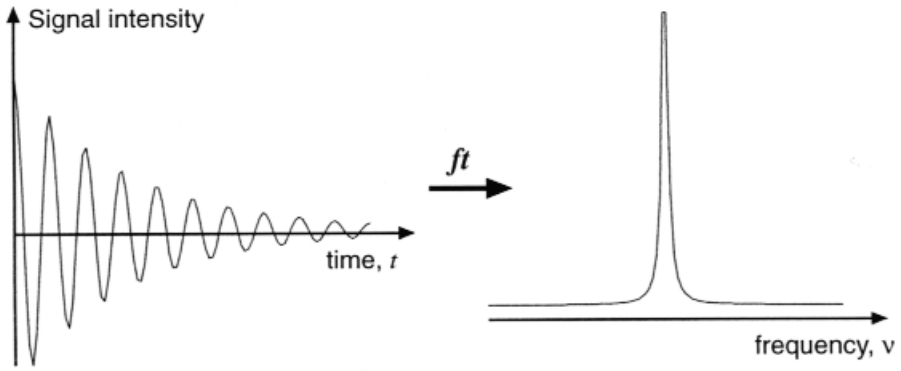

Figure 4.6 From FID to specrum by Fouriere Transformation[26]p26.

The Fourier transformation is described mathematically by:

$$F(\nu) \propto \int_{-\infty}^{\infty} f(t)e^{-i2\pi\nu t}dt \qquad 4-26$$

and this is the mathematical basis of the Fourier Transform (FT) NMR method.

4.9 1D ^{1}H NMR

The sample is placed in the probe-head and the magnetic field surrounding the sample made as homogenious as possible through shimming. Shimming is the adjustment of several circuits to set up an additional magnetic field inside the magnet correcting the original field. The macroscopic magnetization vector M_0 is oriented along the field B_0 at equilibrium. When applying the radio frequency pulse, M_0 is rotated to an angle depending on the pulse length, t_D. As long as no long relaxation times or other time requirements exist to make it impossible, t_D is usually chosen to rotate M_0 90° and thus maximizing the signal output.

This results in $M_z = M_0 = 0$ and $M_y = M_0$. The receiver coil then register the decay of M_y and M_x and the FID is obtained. After a Fourier Transformation of the FID, the 1D NMR spectrum is ready to be investigated.

4.10 Nuclear Overhauser Enhancement (NOE)

The NOE effect increases the intensities of the signals. Two nuclei close in space exhibiting a dipolar coupling will help each other to relax. The NOE effect works through space, not necessarily through scalar couplings. The system for two dipolar coupled nuclei A and X with no scalar coupling is illustrated below:

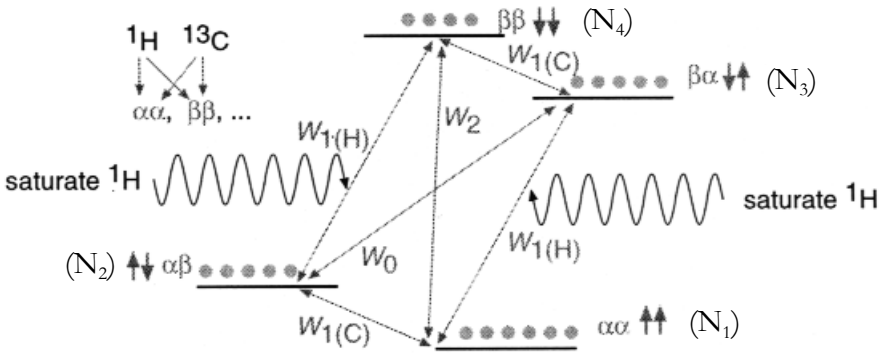

Figure 4.6 Two nuclei A and X (illustrated with H and C) are dipolar coupled and help relax each other through the pathways W_0 and W_2. The usual relaxation pathway W_1 is irradiated[26]p74.

During excitation the only allowed transitions are delta m ± 1 (equation 4 - 14). During relaxation this is not the case. Figure 4.6 describes the possible pathways for relaxation. W_2 is a double quantum transition and W_0 a zero quantum transition. W_0 and W_2 are determined mostly by dipole-dipole relaxation. When non-dipolar mechanisms are relaxing the system, this affects mainly W_1.

Irradiation of the sample with the resonance frequency of A equalizes (i.e. saturates) the populations in the N_1-N_3 and N_2-N_4 levels. The population difference for X has not changed and there seems to be no signal enhancement.

The irradiation shifts the system out of equilibrium, and because the W_{1A} pathway is irradiated and the W_{1X} has not changed from equilibrium, the only pathways to relaxation are W_0 and W_2. When relaxation along W_0 occurs, populations in N_2 are increased and N_3 decreased, thus reducing the difference in populations N_1 - N_2 and N_3 - N_4, thereby reducing the signal intensity from X. Relaxation along W_2, on the other hand, increases population N_1 at the expense of N_4, seemingly increaseing the difference between populations N_1 - N_2 and N_3 - N_4 giving enhanced signal intensity from X. As NOE is a relaxation process it needs some time to build up.

The system is not relaxed by W_0 or W_2, but the two pathways in combination. Both W_0 and W_2 relax the system and are therefore competing pathways. What decides whether W_0 or W_2 dominates in the relaxation process is the correlation time, t_c. Small molecules tumble faster than large ones and thus have shorter t_c. W_2 dominates at short correlation times and W_0 at long correlation times. Thus, small molecules give positive NOE effect and large molecules give negative NOE effect.

The frequency of the applied magnetic field is also an important factor. The fluctuating magnetic fields needed to induce the double quantum transition must contain frequencies close to the sum of the Larmor frequencies of A and X. The zero quantum transition requires much lower frequencies. Thus it is more likely to find negative NOE amplifications in a high field.

The NOE effect will also depend on the distance between the cross-relaxing molecules and will decrease in inverse proportion to the sixth power of the distance. This is an important tool for calculating distances between molecules through space.

Maximum NOEs cannot be achieved, since the dipole-dipole relaxation process is not the only process relaxing the nuclei. In theory the maximum NOE intensity enhancement is given by:

$$\eta + 1 = 1 + \tfrac{1}{2} * \gamma_X/\gamma_A \qquad 4-27$$

The maximum NOE effect for a ^{13}C signal coupling with ^{1}H is roughly 3. In comparison, the maximum NOE effect for ^{1}H relaxing with ^{1}H is only 1.5, since $gamma_X$ and $gamma_A$ will be equal.

4.11 NOESY

NOESY (Nuclear Overhauser Enhancement Spectroscopy) is a 2D NMR technique mainly used to determine structures of larger molecules in solution. There is a relation between the cross peak volume a_{ij} and the distance between spin nuclei i and j for larger molecules with short mixing times:

$$\alpha_{ij} \propto 1/(r_{ij}^{6}) \qquad 4-28$$

Hence the cross peaks will contain information about the distance between nuclei coupling through space. The pulse sequence for a NOESY experiment is given below:

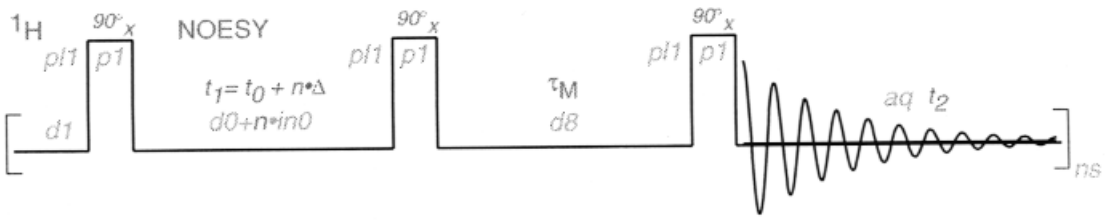

Figure 4.7 The pulse sequense for a simple NOESY experiment[26]p111. The sequence shown is simplified compared to the sequence used in experiments in this thesis.

A simple ^1H 1D NMR experiment is built up with just one pulse and then the acquisition. 2D NMR experiments are a little more complicated. To build in the second time dimension there is an incrementing time delay between the two pulses. The first pulse flips the magnetization vector into the xy-plane. Then, because of the time delay, it fans out from the slightly different Larmor frequencies. The time delay should not be long enough for any T_1 relaxation to occur. The second pulse will flip the magnetization vector in the opposite direction of the magnetic field giving zero signal. But, a component of the magnetization vector is on the x-axis during the second pulse because of the fanning out. This component is not rotated by the second pulse, giving rise to a signal containing information from both time dimensions.

In this thesis NOESY is applied to confirm that the DNA sequence is a duplex and not just single stands and to check the conformation of the oligomer after interaction with Ofloxacin as well as to see where Ofloxacin is interacting.

4.12 Water suppression

Water is a frecuently used solvent. Given the high concentration of ^1H in water, 55M, there is a relatively large signal due to water protons, considering the sample concentrations are between 0.07 mM and 6 mM. This results in baseline distortions and makes it difficult to observe other signals in the same vicinity to the water proton signal. To avoid this problem water suppression methods are used.

Water is either suppressed by presaturation of the water signal before aquisition or the pulsetrainesWATERGATE (WATER GrAdient Tailored Excitation) sequence w5 or the sequence 3-9-19 are used to manipulate the magnetization vectors as to minimise the water signal.

Theory - Part D:
5. Diffusion

Traditionally, self-diffusion constants have been measured through radioactive tracing techniques. These methods still give the most accurate data available experimentally today, but they are rather time consuming and complicated. Self-diffusion constants measurements obtained by NMR techniques require no specific sample preparation and demand no more time than other NMR experiments. NMR techniques can provide individual multicomponent self-diffusion constants with good precision.

Self-diffusion measurements have been utilised ever since the discovery of spin echoes, and during the last three decades the technique has been heavily used to investigate molecular transport. The theory is well known and a number of good reviews including theory and application have been published[27, 28, 29, 30].

5.1 Diffusion

Diffusion is defined as random motion in space. Molecules in solution are constantly in motion both rotationally and translationally. The process of translational motion are referred to as self-diffusion and is defined with a self-diffusion coefficient D (m^2s^{-1})

The self-diffusion coefficient depends on molecular properties such as size, shape, mass and charge. It also depends on environmental factors like viscosity of solution, temperature, solvent and other solutes. The concentration becomes a factor if the distant between two molecules are less than the distance one of the molecules travel in a given time. The concentration is usually not considered to be a factor.
The Stokes-Einstein equation is a special case of the Debye-Einstein equation and ideal for illustrating the relationship between the diffusion constant and the molecular properties. Stokes-Einstein is referring to spherically shaped molecules.

$$\text{Debye-Einstein:} \qquad D = k_B T / f_T \qquad 5-1$$

where D is the self-diffusion constant, k_B is the Boltsman constant, T is the temperature and f_T is the friction constant.

$$\text{Stokes-Einstein:} \qquad D = k_B T / 6\pi\eta R_H \qquad 5-2$$

where h is the viscosity and R_H is the radius of the molecule.

From equations 5 - 1 and 5 - 2 one can see that the self-diffusion coefficient can be found from the shape and radius of the molecule and the viscosity and temperature of the solution. It also follows the possibility of knowing the self-diffusion constant of two separate molecules and then to see from the self-diffusion constant whether two molecules interact in a solution.

5.2 How to measure diffusion by NMR

Diffusion coefficients can be calculated from the echo attenuation if the amplitude and duration of the magnetic field gradient are known; all NMR diffusion measurements are based on this principle.

$$I = I(0) * e^{-(D(\gamma g(i)\delta)\,\mathrm{squ}\,(\Delta - \delta/3)\,10*4)} \qquad 5-3$$

Which means that there is a connection between the amplitude of the signal and the self-diffusion coefficient. Big delta is the waiting time between the two gradients and little delta the duration time of the gradient.

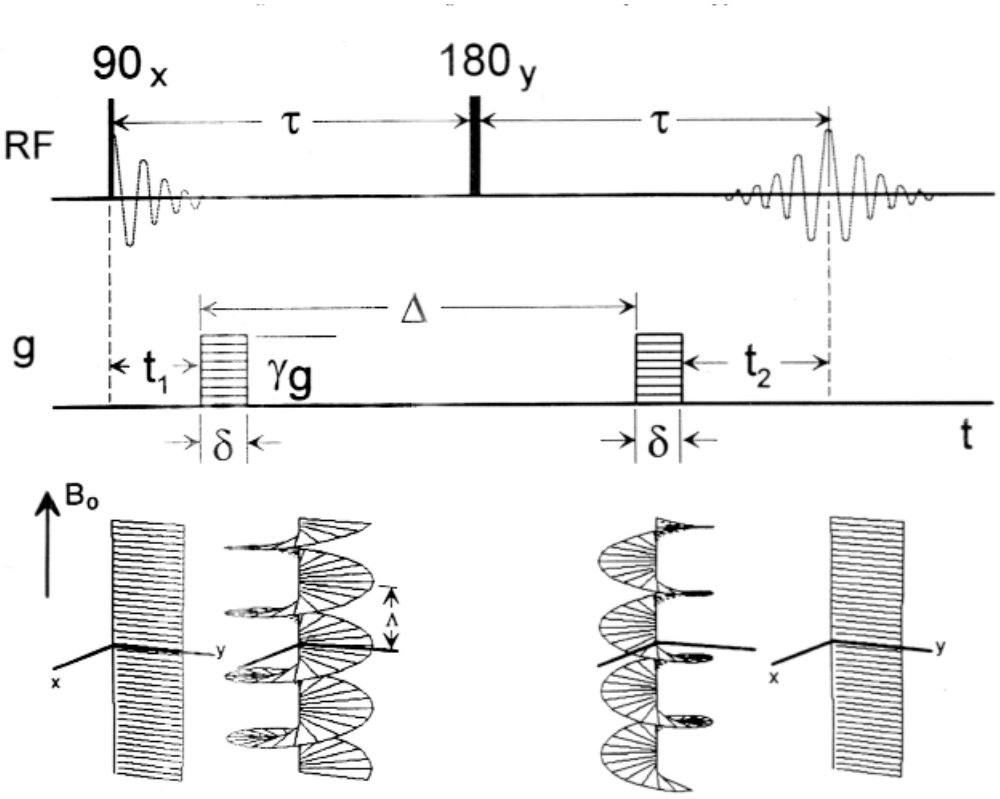

Figure 5.1 The pulse sequence and the implication of the gradients are shown for a simple spin echo experiment[30].

All measurements of diffusion coefficients are based on the fact that one can measure the amplitude or the area of the signal-top.

5.3 Basic theoretic introduction

Every NMR experiment is based on the repression of the Larmor frequency given earlier by equation 4 - 13 which may also be expressed as:

$$\omega_0 = \gamma B_0 \qquad 5 - 4$$

Where gamma is the gamma coefficient, a physical quality of the atom in question and B_0 is the strength of the magnetic field (*see also NMR theory*). One can then influence the system by a gradient given by:

$$g = \delta B_z i/\delta x + \delta B_z j/\delta y + \delta B_z k/\delta z \qquad 5 - 5$$

where i, j and k is unit vectors in the x, y and z direction in a Cartesian coordinate system. The magnetic field exerted on the molecule will then be:

$$B = B_0 + g\, r \qquad 5 - 6$$

where r describes the position of a specific nuclear spin. The gradient in the z-direction is described as:

$$g_z = g\, k \qquad 5 - 7$$

where k is the unit vector in the z-direction. This gradient gives the nuclear spin-system a phase-shift theta(z) in the z-direction described by:

$$\Phi_{(z)} = \gamma\, g_z\, z\, t \qquad 5 - 8$$

z is the distance travelled by the molecule in the time t. The total phase-shift in the magnetic vectors is expressed as:

$$\Phi_{(z)\ total} = \gamma\, B_0\, t + \gamma\, g_z\, z\, t \qquad 5 - 9$$

By exerting the molecules with a gradient pulse for a time, t, one creates a phase-shift. Then, by exerting the same pulse, but with the opposite direction one can read out the resulting phase-shift. If the molecules do not move in the waiting time big delta, the second pulse nullifies the effect

from the first pulse, and no net phase-shift is registered. If, however, the molecule moves a distance during the waiting time big delta, the second gradient pulse will mere reduce, not nullify the effect from the first pulse, and a phase-shift can be registered.

5.4 Spin echo or stimulated spin echo

The T_2 relaxation of small molecules is slow and using a spin-echo sequence does not cause any problems, as it may for larger molecules with faster T_2 relaxation. Because of the fast relaxation there will be no information left using a spin-echo sequence. One should therefore use a stimulated spin-echo when the molecule is larger to avoid this problem. Using a stimulated spin-echo secures that the T_1 relaxation dominates allowing faster T_2 relaxation.

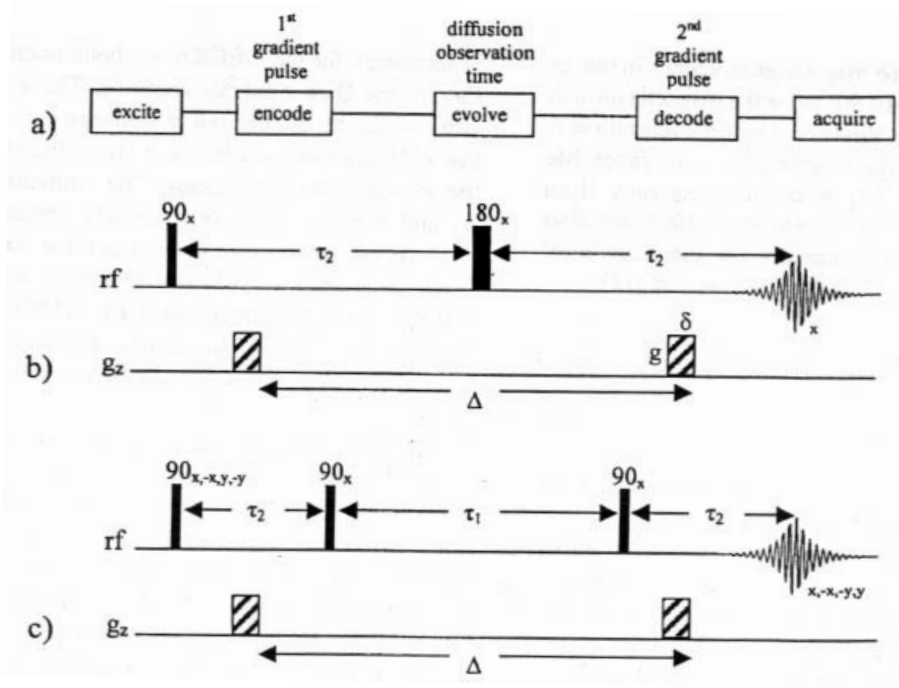

Figure 5.2 a) schematically overwiev of the self-diffusion experiment b) spin echo pulse sequence, T_2 is dominating c) stimulated spin echo pulse sequence T_1 is dominating[27].

5.5 Calculations of diffusion constants and association constants

The intensities of the picked peak are plotted as a function of the gradient strength resulting in a "simfit" plot. The simfit plot is a visual test of the peak attenuation and give an indication on whether the results are reliable. The uncertainty in the intensity is decreasing with gradient strength, since the gradient is suppressing more of the peak with increasing gradient strength. This leads to the conclusion that visual improvement of the simfit plot must be more important in the high intensity/low gradient strength area of the plot.

There are two ways to derive at the diffusion constants. The most complicated way is to simulate

a fitness curve on the simfit plot (the name simfit arrives from simulated fitness) using several iterations to best fit the curve. This is done for spin-echo experiment in the t1/t2 part of the XWinNMR program. The other way is to plot ln $I_{normalised}$ as a function of X where X is given as:

$$X = (g\gamma 2\delta * 100)^2 * (\Delta-(2\delta/3)-(\tau/2)) \qquad 5-10$$

where g is the gradient strength, gamma is the gradient amplitude, little delta the duration of the the gradient pulses and tau the delay between the gradients. X is given for a stimulated spin-echo experiment. This method was applied for stimulated spin-echo experiments as the first spectrum read by the XWinNMR program repeatedly was destroyed by ringing rendering the possibilities for peak picking and the intensities had to be read out manually. Also, the equation used in the t1/t2 program was faulty, as Bruker did not include tau in the calculations. Thus the t1/t2 program will calculate invalid results until this fault is corrected.

When ligands interact, the diffusion constants calculated containes an averaged value from both bound and non bound ligand. The fraction bound ligand (F) may the be calculated from the diffusion constant by:

$$F = (D_{Oflo} - D'_{Oflo})/(D_{Oflo} - D'_{GGCC}) \qquad 5-11$$

where D'_{Oflo} and D'_{GGCC} are the self diffusion constants and D_{Oflo} are the measured diffusion constant in that experiment. When F is known the association constant can be calculated from:

$$K_a = F/((1-F)*(C_{GGCC} - (C_{Oflo} * F))) \qquad 5-12$$

where C_{Oflo} and C_{GGCC} are the concentrations of Oflo and GGCC in the sample. The equations are adapted from reference [31].

5.6 Problems

Diffusion measurements are based on the spin-echo or stimulated spin-echo pulse sequences and the use of gradient pulses. This introduces some problems that should be addressed.

5.6.1 Eddy Current

When gradient pulses are switched quickly on and off eddy currents are set up to oppose the change. These currents induce magnetic fields in the conducting environment of the sample, as the probe and the magnet. The induced magnetic fields are slowly decaying, influating the original magnetic field and introducing spectral distortion or even changing the position of the lock signal introducing a shift in the resonance.

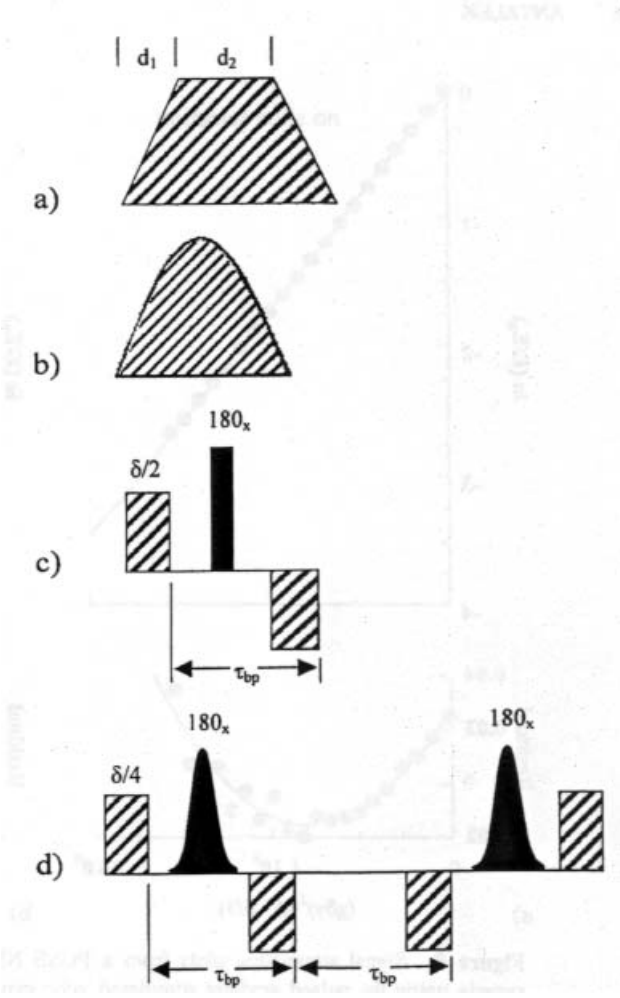

Figure 5.3 Different alternatives to the standard square gradient. a) trapezoidal b) half-sine shape c) bipolar gradient composite and d) the CLUB-sandwich including two 180 degree pulses[27].

To reduce the effect from eddy currents several precautions can be taken. Induced magnetic fields in the inner bore of the magnet can be reduced by the use of wide bore magnets. Induced magnetic fields in the probe can be nullified by a shielded gradient system - a probe with secondary gradient coils outside the primary Maxwell pair constructed to produce a magnetic field identical, but opposite, to the induced magnetic field. This reduces the effect of eddy current, but does not solve the problem completely. Experimental techniques to reduce effects from eddy currents include long waiting time between gradient pulses and design of pulse sequences that take eddy currents into account. A common way is to apply gradients in opposite directions using a 180° hard pulse to turn the system.

5.6.2 Gradient Field Nonuniformity

Basic theoretic outlines assume that gradient pulses are uniform across the z-direction of the sample. Nonuniform gradients will lead to systematic deviations from ideal behaviour and introduce considerable errors in measured diffusion constants.

One way to reduce the problem is to use slice selection of the gradient pulses, that is, only a small region of the sample, where the gradient are uniform, are used to obtain diffusion constants. This

can either be achieved by physically constraining the sample or exciting only the spins in the region of the sample where the gradient is uniform.

5.6.3 Temperature Gradients

The heating/cooling system of the magnet designed to keep a constant temperature in the sample is not optimal. Heating or cooling is either performed from the top of the probe or from the bottom. This results in a small temperature difference along the z-axis of the sample. Diffusion is dependent on temperature, hence the temperature gradient will introduce a velocity term to the diffusion constant.

The problem is difficult to control, but it may be solved by two methods; either reducing the height of the sample or by using a convection current compensated pulse sequence (a variant of the double stimulated echo configuration). If the sample height is reduced, the width of the sample should be reduced first since this has even larger implications.

5.6.4 Other considerations

In addition to the above mentioned problems, there are considerations to take into account during the aquisition of PGSE NMR data.

As gradients temporarily perturb the field, the lock should be controlled frequently. The data should preferably be collected in an interleaved manner, to avoid the occurrence of random errors. Vibrations at the probe are interfering with the diffusion of the molecules in the sample and ought to be avoided. Small vibrations, from for instance airflow in the probe, as well as chemical exchange and cross relaxation may influence the diffusion constant. The general effect from cross relaxation is that D will change as a function of the diffusion time (big delta) when the stimulated spin echo sequence is used. Spin echo exhibits no such effect from cross relaxation.

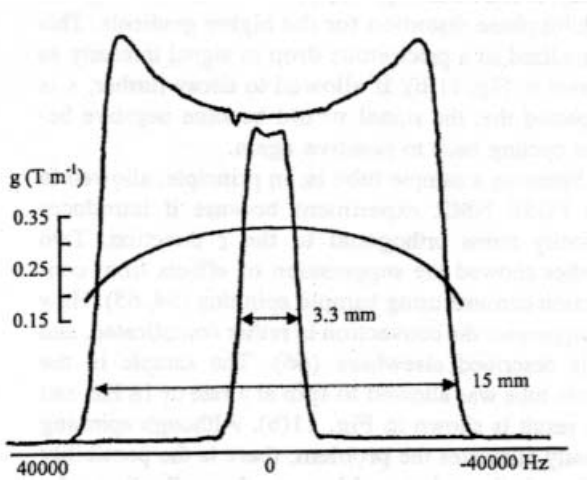

Figure 5.4 Illustration of the 1D profile experiment showing the effect of slice selection[27].

6. Experimental

6.1 Sample preparation

6.1.1 Preparation of the NMR sample of the DNA-oligomer GGCC

The oligomer GGCC delivered was not sufficiently pure, additional purification by HPLC ion-exchange was therefore needed. The purification was carried out with the eluents A: 10 mM NaOH, 0.3 M NaCl, pH 12.5 and B: 10 mM NaOH, 1.0 M NaCl, pH 12.5 with a detection wavelength of 260 nm. A 60 minutes linear gradient run from 100% A to 60% B was applied. Immediately after purification the oligomer pH was adjusted using a phosphate buffer ($NaH_2PO_4 * H_2O$). The sample was then desalted by filtration. Purification for paramagnetic impurities was not conducted.

After purification the sample was freeze-dried and resolved in 450 microL deionised water.

Table 6.1 Description of chemicals

Chemical	**Purchased/Manufacturer**	**Description**
Oligomer	DNA Technology, Denmark	A palindromic decamer
Phosphate buffer	Merck	p.a. quality
HCl	Merck	For the purification process
NaOH	Merck	For the purification process
Sephadex G-25		Used for desalting
Deionised water	Barnstead	From NANOpure deionising apparatus
Deuterated water	Cambridge Isotope Laboratories Inc.	99.9% purity
EDTA	Merck	p. a. quality

Table 6.2 Description of the equipment

Equipment	**Purchased/Manufacturer**	**Description**
Pump	Waters	626 LC model
Coloumn	Pharmacia Biotech	MonoQ HR 10/10
FlowDetector	Waters	W600s model
UV-detector	Dual	W2487 model
Software	Waters	Waters Millenium32 ver.3.05.01 software package
Hardware	Pentium	Standard PC
UV	Perkin-Elmer	Lamda 6 UV/VIS Spectrophotometer
Freeze-drying	GENEVAC	CVP 100/2 vacuum pump
pH measurements	Philips	PW9420 pH-meter with a Sentron pH ISFET Probe

To determine the concentration a 5 microL amount of the sample was imbedded in a solution of 500 microL 10 mM phosphate buffer, 500 microL 0.5M $NaClO_4$ and 1000 microL deionised water. The concentration of the oligonucleotide in the solution was thereafter determined by UV.

6.1.2 Preparation of NMR samples of Ofloxacin

Ofloxacin was given as the neutral molecule in solid state and no further purification was required.

Two stock solutions of Oflo were made. A series of samples with different concentrations was prepared from one of the stock-solutions and the other used for titrating GGCC.

First a 7.8 mM stock-solution of Oflo was prepared using stock-solutions of HCl and NaOH to control pH.

Table 6.3 The making of 7.8 mM stock-solution Oflo*

Oflo	**H_2O**	**0.05M HCl**	**0.05M NaOH**	**pH**
0.0043g	1280microL	200microL	40microL	7.15

** pH was measured during the dilution and the final concentration is corrected for volume changes*

A series of samples with concentrations ranging between approximately 1 mM and up to 6 mM was prepared from this stock-solution. Ofloxacin is more easily dissolved at low pH, therefore HCl was added first followed by NaOH to neutralize the solution.

Table 6.4 Concentration series for measuring stacking of Ofloxacin

Stock-solution (microL)	**Deuterated water (microL)**	**Deionised water (microL)**	**Concentration (M)**	**Measured pH**
65	50	385	1.02	6.33
130	50	320	2.04	6.70
190	50	260	2.98	6.80
250	50	200	3.91	6.88
320	50	130	5.01	6.99
380	50	70	5.95	7.03

These samples were used for measuring stacking of Oflo. The 5.01 M solution was also used for assignment purposes and for investigating the dynamics of the methylpiperazine ring. A new stock-solution 5.22 mM Oflo with pH 6.78 was prepared for the titration with GGCC.

Table 6.5 The making of 5.22 mM stock-solution Oflo*

Oflo	**H_2O**	**0.05M HCl**	**0.05M NaOH****	**pH**
0.0020g	1020 microL	30 microL	0 microL	6.78

** pH was measured during the dillution and the final concentration corrected for volum changes*

*** No NaOH was needed for pH correction of the solution*

6.1.3 Cleaning procedures

The samples are very sensible to contamination, particularly in the small concentration range studied in this thesis. It is therefore of great importance that the NMR-tubes are free from dust and other contaminating particles.

The NMR-tubes were first filled with a deconex solution and left for several hours. They were then rinsed three times with 5 mM EDTA and finally 10 to 15 times with deionised water. Disposable equipment was washed three times with deionised water.

6.2 Setup for NMR experiments

Three main techniques have been used in this thesis:
1) 1D ^{1}H NMR for assigning both GGCC and Ofloxacin and investigating the dynamics in the methylpiperazine ring.
2) 2D NOESY for assisting the assignment of GGCC.
3) Diffusion measurements to extract information on both stacking conditions in Ofloxacin and the affinity between GGCC and Ofloxacin.

The experiments were conducted on a Bruker DRX 600 MHz instrument. Processing of the data was performed on a Silicon Graphics INDY workstation using Bruker XWIN-NMR software suite v. 2.6. The spectra were analysed mainly on the same equipment.

For an explanation of the NMR parameters see Appendix C.

6.2.1 Calibration of the temperature

The temperature in the probe-head is controlled by a temperature-control unit. This unit does not present actual temperatures and thus has to be calibrated. The temperatures are chosen by setting the *te* parameter followed by the *teset* command. Temperatures given in this thesis are the temperature set to the temperature control unit unless otherwise stated. Most experiments in this thesis are performed at 298K, except the dynamics experiments.

Table 6.6 Some actual examples of reading temperatures on the spectrometer

Reading (K)	**Actual (K)**
270.0	267.4
275.0	273.0
280.0	278.5
285.0	284.1
290.0	289.8
295.0	295.5
300.0	301.3

This render the formula:

$$T_{actual} = (1.1312 \pm 0.0038) * (T_{reading}-(38.2 \pm 1.1)) \qquad 6 - 1$$

6.2.2 Calibration of the pulse

The 90° pulse flip angle was used for maximum signal intensity in most of the experiments in this thesis. The pulse angle is determined by two parameters: pl1 and p1. The pulse strength, pl1, is set on 0.00 dB in all experiments. It is given as attenuation values, meaning that greater pl1 values gives a weaker pulse.

The duration of the pulse, p1, was calibrated using the 360° method before each session of experiments[26]p62.

6.2.3 Adjusting the receiver gain

The receiver gain (rg) is set automatically in most experiments except in diffusion measurements where the *rga* command (set receiver gain automatically) cannot be used. The *rg* is then set in a 1D experiment and the FID controlled during the first scans in the diffusion experiment to check the *rg* value. The intensity of the FID should be just below ± 50.000 on the absolute scale. The *rg* value was adjusted manually whenever necessary.

6.2.4 1D ^{1}H NMR

Adjustments of *p1*, *o1p* and *sw* were carried out through the simple 1D pulse program *zg*. 1D ^{1}H NMR spectra were obtained for pure Oflo and pure GGCC and the Oflo/GGCC titration samples. All samples contained water as solvent and 10% deuterium to secure a lock signal.

Table 6.7 Adjustable parameters in 1D NMR experiments

	Oflo	**GGCC**	**Oflo/GGCC**
Pulse program	dpfgsew5	dpfgsew5	dpfgsew5
ns	256	256	1 k
p1	9.65 microseconds	15 microseconds	15 microseconds*
o1p	4.750 ppm	4.752 ppm	4.753 ppm**
rg	1024	1024	1024***
d1	6 seconds	2 seconds	2 seconds
td	32 k	64 k	64 k
sw	12.977 ppm	20.0276 ppm	20.028 ppm
pl18	6.00 dB	6.02 dB	6.02 dB
p0	19.25 microseconds	30.00 microseconds	30.00 microseconds****
p28	19.25 microseconds	30.00 microseconds	30.00 microseconds****
d19	143 microseconds	150 microseconds	150 microseconds
te	298 K	298 K	298 K

* *changed to 13.5 microseconds from sample number 3*

** *changed to 4.752 ppm from sample number 3*

*** *changed arbitrary, see table 6.8*

**** *changed to 25.70 microseconds from sample number 3*

Table 6.8 *rg* values for acquisition of ^{1}H NMR spectra of Oflo/GGCC in mixture

	rg-values
GGCC without* stock-solution Oflo	1024
with 10 microL stock-solution Oflo	1024
with 20 microL stock-solution Oflo	645.1
with 30 microL stock-solution Oflo	1824.6
with 40 microL stock-solution Oflo	1625.5
with 50 microL stock-solution Oflo	1625.5
with 60 microL stock-solution Oflo	1625.5
with 70 microL stock-solution Oflo	1625.5
with 80 microL stock-solution Oflo	1625.5
with 90 microL stock-solution Oflo	1625.5
with 100 microL stock-solution Oflo	1625.5

** The first NMR sample tube broke and made it impossible to tell how much Oflo from stock-solution was supplied. This sample is the deluted, recovered sample after the incident without measurable addition of stock-solution Oflo. The concentrations of the Oflo samples were calculated using intensities from the Oflo/GGCC spectra. Intensities were corrected for different rg-values as shown above.*

1D ^{1}H NMR spectra were also obtained to determine the 90° pulse, the position of the water signal, the sweep width and checking for contamination before other spectra were acquired.

1D ^{1}H NMR experiments on Oflo were also carried out with presaturation of the water signal since not all protons were accounted for in the w5-water suppression experiment. Spectra at 278, 288, 298, 300, 310, 315, 320, 325 and 330K were obtained.

Table 6.9 Adjustable parameters for acquisition of spectra of Oflo with presaturation of water

Parameter	**Values**
Pulse program	zgpr
td	32768
ns	8
ds	2
sw	11.9705 ppm*
aq	2.2807028 seconds
rg	90.5
dw	69.600 microseconds
de	6.00 microseconds
d1	2 seconds
p1	14.70 microseconds
pl9	40 dB

** for experiments at 278, 288 and 230K the value 26.7035 ppm was used, aq changed accordingly.*

A temperature change induces a drift in the chemical shift for the water signal and *o1p* therefore

moved from 4.745 ppm at 278K to 4.766 ppm at 230K.

All spectra were processed with *si* equal to *td* for maximum resolution. The FID was multiplied with an exponential weightening function, *em*, and line broadening was set to secure good signal to noise ratio, typically 0.50 - 2.00 Hz.

6.2.5 2D NOESY

The NOESY technique was used to assist the assignment of GGCC and to obtain information on any cross-linking between GGCC and Oflo. Two NOESY spectra were obtained, one of pure GGCC and one of GGCC/Oflo after the last titration.
To secure equal conditions, no aquisition- or processing parametres were changed between the two acquisitions.

Table 6.10 Adjustable parameters of the NOESY experiments

Acquisition parameter	**Values**	
	F2	**F1**
td	2 k	1 k
sw	20.0276 ppm	20.0276 ppm
pulse program	noesydpfgsew5	
o1p	4.754 ppm	
rg	1448.2	
d1	1.3 sec	
p1	14.00 micro sec	
pl18	6.02 dB	
p0	28.76 micro sec	
p28	28.76 micro sec	
d19	150.00 micro sec	
d8	250 milli sec	
Processing parameter		
si	2 k	2 k
WDW	QSINE	QSINE
SSB	2	2
lb	2 Hz	2 Hz
ME_mod	no	LPfc
LPBIN	0	2048
MC2		States-TPPI

Water suppression was conducted using the w5 pulse sequence and linear prediction applied to enhance signal to noise ratio.

6.2.6 Diffusion measurements

Three different diffusion measurements were performed:

1) The self diffusion constants for Ofloxacin and GGCC.

2) Diffusion measurements on different concentrations of Ofloxacin to check for stacking.

3) Measurements on a GGCC sample with different concentrations of Ofloxacin to measure the association between Ofloxacin and GGCC.

6.2.6.1 Self diffusion constants

The self-diffusion constant for Ofloxacin was calculated from the stacking experiment.
The self-diffusion constant for GGCC was determined using four different peaks at 7.12, 7.81, 8.18 and 8.28 ppm to rule out mistakes.

The diffusion measurements for GGCC cannot be based on the same pulse sequence as for Oflo (*see theory chapter 5.4*). Because of the different pulse sequences, the parameters are also set differently.

Table 6.11 Acquisition parameters for the determination of the self-diffusion constant for GGCC

Parameter	**Values**
Pulse program	ledbp19gs2s.nf
td	16384
ns	64
ds	16
sw	22.0410 ppm
rg	32
dw	37.800 micro sec
de	6.00 micro sec
d1	6.00 sec
d16 (Tau)	0.005 sec
p16 (Little delta)	2300.00 micro sec
d20 (Big delta)	0.065 sec
d21	0.005 sec
p1	15.0 micro sec
p28	29.93 micro sec
pl18	6.02 dB

6.2.6.2 Stacking measurements for Ofloxacin

The stacking measurements are based on the self-diffusion constant for Ofloxacin at different concentrations. Stacking leads to greater clusters of molecules and therefore a smaller diffusion constant.

The diffusion constant was measured at six different concentrations of Ofloxacin; 1.02, 2.04, 2.98, 3.91, 5.01 and 5.95 M. The acquisition parameters used in all the experiments were not changed to secure equal conditions for comparison of results.

Table 6.12 Adjustable parameters in diffusion measurements of Oflo to investigate stacking

Parameter	**Value**
Pulse program	segsw5
td	8192
sw	5.0069 ppm*
ns	22
ds	4
rg	30
dw	166.400 microseconds
de	6 microseconds
d1	6 seconds
d16	0.012 seconds
p16 (Little delta)	4 milliseconds
d19	0.0002 seconds
p0	19.30 microseconds
p1	9.65 microseconds
p28	19.30 microseconds
pl18	6.02 dB

* *changed to 12.977 ppm from experiment number 4, dw is changed accordingly*

Big delta is not a directly adjustable parameter in the pulse program and is calculated in a spin echo experiment using the equation:

$$\Delta = p16 + d16 + 5.949 * p28 + 18 * d19 + 46\ \mu s \qquad 6 - 2$$

In this experiment big delta was calculated to be 19.76 milliseconds.

6.2.6.3 Measurements of the affinity between Ofloxacin and GGCC

The affinity measurements were carried out exactly as the diffusion measurements. Diffusion measurements were performed on both Oflo and GGCC for comparison of results.

Measurements with focus on GGCC used the same parameters as in table 6.11 and measurements with focus on Oflo used the same parameters as in table 6.12, adjusting *p1*, *o1p* and *rg* to fit the experiments. Adjustments of these parameters do not affect the experiment.

6.2.7 Calculating the diffusion constants

After acquisition the t1/t2 part of XWin NMR was used to calculate the constants. After phasing the spectra, the t1/t2 program is opened with the *t1/t2* command. The program reads the spectra applying the *rspc* command and the marker is set on the peak in question. The program, using the *ppt1* command, then reads all intensities of the peak in the second dimension. For some reason (a logical mistake in the program) the t1/t2 program then needs to be opened again. The *pd* command now gives a curve with all the intensities, normalizing the first peak to 1. The simfit command present a simulated fitness curve on the plot and the diffusion constant reads out directly from the program.

Noise and ringing left the first spectrum in the diffusion measurement series impossible to use at the peak in question when applying a stimulated spin echo pulse sequence. This unabled the t1/t2 program to calculate the diffusion constant, but the peak from the water signal made it possible to define the gradient strength and the intensities of the peak in all the spectra in the series were read out and the diffusion constant calculated manually as described in chapter 5.5.

7. Results

7.1 Ofloxacin (Oflo)

7.1.1 Assignment of ^{1}H NMR spectrum of Oflo

Oflo contains two aromatic protons, in positions 5 and 8, expected to have chemical shifts somewhere between 6 and 9 ppm. The two methyl groups positioned at C3 and N4´ are expected to give signals in the region 0.5 - 3 ppm. The protons sited on the methylpiperazin ring and on C2 and C3, are expected to have chemical shifts somewhere between the methyl groups and the water signal.

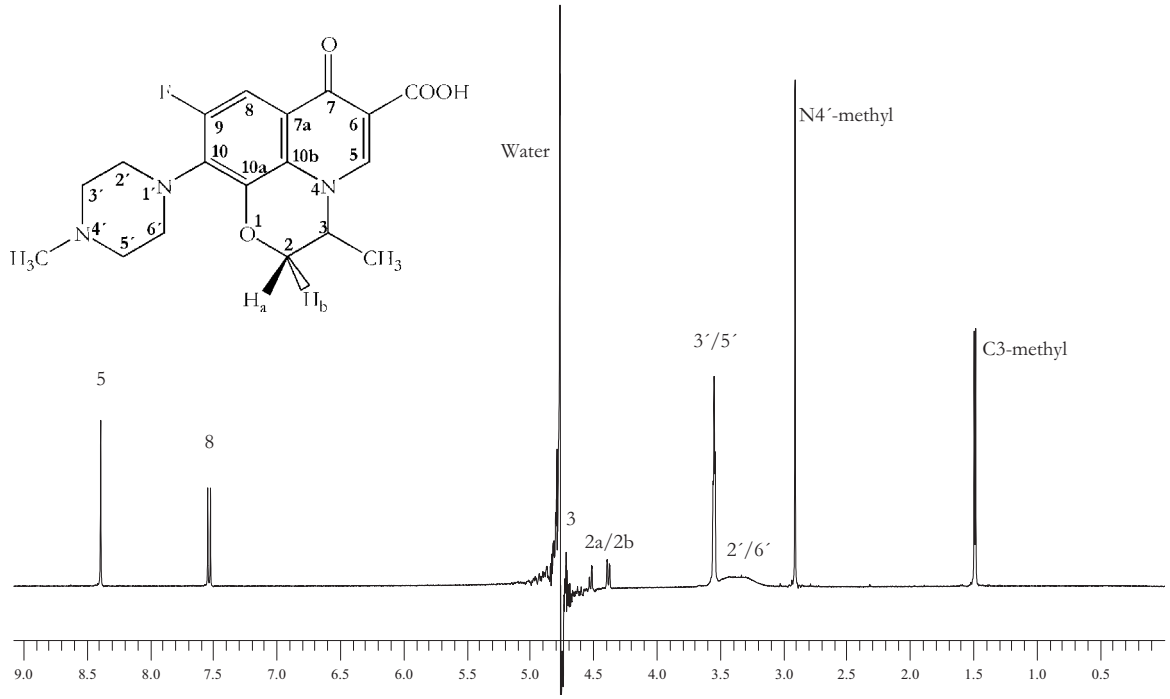

Figure 7.1 ^{1}H NMR spectrum of 5.01mM Ofloxacin in water (pH 6.99) and D_2O (10%). The spectrum was aquired at 294K (actual temperature), and the water signal was suppressed by presaturation.

Due to the fluorine in position 9 the signal from H8 is splitted in a dublett. The other signal in the aromatic region must therefore result from H5. The two protons H2a and H2b are not chemically identical and will split each other. It is not possible to predict which of the two signals is from which proton from the available data. The assignment of H3 on the other hand is now obvious although difficult to observe due to the water signal. The signal from H3 was easier to observe in a spectrum obtained using D_2O as solvent (*see Appendix A*). Because of the suppressed water signal the coupling constant in the H3 signal is not very reliable, but from the structure one can see that the only methyl group splitted from one proton is C3-methyl. J-coupling similar to that measured for C3-methyl is expected. The two methyl signals are easily distinguished; the N4´-methyl is situated on a nitrogen atom giving a downfield singlet and the C3-methyl protons couple

with H3, hence the most upfield signal with the splitting must be the C3-methyl-group. The broad bump at ~3,3 ppm are the 2´/6´ protons. The methylpiperazine ring has a hindered motion and the signal from 2´/6´ is at coalescence at this temperature. A further investigation of this phenomenon is given in the following session.

Table 7.1 Chemical shift-values for Oflo

Proton (s)	**ppm**	**multiplicity**	**J (Hz)**
C3-methyl	1.48	d	6.9
N4´-methyl	2.91	s	-
2´/6´	coalecence	-	-
3´/5´	3.55	t	4.7
2a[2]	4.52	dd	11.4/1.7
2b[2]	4.39	dd	11.4/2.4
3[1]	4.7	m	-
8	7.52	d	12.7
5	8.39	s	-

[1] *From D_2O spectrum without water suppression (spectrum appended)*

[2] *It is not possible to separate the two tops from the data available*

7.1.2 Dynamics of the methylpiperazine ring

As can be seen from figure 7.1, 294 K is the coalescence temperature for the motion of the methylpiperazine ring. The development of the top from the 2´/6´ protons are shown in figure 7.2. The rate constants for the dynamics can be calculated using the following equations:
Slow exchange (i.e. distinct resonances observed for each pair of protons)

$$k = \pi(w-w_0) \qquad 7-1$$

Coalescence (i.e. exhanging resonances just merge into a single peak)

$$k = \pi(\delta\nu)(2)^{-1/2} \qquad 7-2$$

Fast exchange (i.e. one averaged resonance observed)

$$k = \pi(\delta\nu)^2(w-w_f)^{-1}(2)^{-1/2} \qquad 7-3$$

where
w_0 is the width at half height for the peak at the low temperature limit, w_f the half height for the peak at high temperature limit and w is the width at half height for the peak in question.
(delta v) is the chemical shift difference between the reconances in the low temperature limit.
The upper and lower temperature limits was found and w_0, w_f, w and (delta v) measured.

Table 7.2 Summary of parameters obtained from the temperature series of the methylpiperazine protons

T (K)	**w (Hz)**	**Peak distanse (Hz)**	**Calculated k (Hz)**
271	33.3 (w_0)	156.5 (delta v)	--*
283	58.2	155.0	78.3
294	--	--	347.5
308	46.9	--	1810.3
313	31.4	--	3758.2
319	23.5	--	8264.5
324	18.0	--	49436.8
330	16.9 (w_f)	--	--*

**k cannot be calculated for the upper and lower temperature limits.*

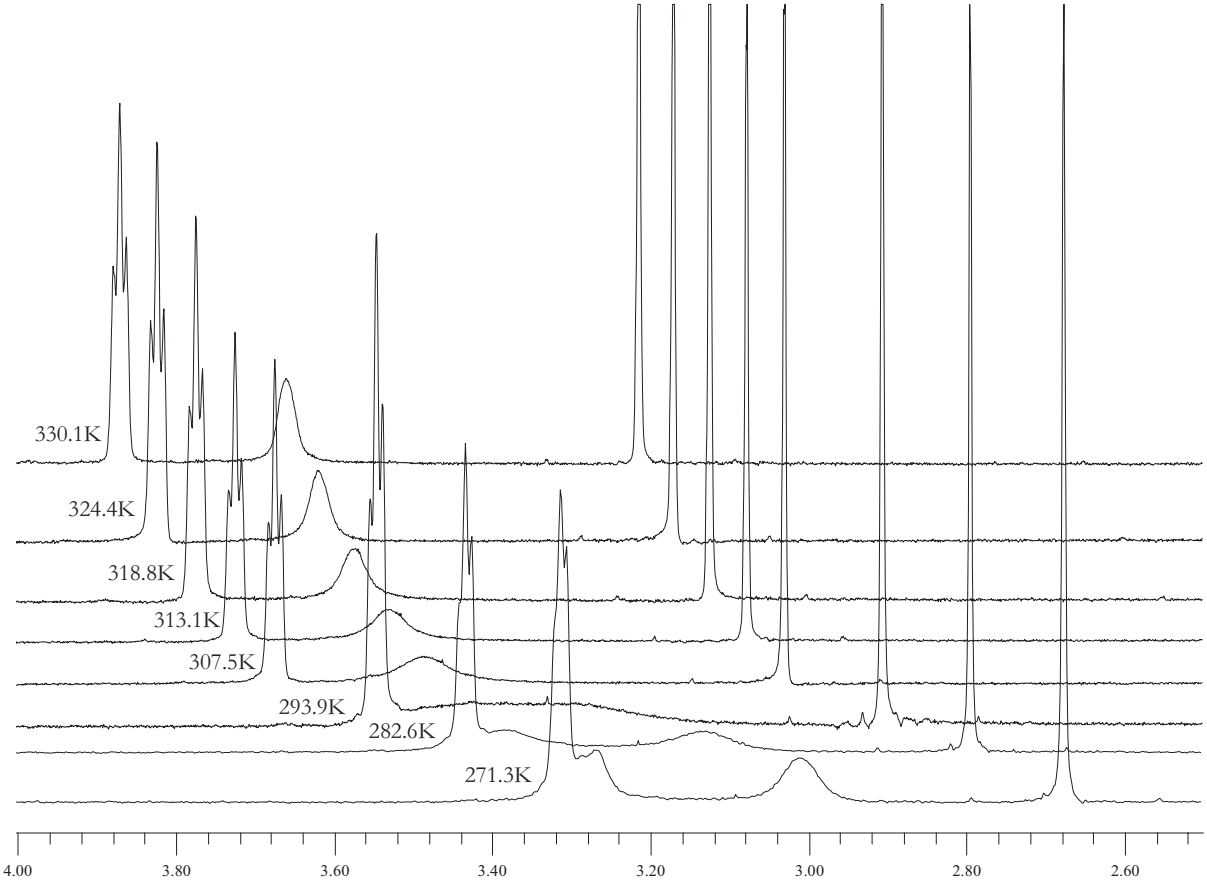

Figure 7.2 The developement of the 2´/6´ signal with changing temperature. Sample and conditions are the same as for spectrum in figure 7.1. The spectra are placed on top of each other and due to temperature change the chemical shifts drift.

Both Eyring and Arrhenius plots were prepared and thermodynamic parameters for the rotation calculated. The plots are shown in figure 7.3.

Table 7.3 Calculated thermodynamic parameters for the rotation of the methylpiperazine ring

Delta H	**Delta S**	**Delta G**	**E_a**
91 kJ/mol	120 J/Kmol	58 kJ/mol	107 kJ/mol

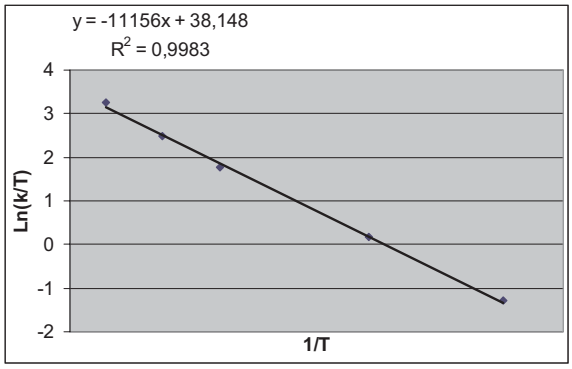

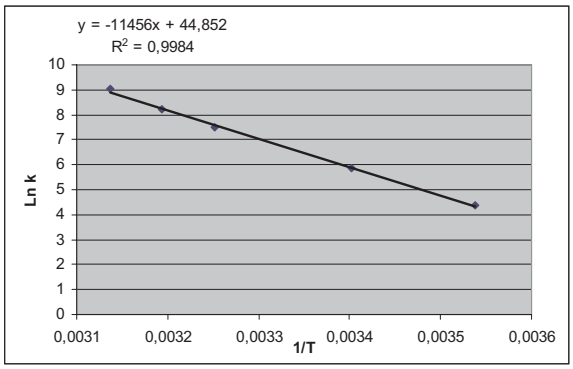

Figure 7.3 Eyring plot and Arrhenius plot of the dynamic of methylpiperazine.

Table 7.4 Data for Eyring and Arrhenius plots

T (K)	**Ln [k/T]**	**1/T (K^{-1})**	**Ln k**
283	-1.283	0.00354	4.361
294	0.171	0.00341	5.851
308	1.773	0.00325	7.502
313	2.486	0.00319	8.232
319	3.256	0.00314	9.020

7.1.3 Stacking measurements

Investigations of the stacking conditions in Oflo were performed by measuring the self-diffusion constant in a series of concentrations using the spin echo sequence. The constants were calculated directly in the t1/t2 part of the XWinNMR program.

Table 7.5 Self-diffusion constants for Oflo at different consentrations

Concentration	**pH**	**$D_{2.9}$ ($*10^{-10}m^2s^{-1}$)**	**$D_{3.5}$ ($*10^{-10}m^2s^{-1}$)**	**$D_{8.4}$ ($*10^{-10}m^2s^{-1}$)**
1.02 ± 0.09 mM	6.33	4.44 ± 0.06	4.38 ± 0.06	--*
2.04	6.70	4.41	4.36	--*
2.98	6.80	4.38	4.33	--*
3.91	6.88	4.33	4.34	4.31 ± 0.06
5.01	6.99	4.38	4.29	4.36
5.95	7.03	4.23	4.21	4.27

The uncertainty is indicated at the first constant in each case.

* *The diffusion constant at 8.4 ppm was not measured for all concentrations since the width of the spectra was maladjusted for the first three concentrations.*

The diffusion constant at 8.4 ppm is included as a reference to the diffusion constant for GGCC which was measured at peaks in the same region. The samples were not adjusted for pH, but pH is well in between the pKa-values (*6.05 and 8.22 respectively*) and is thus not expected to have considerable effect on the diffusion constant. The concentration might also affect diffusion constants. Diffusion constants plotted against pH and concentration are given in figure 7.4.

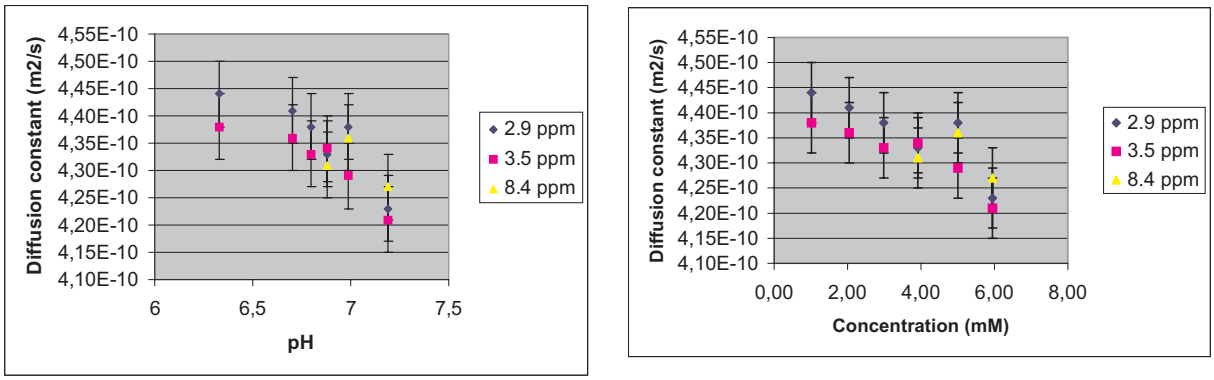

Figure 7.4 Diffusion constants plotted against pH and concentrations for Oflo. The plots show all the peaks and uncertainties in the diffusion constants are shown in each point. The uncertainty in the x-direction is not shown.

Without concern of variations from sample concentration and pH, Oflo has a mean diffusion constant of $D = 4.36 \pm 0.06 * 10^{-10}$ m^2s^{-1} (*taken from the peak at 2.9 ppm only*)

7.2 The DNA-oligomer GGCC

7.2.1 Assignment of NMR spectra of the oligomer GGCC

The GGCC oligomer is a palindromic, self-complementary sequence and has two identical strands in the double helix, namely:

5´ - T_1 A_2 T_3 G_4 G_5 C_6 C_7 A_8 T_9 A_{10} - 3´

The two sequences give rise to two sets of equal signals from the ten base pairs.

7.2.1.1 ^{1}H NMR spectrum of GGCC

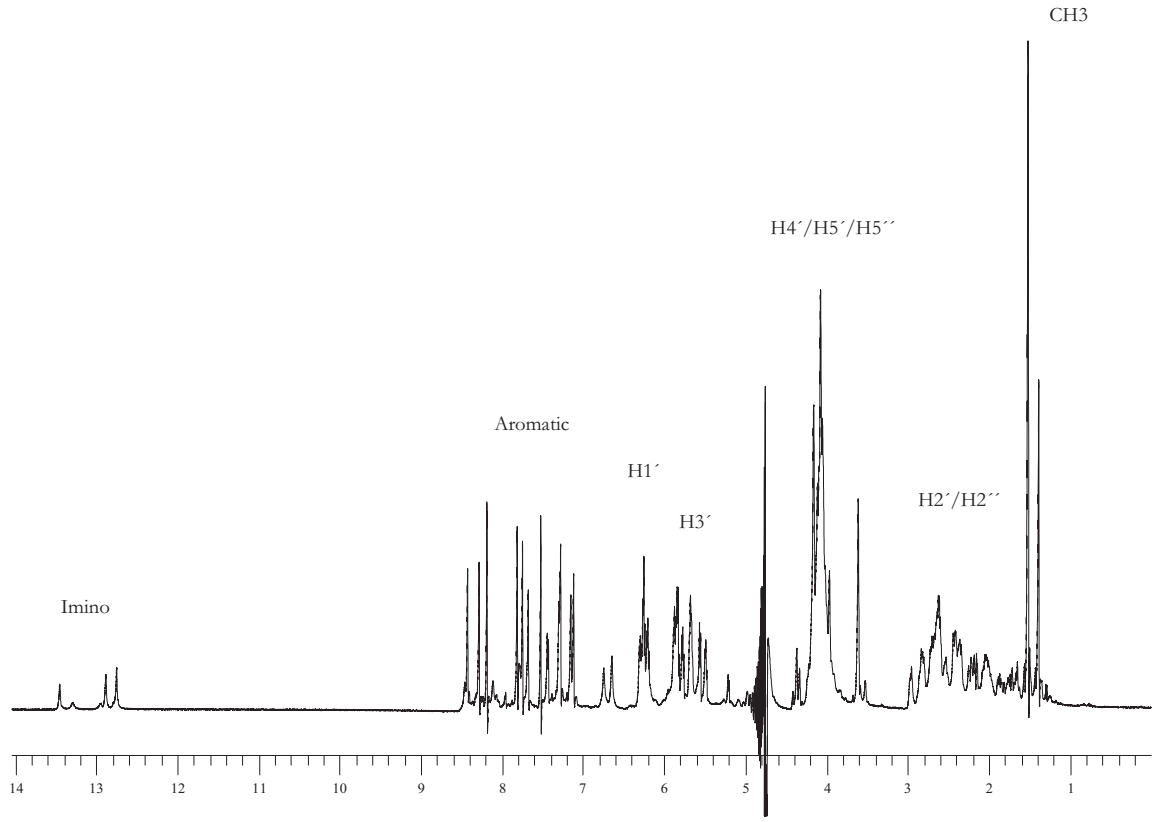

Figure 7.5 ^{1}H NMR spectrum of 0.58 mM GGCC with phosphate buffer acquired at 298 K. The regions for the different groups of protons are indicated.

A complete assignment of the oligomer was not conducted although most of the aromatic region of the oligomer had to be assigned by ^{1}H NMR and NOESY to investigate the development during the titration with Oflo. The assignment was assisted by a previous assignment by Vinje et al.[32]. Only parts of the assignment is published, but the rest was kindly handed out by mr. Vinje.

From figure 7.7 it is obvious that the DNA is in double helix state since all five imino protons are observable. The imino protons exchange too fast on the NMR time scale to be observed unless they are involved in hydrogen bonds in a double helix. Signals from T1 and T9 have low intensi-

ties as the outer base pairs are expected to be less stable than the rest of the base pairs. Also, Thymine - Adenine pairs only have two hydrogen bonds and Guanine - Cytosine has three hydrogen bonds. The low intensities of the Guanine signals, especially G4, are caused by paramagnetic impurities. This was expected as purification for paramagnetic impurities was not conducted. The C6 and T1 signals in the aromatic region are overlapping.

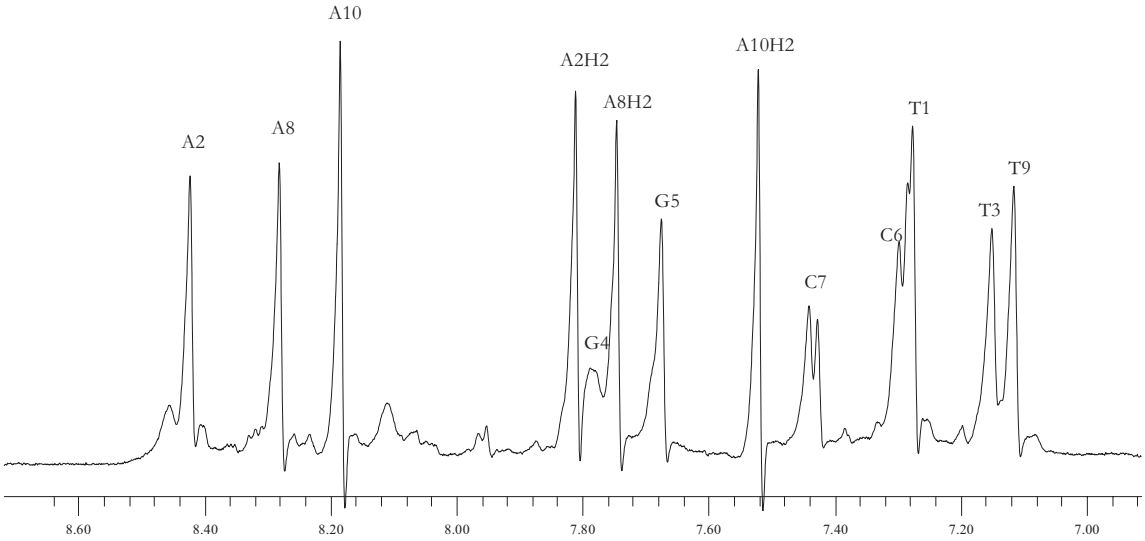

Figure 7.6 The ^{1}H NMR spectrum of GGCC expanded in the aromatic region.

Table 7.6 ^{1}H chemical shifts in the aromatic and imino regions of the ^{1}H NMR spectrum of pure GGCC

Aromatic protons	**Chemical shifts (ppm)**
T1	7.28
A2	8.42
T3	7.15
G4	7.79
G5	7.68
C6	7.30
C7	7.43
A8	8.28
T9	7.12
A10	8.18
A2H2	7.81
A8H2	7.74
A10H2	7.52
Imino protons	
T1	12.95
T3	13.45
T9	13.29
G4	12.75
G5	12.88

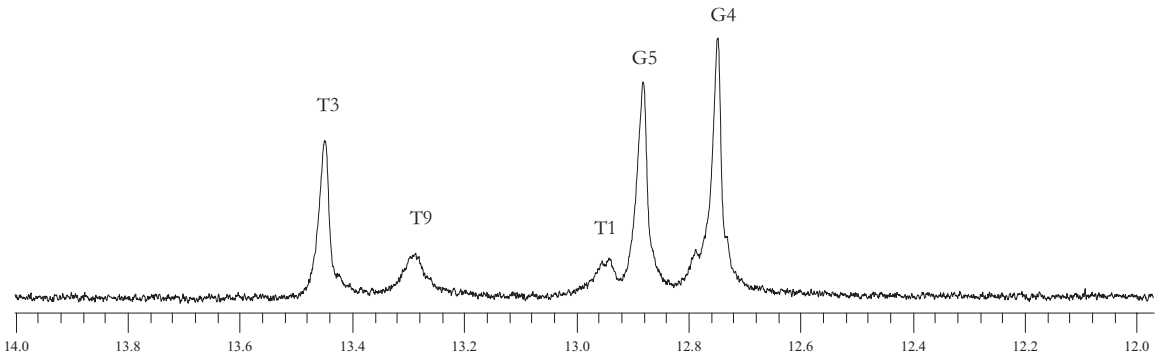

Figure 7.7 The ^{1}H NMR spectrum of GGCC expanded in the imino region.

7.2.1.1 NOESY spectrum of pure GGCC

The NOESY spectrum is helpful in confirming the helix structure of the oligomer. A NOESY sequential walk has been conducted in the aromatic region.

As can be seen in the NOESY spectrum some overlap of peaks in the aromatic region occures. The sequential walk is based on reference [30].

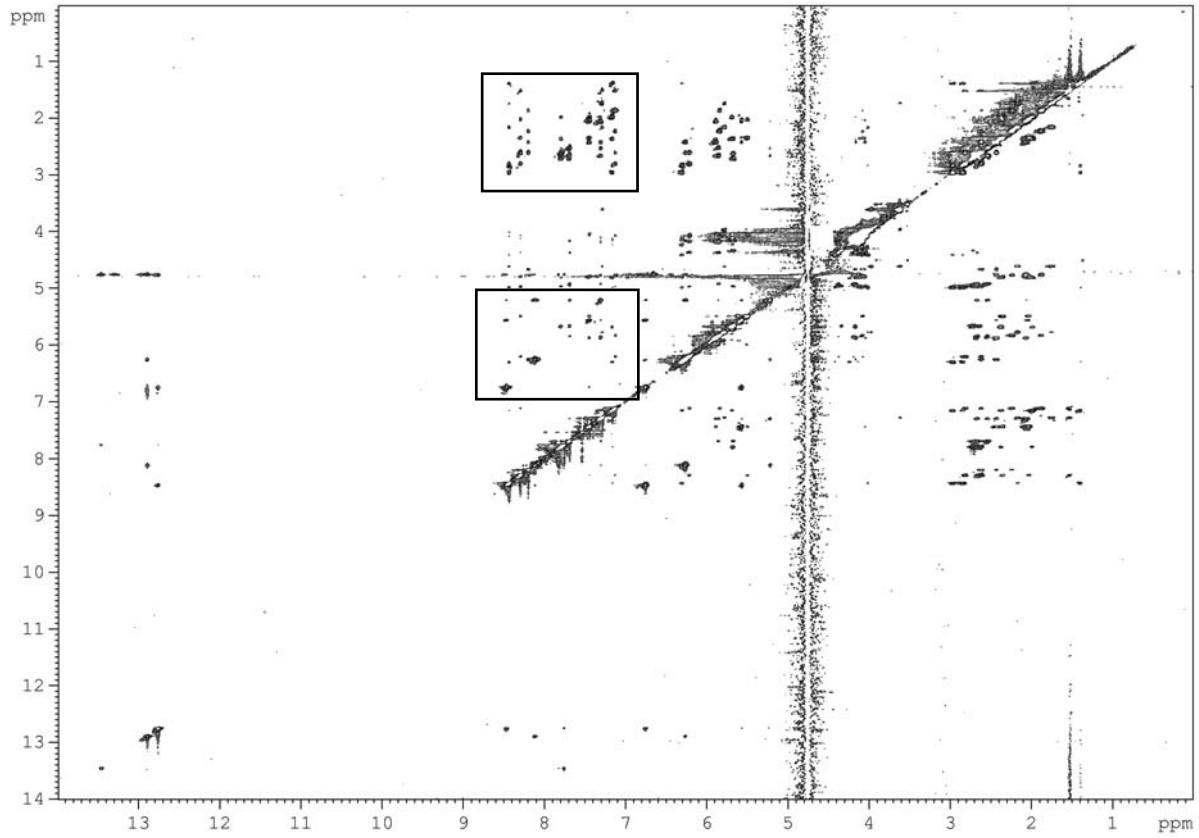

Figure 7.8 The NOESY spectrum of 0.58mM GGCC at 298 K. Two parts of the spectrum is further investigated and expansions are given in the following figures.

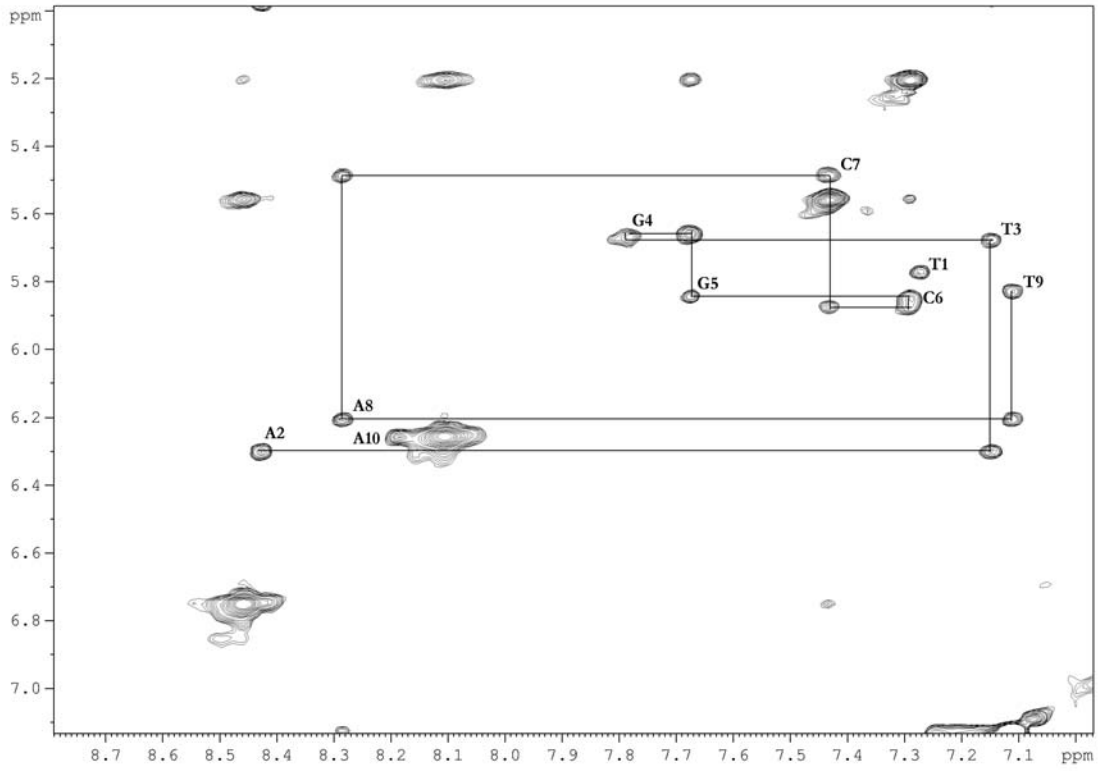

Figure 7.9 NOESY sequential walk in the expanded aromatic region of the NOESY spectrum of GGCC.

The NOESY sequential walk is performed in the aromatic-aromatic region. Crosspeaks between the H6/H8 protons on the base and H1' on the sugar are marked in the spectrum with the name of the bases. Between each internal crosspeak there is a crosspeak between the H1' on the sugar and H6/H8 on the base below. These crosspeaks are not specifically marked in the spectrum. As example; A2 and T3 are marked in the spectrum. These crosspeaks result from H8 on A2 and H1' on the sugar to whom A2 is attached, and H6 on T3 and H1' on the sugar to whom T3 is attached respectively. Between these two crosspeaks there is an unmarked crosspeak, this is the H1' on the sugar to whom A2 is attached and H6 on T3.

Only two crosspeaks are missing in the sequential walk; crosspeaks between T1 and A2 and between T9 and A10. This is expected as the outer base pairs are less stable than the rest of the base pairs.

Another expansion is shown in figure 7.10. In this region the crosspeaks between H2' and H2" on the sugar ring and the H6/H8 on the bases are observable. This is also a sequential walk, although more complicated. The bases each result in four crosspeaks; two from H6/H8 to H2' and H2" on the sugar to whom they are attached and two from H6/H8 to the H2' and H2" on the sugar on the previous base. T1 without a sugar attached in 5' position will only give rise to two crosspeaks. Although not illustrated by lines, all the crosspeaks expected are present in the

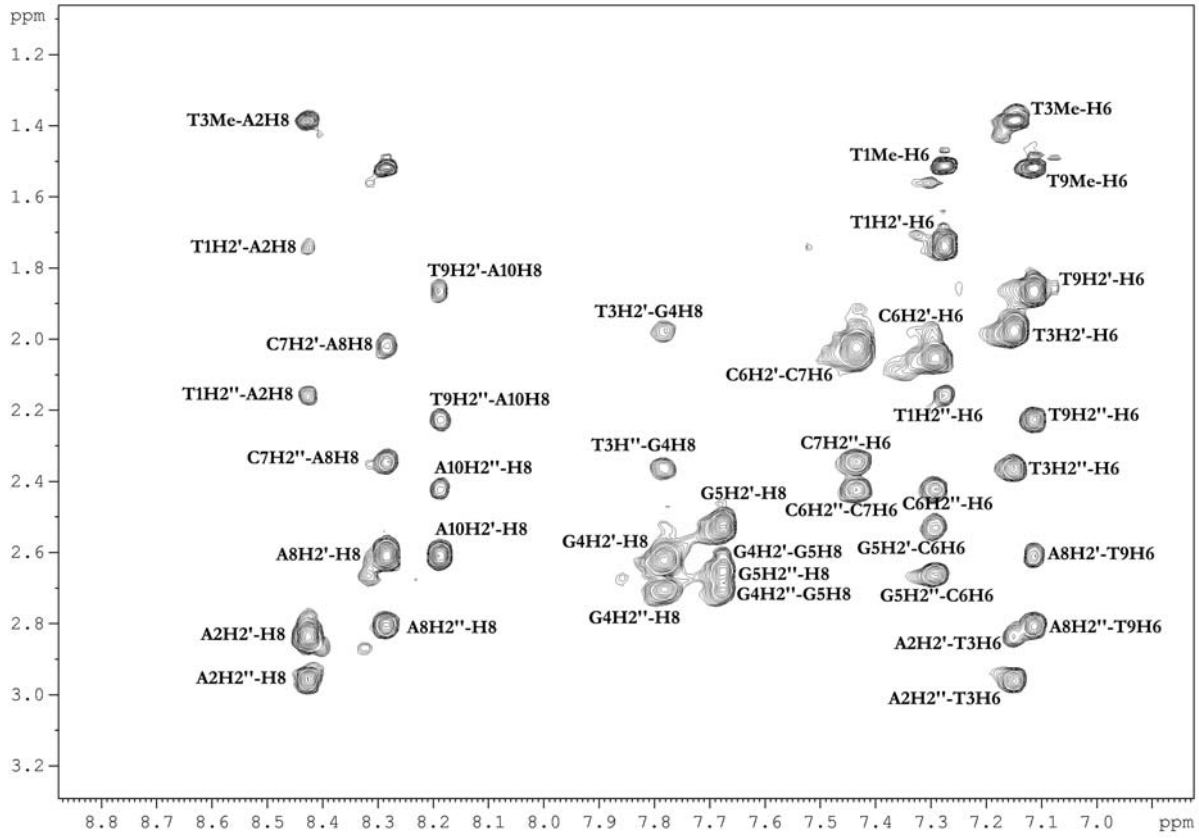

Figure 7.10 An expansion of the aromatic-anomeric region of the NOESY spectrum of GGCC.

spectrum indicating a completely intact double helix. The ppm values for the crosspeaks are summarised in table 7.13.

7.2.2 Measurements of the self diffusion constant of GGCC

The calculations in XWinNMR do not take into account the effect of tau when bipolar pulses are used. For that reason the intensities from all the scans had to be read out and the diffusion constant calculated manually. First the normalised intensities were plotted against the gradient strength to rule out any abnormal points (*so-called "Simfit" plot*) and then the natural logarithms to the normalised intensities were plotted against x (*see equation 5 - 11*). The resulting coefficient will give the diffusion constant.

A 0.58 mM sample of GGCC was used for self-diffusion constant measurements. The diffusion constant of GGCC is not expected to depend on the concentration. No experiments were conducted to confirm this assumption. The Simfit plot and regression plot for the peak at 7.81 ppm are shown in figure 7.11. Intensities and some of the other simfit and regression plots are appended in appendix A. Four peaks were used to control the results and calculate the uncertainty.

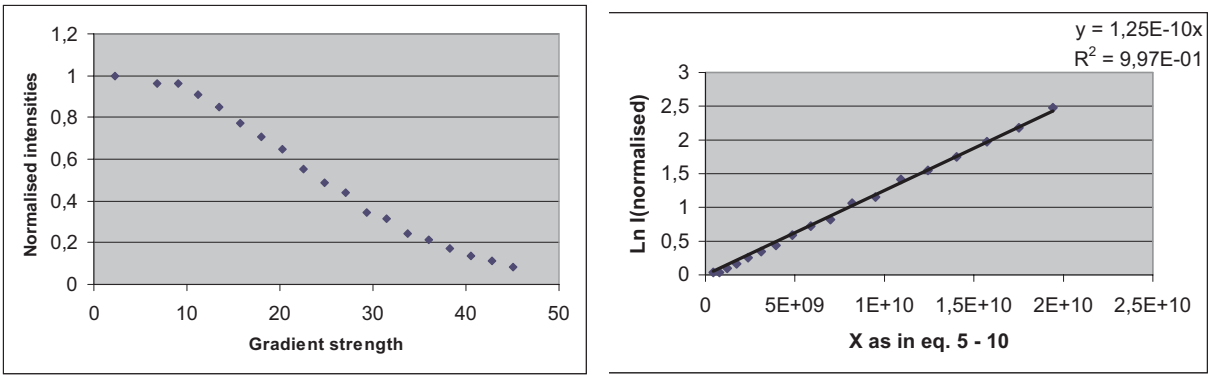

Figure 7.11 Simfit and regression plots for diffusion measurements of GGCC for peak at 7.28 ppm

Table 7.7 Diffusion constant of GGCC calculated at different chemical shifts

Chemical shift	**7.12 ppm**	**7.81 ppm**	**8.18 ppm**	**8.28 ppm**
Diff. constant	$1.42 * 10^{-10} m^2 s^{-1}$	$1.25 * 10^{-10} m^2 s^{-1}$	$1.31 * 10^{-10} m^2 s^{-1}$	$1.36 * 10^{-10} m^2 s^{-1}$

This gives a mean diffusion constant of $1.34 (\pm 0.07) * 10^{-10} m^2 s^{-1}$

The uncertainty in all diffusion constants in GGCC are taken to be $\pm$ 0.07

7.3 Oflo and GGCC titration

7.3.1 Oflo concentration

Unfortunately, immediately after 10 microL stock-solution Oflo was imbedded in the sample of pure GGCC, the NMR-tube was dropped on the floor and broke. The sample was reproducible, but there were no means of telling how much of the Oflo stock-solution got into the GGCC sample. UV-measurements were tempted, but unfortunately the Oflo concentration was too small. We decided to maintain the experiment rather than to start over , which would have set the experi-

mental time back two to three weeks. The concentration of Oflo in the GGCC sample was calculated after the experiments were ended. The N4´-methyl protons from Oflo appear in a part of the spectrum where GGCC protons do not have any signal and the intensities from this signal were used to calculate the concentration of Oflo. As can be seen from the spectra of the Oflo-GGCC titration, the N4´-methyl signal divides into two distinct peaks, labeled N4´-methyl (a) and N4´-methyl (b). The development of both these peaks taken together resulted in a good regression line giving the initial Oflo concentration.

Table 7.8 Data used to calculate the initial concentration of Oflo in the Oflo-GGCC titration

Total volume (microL)	**Intensities N4´-methyl**	**Intensities N4´-methyl (a)**	**Intensities N4´-methyl (b)**	**Concentration (mM)**
450	37759020	23420351	14338670	0.07
460	61711756	33883856	27827900	0.13
470	120743385	60371693	60371693	0.24
480	184438117	113001393	71436724	0.35
490	241256290	172066726	69189564	0.45
500	298115926	213504437	84611489	0.56
510	311314224	213364334	97949890	0.66
520	405830963	288835929	116995034	0.76
530	453484661	320176475	133308186	0.86
540	502948887	353626474	149322413	0.95
550	542229480	378896227	163333253	1.05

The applied volume Oflo after the accident was of course known. The initial concentrations could therefore be calculated by first plotting the applied concentrations as a function of intensities and doing a linear regression on the plot. The regression equation then allows the concentrations to be adjusted to make the regression-line go through origo. This resulted in the initial concentrations summarised in table 7.8. The plots of the intensities from the N4´-methyl signals (a) and (b)

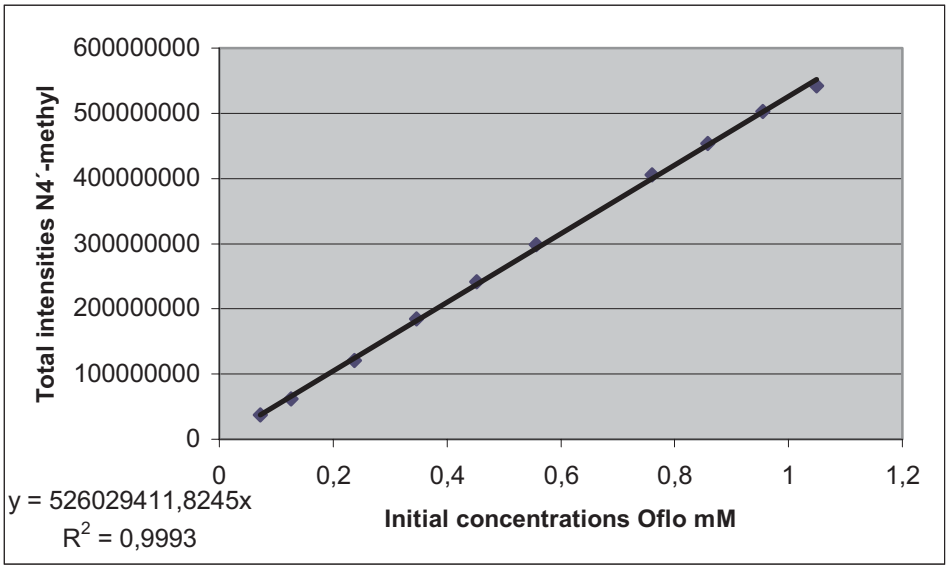

Figure 7.12 Intensities of both Oflo tops plotted against initial concentrations

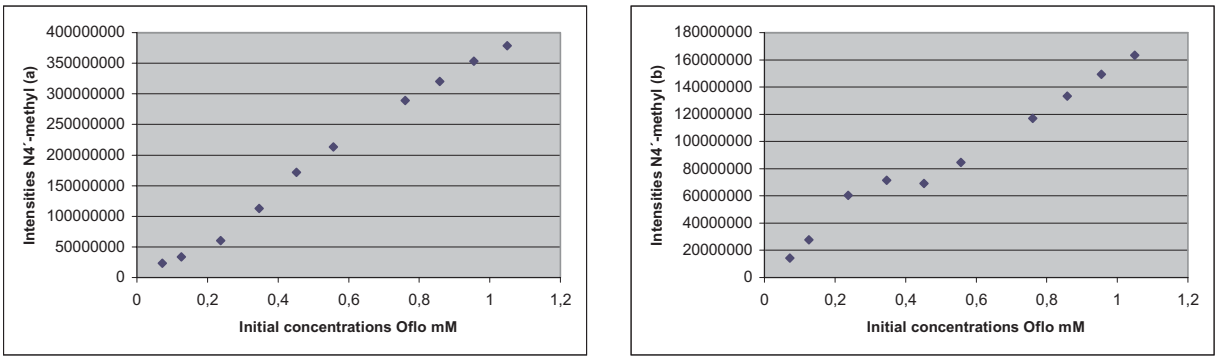

Figure 7.13 Intensities of the N4´-methyl (a) signal and the N4´-methyl (b) signal plotted against initial concentration of Oflo

and both taken together against the concentration are given in figures 7.12 and 7.13.

Two signals from N4´-methyl were not expected, this is further discussed in chapter 8.3.2

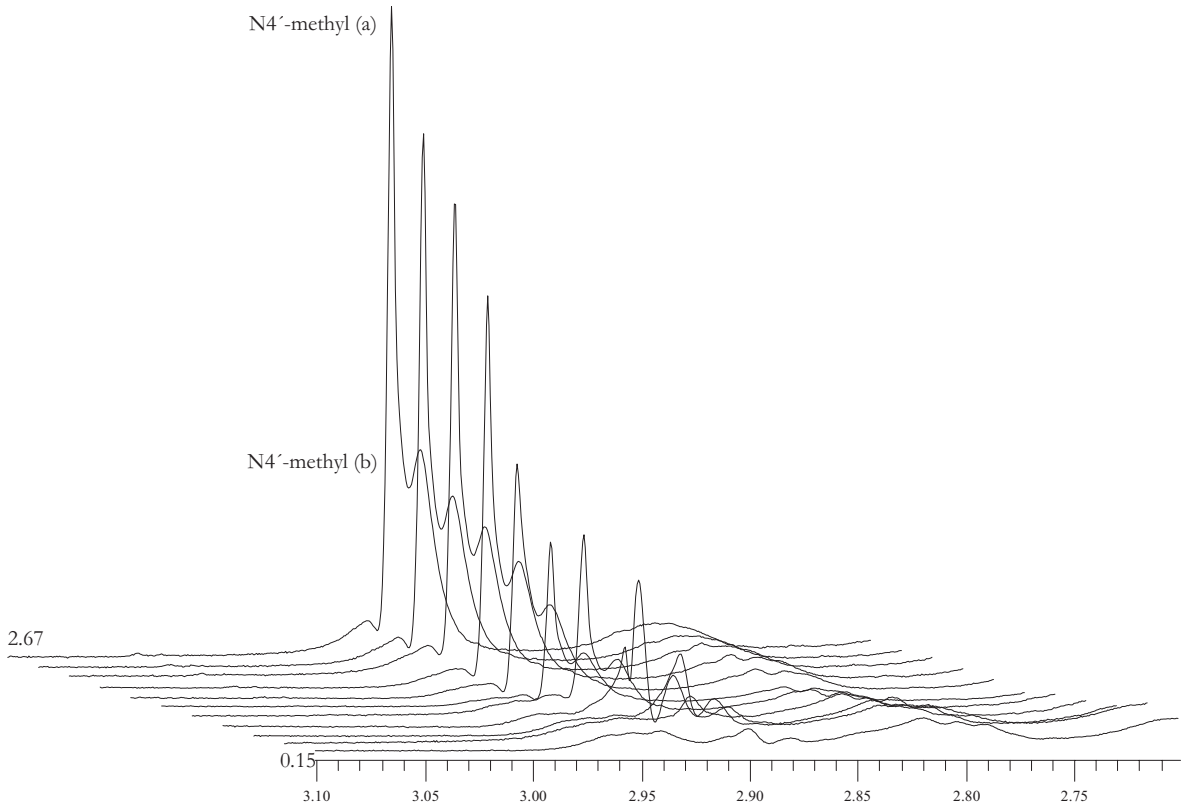

Figure 7.14 The development of the Oflo top at 2.9 ppm through the different concentrations, from 0.07 mM (lower) to 1.05 mM (upper). Oflo:GGCC ratios at first and final spectra are shown.

This method complicated the calculations of the uncertainty of the concentrations as the intensities are read out from the XWinNMR program without any uncertainty given. The uncertainty of ± 0.09 from the stock-solution is used.

The relative development of the peaks was calculated using intensities (*see table 7.8*) and is given in the table below.

Table 7.9 Relative development of the two N4´-methyl signals

Ratio Oflo:GGCC	**% from total (N4´-methyl(b))**
0.15	38.0
0.27	45.1
0.52	50.0
0.77	38.7
1.03	28.7
1.29	28.4
1.56	31.5
1.83	28.8
2.11	29.4
2.39	29.7
2.67	30.1

If the splitting of the N4´-methyl signal arises from interactions with DNA this gives the ratio between interacting and non interacting Oflo. This is further discussed in chapter 8.3.2.

7.3.2 Titration of GGCC with Oflo

7.3.2.1 1D spectra

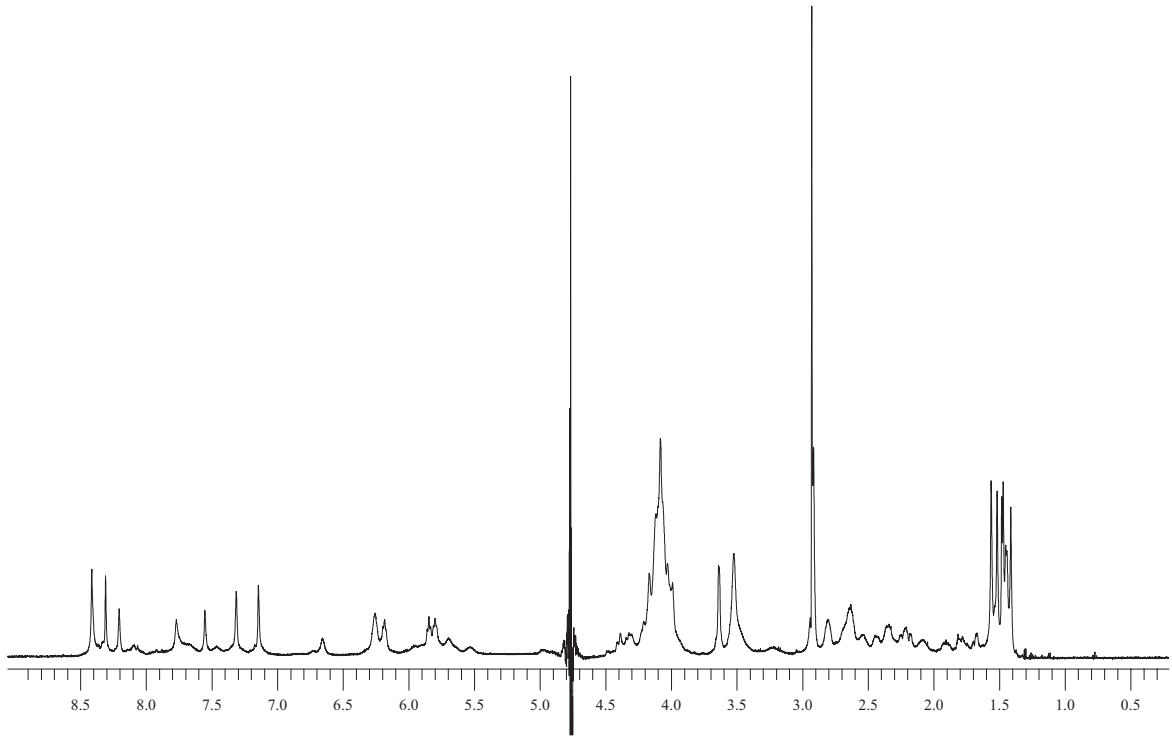

Figure 7.15 The final ^{1}H NMR spectrum in the titration, the ratio Oflo:GGCC is 2.67.

The rest of the 1D ^{1}H NMR spectra is appended.

The development of the peaks may be seen in three different areas; the imino, the aromatic and the 1.0 - 4.5 ppm regions of the proton spectra. The development in the three different regions are shown in figures 7.16 to 7.18.

<u>The imino region:</u>
All imino signals are behaving rather similar. With the exception of T1, which is completely lost at ratio 0.27, all imino signals are decreasing, showing the largest decrease between ratios 0.52 and 0.77. Only signals from T3 and T9 are observable in the last spectrum (ratio 2.67). The G5 signal are lost at ratio 1.56, and the same applies to the G4 signal.

<u>The aromatic region:</u>
There are three things worth noticing in this region. The adenine signals are only slightly changing, showing a decrease in intensity (*especially at A10*) and a broadening of the peaks, but are essentially the same. The Guanine peaks from G4 and G5 are broadening and decreasing, almost vanishing, and already at ratio 0.52 the peaks are almost indistinguishable, with the exception of the

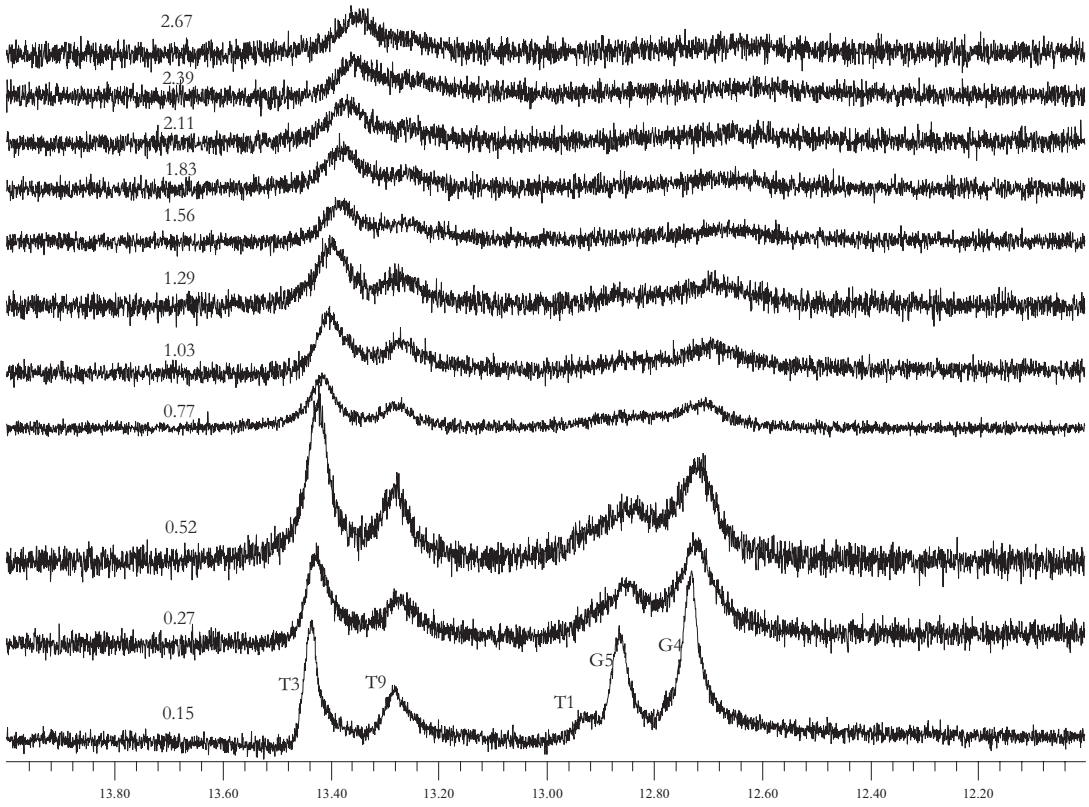

Figure 7.16 The development of the imino proton region in the titration, ranging from ratio Oflo:GGCC 0.15 (lower) to 2.67 (upper). The spectra are placed on top of each other.

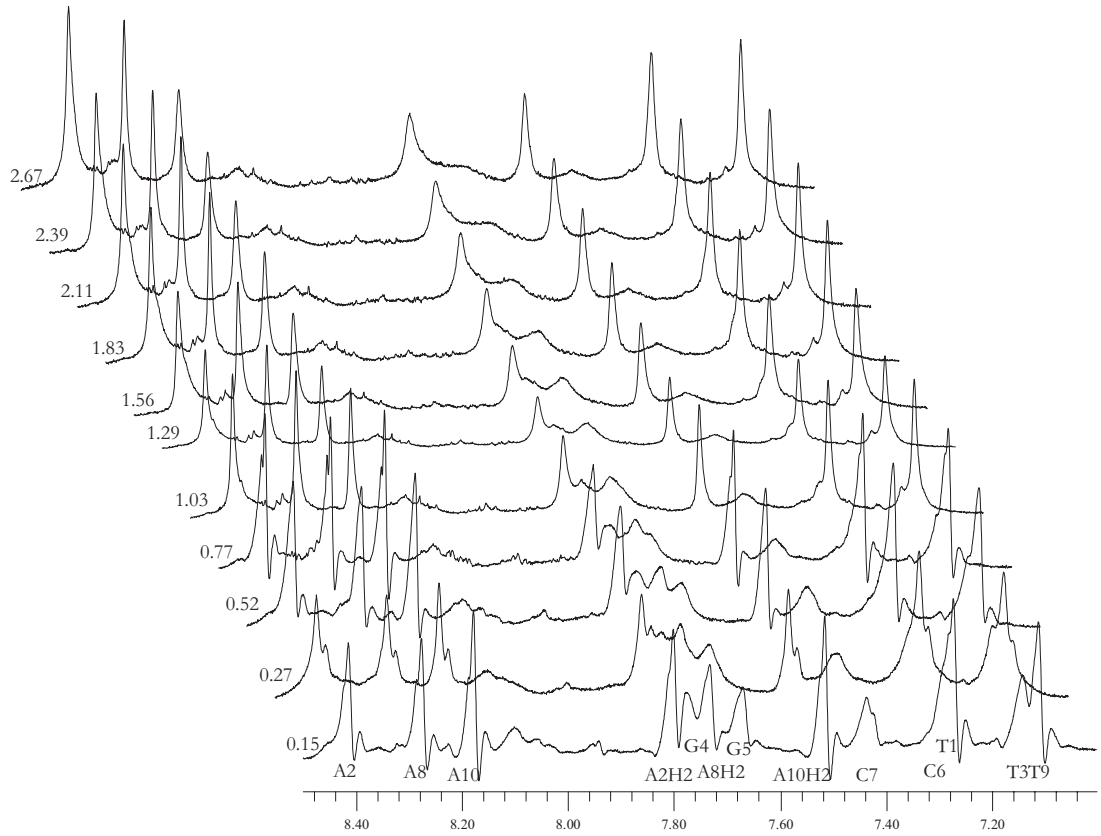

Figure 7.17 The development in the aromatic region in the titration, ranging from ratio Oflo:GGCC 0.15 (lower) to 2.67 (upper)

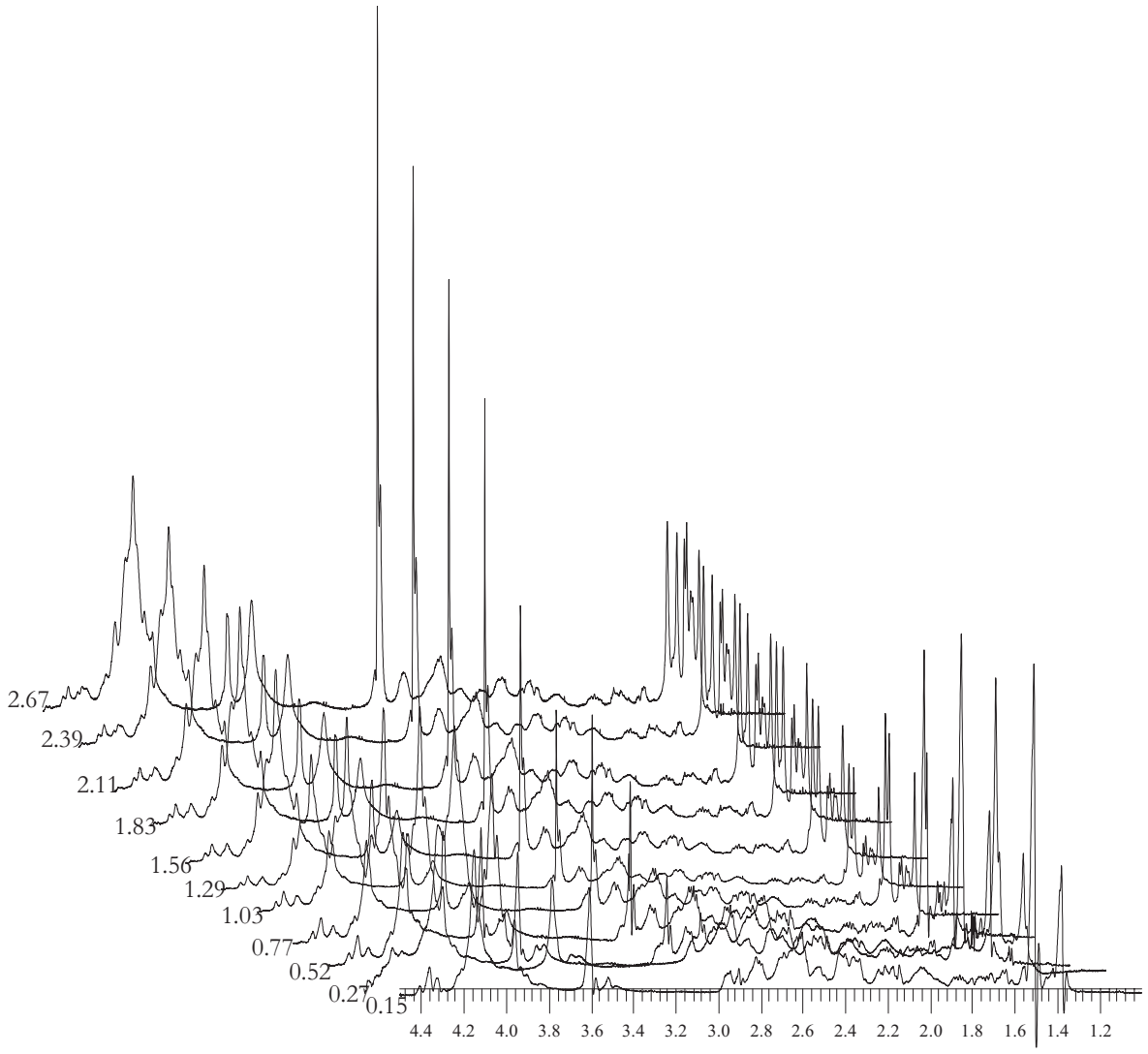

Figure 7.18 The development of the peaks in the 1.0 - 4.5 ppm region in the titration, ranging from ratio Oflo:GGCC 0.15 (lower) to 2.67 (upper)

A2H2 signal. The only signals remaining at the end, although broadened and decreased are the A2H2 and A10H2 signals and the T1 and T9 signals. The T3 signal disappears quickly, probably shifting to the same ppm value as T9.

The 1.0 - 4.5 ppm region:

This region has not been completely assigned and are also more complicated as there is heavy overlap between the peaks. The most distinct changes, however, in this region are increasing signals from the N4´-methyl and 3'/5' protons in Oflo at 2.9 and 3.5 ppm respectively. An interesting feature, although difficult to observe in figure 7.18, are the methyl signals completely separated in the final spectrum giving rise to five different peaks, although only four methyl groups are present to give signals in this area. The intensities of the methyl signals are clearly increasing until ratio 0.77, decreasing at ratios 1.03 and 1.29 and then increasing again. The fifth methyl signal arises from the C3-methyl group in Oflo separating like the N4´-methyl signal, but not in a similar manner.

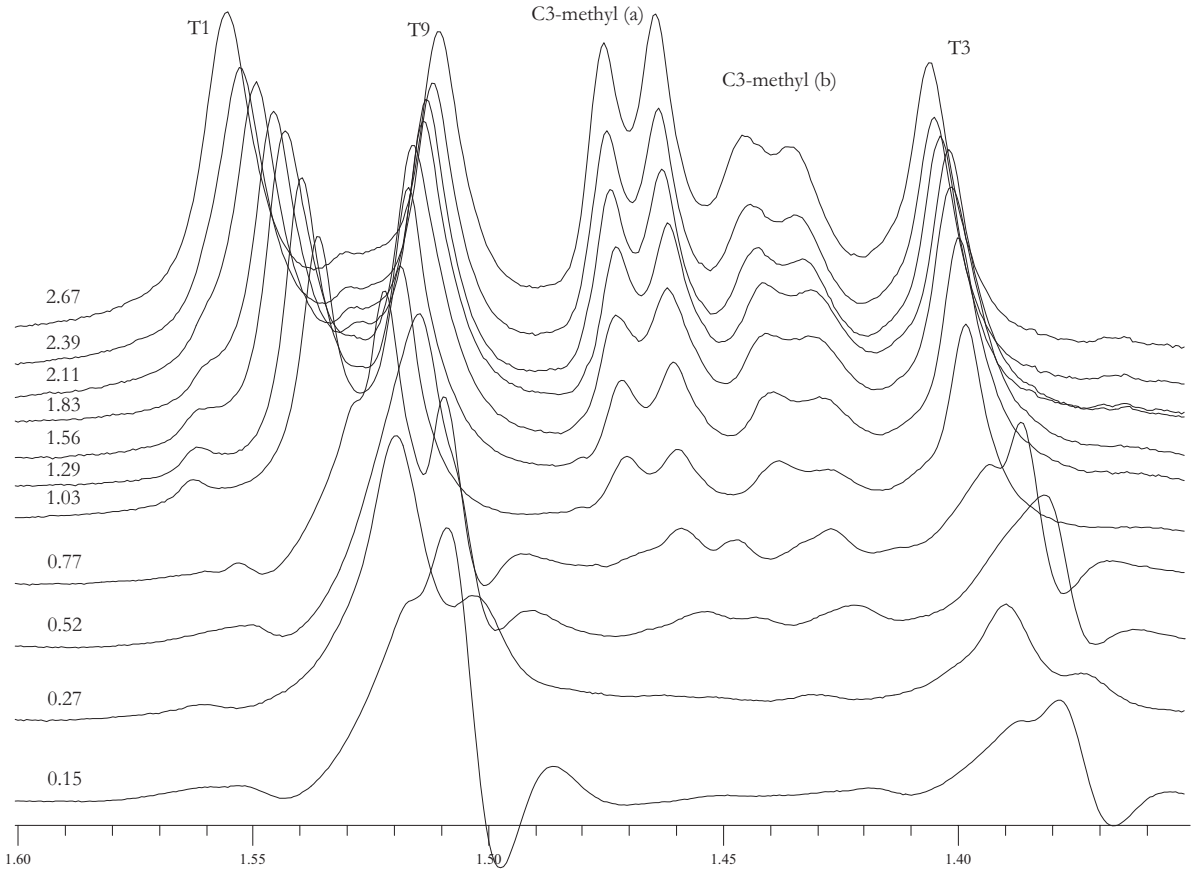

Figure 7.19 The development of the methyl-signals from both GGCC and Oflo. The signals are labelled and the ratio Oflo:GGCC is shown to the left.

The relationship between the peaks has been calculated as with the N4´-methyl group

Table 7.10 The relationship between C3-methyl groups a) and b)

Ratio Oflo:GGCC	**% from total (C3-methyl (b))**
1.03	47.4
1.29	45.7
1.56	45.3
1.83	43.7
2.11	43.2
2.39	42.5
2.67	42.2

The results are based on calculations using the intensities from both peaks in the doublet. It was not possible to separate the two peaks to read out intensities below a Oflo:GGCC ratio of 1.03.

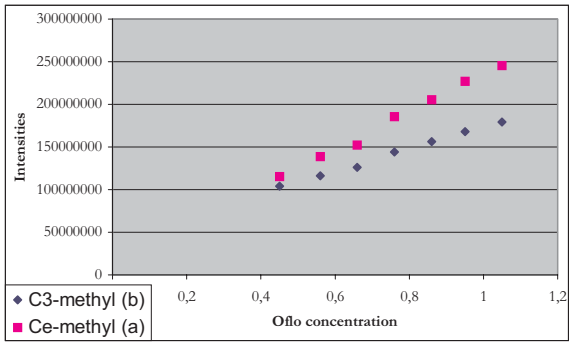

Figure 7.20 Intensities of the two C3-methyl peaks against Oflo concentration

7.3.2.2 NOESY spectra

Unfortunately, no NOESY spectra were recorded during the titration. The only NOESY spectra available are that of pure GGCC and the final sample in the titration series of Oflo and GGCC.

Two regions have been investigated as mentioned in chapter 7.2.3; the H6/H8 - H1' and the H6/H8 - H2'/H2" regions. Chemical shifts in both dimensions for pure GGCC and for the final sample in the Oflo and GGCC titration are summarised in tables 7.11 and 7.12 for comparison.

Table 7.11 Chemical shifts in ppm for crosspeaks for H6/H8 and H1' in the NOESY spectre of both dimensions for pure GGCC and the final sample in the Oflo GGCC titration

Crosspeak between	**Pure GGCC**		**Oflo and GGCC mixture**	
	F2	**F1**	**F2**	**F1**
T1H6 - T1H1'	7.28	5.78	7.30	5.80
A2H8 - T1H1'	--	--	--	--
A2H8 - A2H1'	8.43	6.30	8.41	6.26
T3H6 - A2H1'	7.16	6.30	--	--
T3H6 - T3H1'	7.16	5.69	--	--
G4H8 - T3H1'	7.79	5.69	--	--
G4H8 - G4H1'	7.79	5.67	--	--
G5H8 - G4H1'	7.68	5.67	--	--
G5H8 - G5H1'	7.68	5.85	--	--
C6H6 - G5H1'	7.30	5.85	--	--
C6H6 - C6H1'	7.30	5.88	--	--
C7H6 - C6H1'	7.44	5.88	--	--
C7H6 - C7H1'	7.44	5.49	--	--
A8H8 - C7H1'	8.29	5.49	8.30	5.53
A8H8 - A8H1'	8.29	6.21	8.30	6.18
T9H6 - A8H1'	7.12	6.21	7.14	6.17
T9H6 - T9H1'	7.12	5.83	7.17	5.84
A10H8 - T9H1'	--	--	--	--
A10H8 - A10H1'	8.19	6.26	8.20	6.24

-- means the crosspeak are missing in the NOESY spectrum

Crosspeaks between the two pairs at both ends are missing from the NOESY spectrum of pure GGCC, otherwise all crosspeaks are accounted for. In the Oflo GGCC mixture most crosspeaks between the base pairs are missing with the exception of the crosspeaks between C6 and C7 and between A8 and T9. All the internal crosspeaks between H6/H8 and H1' in the bases and their respective sugars are observable, with a possible exception of the crosspeak between G5H8 and G5H1'.

Although some of the peaks are weak and broad, they are found symmetrically across the diagonal and thereby confirmed. Their positions are in good coherence with expected positions in the spectra. In figures 7.17 and 7.18 low resolution are used and some of the crosspeaks may not appear but this does not imply that they are not present.

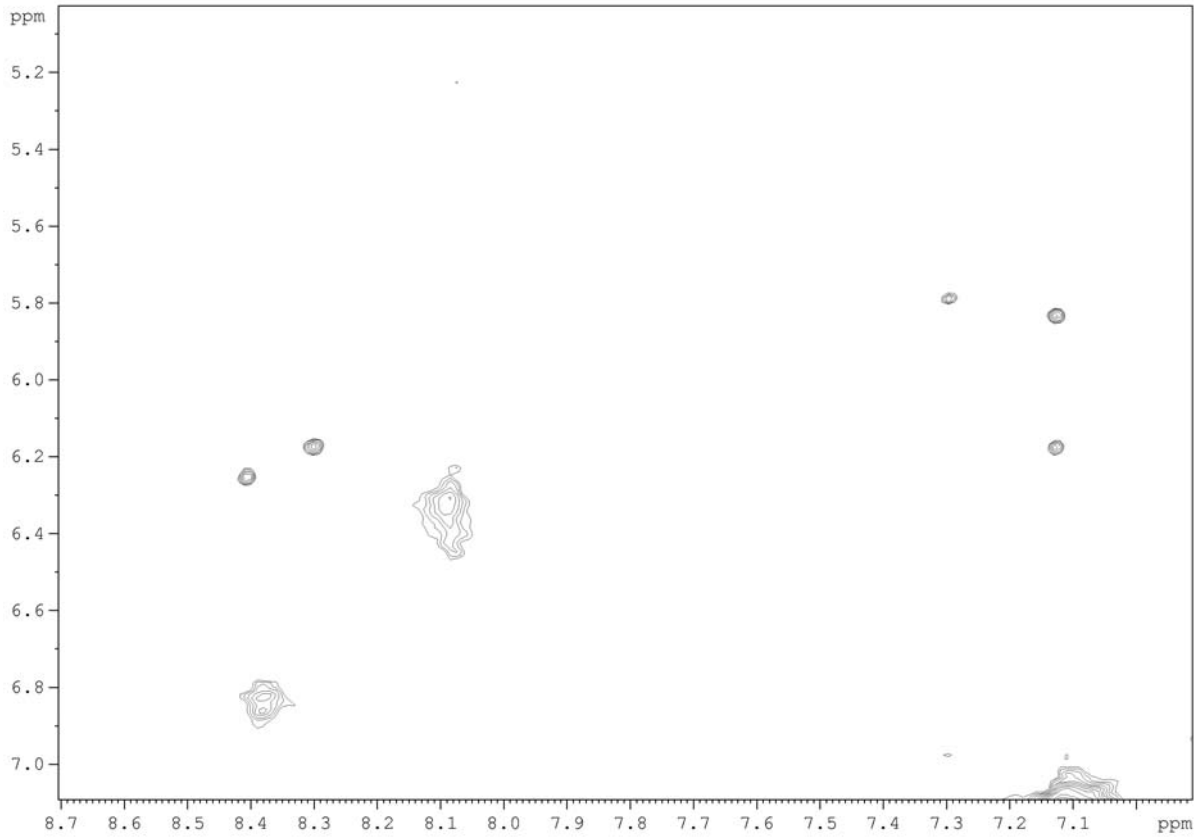

Figure 7.21 Expansion of the H6/h8-H1' region of the NOESY spectrum of the Oflo-GGCC mixture

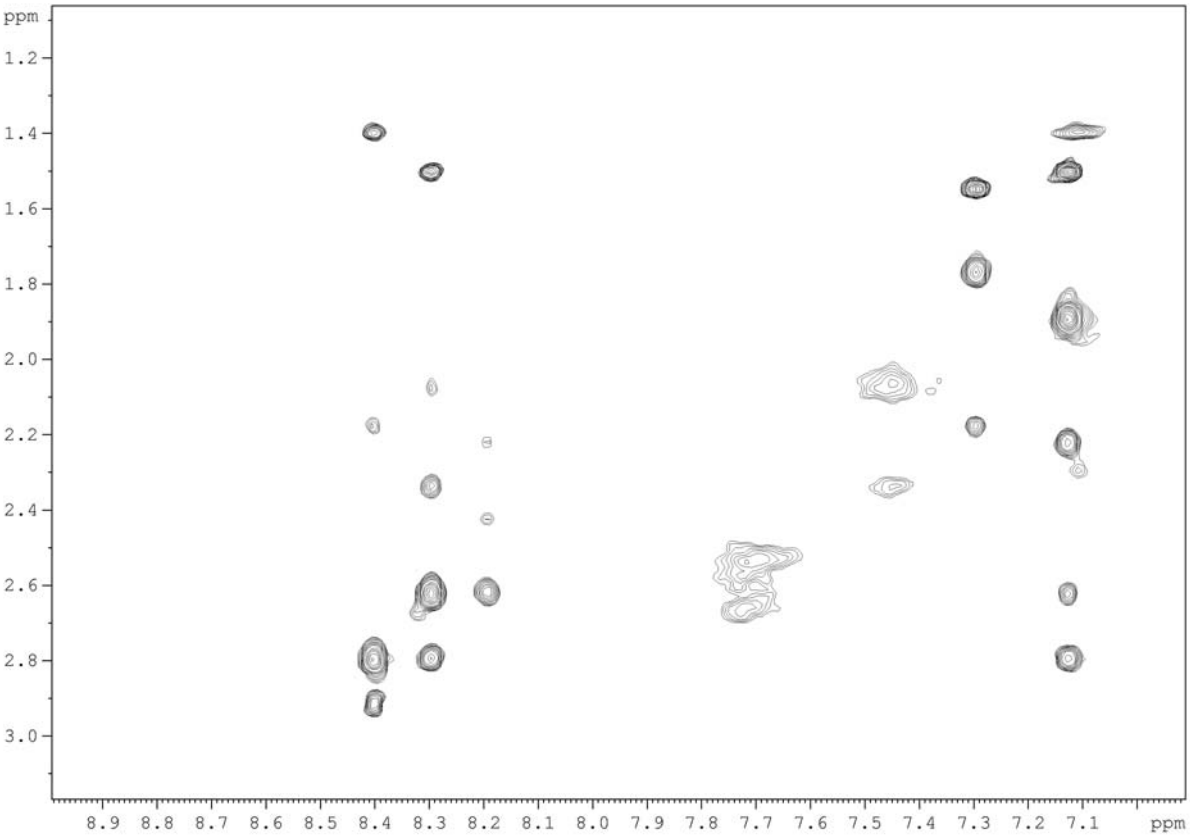

Figure 7.22 Expansion of the H6/H8-H2'/H2" region of the NOESY spectrum of the Oflo-GGCC mixture

Table 7.12 Chemical shifts in ppm for crosspeaks resulting from H6/H8 and H2'/H2" in the NOESY spectra of both dimensions for pure GGCC and the final sample in the Oflo-GGCC titration

Crosspeaks between	**Pure GGCC**		**Oflo-GGCC mixture**	
	F2	**F1**	**F2**	**F1**
T1H6 - T1H2'	7.28	1.74	7.31	1.77
T1H6 - T1H2"	7.28	2.16	7.31	2.18
A2H8 - T1H2'	8.43	1.75	8.41	1.77
A2H8 - T1H2"	8.43	2.16	8.41	2.18
A2H8 - A2H2'	8.43	2.84	8.41	2.80
A2H8 - A2H2"	8.43	2.96	8.41	2.92
T3H6 - A2H2'	7.16	2.84	(7.11)	(2.80)
T3H6 - A2H2"	7.16	2.96	(7.11)	(2.94)
T3H6 - T3H2'	7.16	1.98	(7.11)	(2.01)
T3H6 - T3H2"	7.16	2.37	(7.11)	(2.30)
G4H8 - T3H2'	7.79	1.98		
G4H8 - T3H2"	7.79	2.37		
G4H8 - G4H2'	7.79	2.63		
G4H8 - G4H2"	7.79	2.71		
G5H8 - G4H2'	7.68	2.61		
G5H8 - G4H2"	7.68	2.71		
G5H8 - G5H2'	7.68	2.53		
G5H8 - G5H2"	7.68	2.66		
C6H6 - G5H2'	7.30	2.53		
C6H6 - G5H2"	7.30	2.67		
C6H6 - C6H2'	7.30	2.06		
C6H6 - C6H2"	7.30	2.43		
C7H6 - C6H2'	7.44	2.06		
C7H6 - C6H2"	7.44	2.43		
C7H6 - C7H2'	7.44	2.03	(7.46)	(2.07)
C7H6 - C7H2"	7.44	2.35	(7.46)	(2.34)
A8H8 - C7H2'	8.29	2.03	8.30	2.07
A8H8 - C7H2"	8.29	2.35	8.30	2.34
A8H8 - A8H2'	8.29	2.62	8.30	2.62
A8H8 - A8H2"	8.29	2.81	8.30	2.80
T9H6 - A8H2'	7.12	2.62	7.14	2.62
T9H6 - A8H2"	7.12	2.81	7.14	2.80
T9H6 - T9H2'	7.12	1.87	7.14	1.90
T9H6 - T9H2"	7.12	2.23	7.14	2.22
A10H8 - T9H2'	8.19	1.87	8.20	1.90
A10H8 - T9H2"	8.19	2.23	8.20	2.22
A10H8 - A10H2'	8.19	2.62	8.20	2.62
A10H8 - A10H2"	8.19	2.43	8.20	2.43

( ) indicates weak signals which are confirmed from the symmetric side of the diagonal.

As the table shows, there is a big gap of missing peaks from G4H8 and the T3 sugar ring and all the way down to C7H6 and the C6 sugar ring. There are still crosspeaks in this region, but they

are difficult to assign. It appears that the guanine signals are broadened and overlapping. The broadened signals from the Guanines are observable, but are impossible to assign to G4, G5 or both, they are therefore not included in the table.

Table 7.13 Assignment table for pure GGCC indicating drift in the chemical shifts as Oflo is applied

	CH3	**H1'**	**H2'**	**H2"**	**H6**	**H8**	**NH**	**NH2b**	**NH2f**
T1	1.52	5.78	1.75	2.16	7.28		no		
Delta	*0.03*	*0.02*	*0.02*	*0.02*	*0.03*		*no*		
A2		6.30	2.84	2.96		8.43			
Delta		*-0.04*	*-0.04*	*-0.04*		*-0.02*			
T3	1.39	5.68	1.98	2.37	7.16		13.46		
Delta	*0.02*	*no*	*0.03*	*-0.07*	*-0.05*		*no*		
G4		5.67	2.63	2.71		7.79	12.75		
Delta		*no*	*nr*	*nr*		*nr*	*no*		
G5		5.85	2.53	2.66		7.68	12.89		
Delta		*no*	*nr*	*nr*		*nr*	*no*		
C6		5.88	2.06	2.43	7.30			8.11	6.26
Delta		*no*	*no*	*no*	*no*			--	--
C7		5.50	2.03	2.35	7.44			8.46	6.75
Delta		*no*	*0.04*	*-0.01*	*0.02*			--	--
A8		6.21	2.61	2.81		8.29			
Delta		*-0.03*	*0.01*	*-0.01*		*0.01*			
T9	1.52	5.84	1.87	2.23	7.12		no		
Delta	*-0.01*	*0.00*	*0.03*	*-0.01*	*0.02*		*no*		
A10		6.26	2.62	2.43		8.19			
Delta		*-0.02*	*0.00*	*0.00*		*0.01*			

no means not observed, and nr observed, but not reliable to assign

7.4 Association constants

From the diffusion constants found earlier the association constants may be calculated. GGCC and Oflo diffusion constants are as good as constant, being 1.34 * 10^{-10} and 4.36 * 10^{-10} m^2s^{-1} respectively. Table 7.6 gives the information required to calculate association constants. Calculation of association from diffusion constants is given in chapter 5.5.2

Table 7.14 Information for calculating the association constants using the N4´-methyl signal

Conc. Oflo (mM)	**Conc. GGCC (mM)**	**Diff.Oflo(*$10^{-10}m^2s^{-1}$)**	**% interacting Oflo**
0.07	0.48	2.64	57.2
0.13	0.47	2.78	52.4
0.24	0.46	3.26	36.8
0.35	0.45	3.22	38.1
0.45	0.44	3.31	35.1
0.56	0.43	3.38	32.7
0.67	0.42	3.53	27.8
0.77	0.42	3.42	31.5
0.86	0.41	3.41	32.0
0.95	0.40	3.44	30.8
1.05	0.39	3.51	28.6

The diffusion constants were calculated using the N4´-methyl signal, as this was the only Oflo peak available at all titrations. The peaks at 3.5 ppm and 8.4 ppm were relatively weak and resulted in diffusion constants quite similar to pure GGCC (results not shown).

The fact that only the N4´-methyl signal at 2.9 ppm could be used to calculate diffusion constants complicated the calculations, as this peak is splitted. The largest signal from the N4´-methyl group was used to calculate the diffusion constant.

The association constants were calculated as follows:
- The diffusion constants of the largest N4´-methyl peak were calculated.
- Percentage interacting Oflo was calculated from the diffusion constant.
- Percentage interacting Oflo was adjusted since the peak used to calculate the diffusion constant is not representing all Oflo in the solution.

To illustrate the calculations: In the 0.15 ratio Oflo:GGCC 57.2% Oflo is calculated to interact with GGCC. But the peak investigated is only representing 62% of the Oflo present. The remaining signal from Oflo is imbedded in the second peak, which is already assumed to interact. This gives a corrected percentage interacting Oflo from the diffusion constant of 35.5% and a total of 73.5% Oflo interacting with GGCC.

Association constants were also calculated using the percentage development of the small N4´-methyl signal and the C3-methyl (b) signal.

Table 7.15 Association constants calculated using the development of the N4´-methyl signal

Ratio Oflo:GGCC	**% from N4´-methyl (a)**	**K_a from N4´-methyl (a)**	**% from N4´-methyl (b)**	**K_a from N4´-methyl (b)**
0.15	35.5	$1.21 * 10^{03}$	38.0	$1.35 * 10^{03}$
0.27	28.8	$9.35 * 10^{02}$	45.1	$2.00 * 10^{03}$
0.52	18.4	$5.42 * 10^{02}$	50.0	$2.94 * 10^{03}$
0.77	23.4	$8.30 * 10^{02}$	38.7	$2.01 * 10^{03}$
1.03	25.0	$1.02 * 10^{03}$	28.7	$1.29 * 10^{03}$
1.29	23.4	$1.02 * 10^{03}$	28.4	$1.46 * 10^{03}$
1.56	19.0	$7.96 * 10^{02}$	31.5	$2.17 * 10^{03}$
1.83	22.4	$1.16 * 10^{03}$	28.8	$2.01 * 10^{03}$
2.11	22.6	$1.35 * 10^{03}$	29.4	$2.65 * 10^{03}$
2.39	21.7	$1.43 * 10^{03}$	29.7	$3.58 * 10^{03}$
2.67	20.0	$1.39 * 10^{03}$	30.1	$5.82 * 10^{03}$

Table 7.16 Association constants calculated using the development of the C3-methyl signal

Ratio Oflo:GGCC	**% from C3-methyl (b)**	**K_a from C3-methyl (b)**
1.03	47.4	$3.98 * 10^{03}$
1.29	45.7	$4.83 * 10^{03}$
1.56	45.3	$6.84 * 10^{03}$
1.83	43.7	$8.83 * 10^{03}$
2.11	43.2	$1.98 * 10^{04}$
2.39	42.5	$1.97 * 10^{05}$
2.67	42.2	$1.37 * 10^{04}$

The N4´-methyl signal indicates at least two different interacting modes, one that causes the difference in chemical shift and others measured from the diffusion constant. This gives the total percentage interacting Oflo.

Table 7.17 Total percentage interacting Oflo calculated from the N4´-methyl signal

Ratio Oflo:GGCC	**Total percentage Oflo interacting**
0.15	73.5
0.27	73.9
0.52	68.4
0.77	62.1
1.03	53.7
1.29	51.8
1.56	50.5
1.83	51.2
2.11	52.0
2.39	51.4
2.67	50.1

The percentage Oflo interacting and the K_a values can be presented as plots against the Oflo:GGCC ratio as illustrated in the following figures.

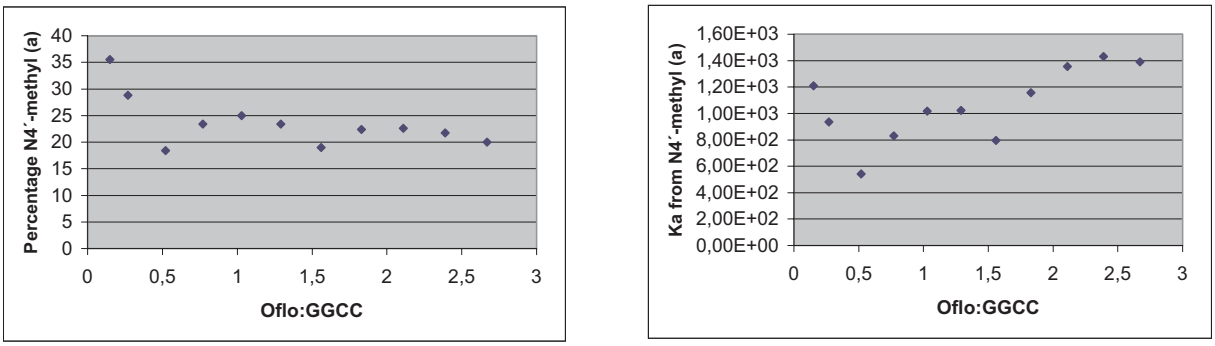

Figure 7.23 Percentage interacting Oflo and K_a plotted against the Oflo:GGCC ratio as calculated using the N4´-methyl (a) signal in Oflo

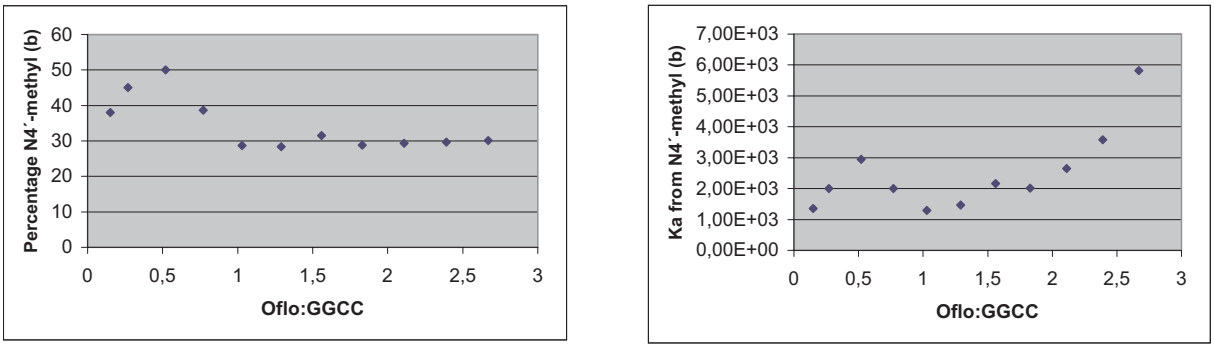

Figure 7.24 Percentage interacting Oflo and K_a plotted against the Oflo:GGCC ratio as calculated using the N4´-methyl (b) signal in Oflo

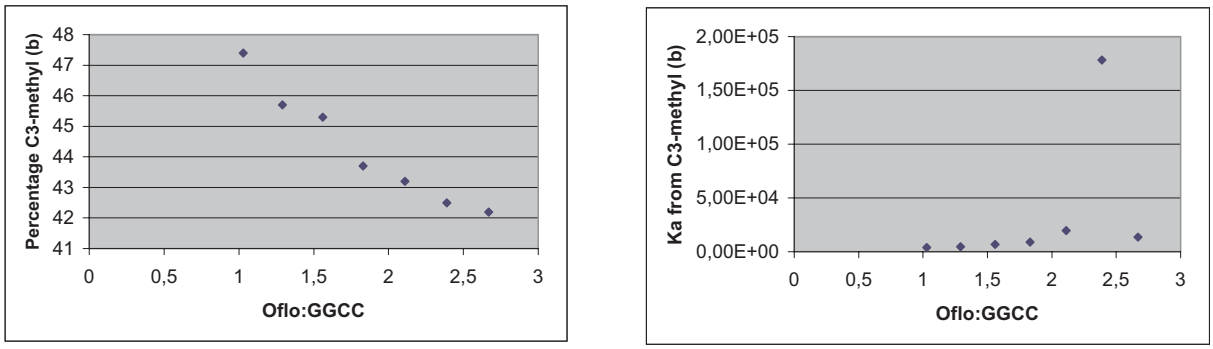

Figure 7.25 Percentage interacting Oflo and K_a plotted against the Oflo:GGCC ratio as calculated using the signal from the C3-methyl group in Oflo

8. Discussion

8.1 Ofloxacin (Oflo)

8.1.1 Assignment of ^{1}H NMR spectrum of Oflo

The assignment of the NMR spectrum of Oflo is relatively straight forward in most regions, but the 2´/6´ and 3´/5´ protons are complicated to separate. No spectra were recorded enabling the separation of the two groups. Mucci et al.[11] previously published an article investigating the structural properties of Oflo using different NMR techniques. They reported the 3´/5´ protons to give signals at 2.54 ppm and two sets of signals resulting from 2´/6´ protons at 3.39 and 3.44 ppm (spectrum obtained at 300 and 340K using DMSO-d6 as solvent, pH not indicated). They proposed that the 2´/6´ protons are closer to the aromatic ring system and hence had a deshielding effect resulting in a downfield signal compared to the 3´/5´ protons. This reasoning would lead to the conclusion that the 2´/6´ protons results in the signal at 3.55 ppm in figure 7.1. However, it is not probable that 3´/5´ is the signal at coalescence, since the reason for split in the signal must be either hindering of ring rotation or ring inversion. The difference in chemical environment leading to splitting is likely to occur at 2´/6´, as these protons are positioned near the sites where the change is likely to occur. Mucci et al. also reported splitting of the 2´/6´ signal at 300K and there is obvious coalescence at ~3.3 ppm in figure 7.1. From this it can be concluded that the suggested assignment of the ^{1}H NMR spectrum of Oflo is correct.

In addition Oflo contains exchangeable protons at the carboxyl group and at N4´. These protons are not observable in the proton specrum as they exchange too fast on the NMR time scale.
It is not possible to separate the H2a and H2b protons, but their vicinal coupling to H3 give information about the conformation of the benzoxacine ring. The C3-methyl group can either be positioned in a pseudo equatorial or a pseudo axial manner. The two possible conformations will give approximately the dihedral angles given below.

Table 8.1 Expected coupling constants at different possible dihedral angles between H2a/H2b and H3

C3 conformation	H2a - H3	Expected J^3	H2b - H3	Expected J^3
C3 p-e	~180^o	~9 - 16 Hz	~60^o	~ 1 - 5 Hz
C3 p-a	~60^o	~1 - 5 Hz	~60^o	~ 1 - 5 Hz

p-e means pseudo equatorial and p-a pseudo axial, the proton positioned upwards is labelled H2a. All angles are approximations as the conformation never will be completely locked.

The coupling constants are very low (2.4 and 1.7 Hz), the conclusion must therefore be that the C3-methyl group are positioned in a pseudo axial manner, as angles near 180 degrees result in hig-

her coupling constants according to the Karplus equations. Mucci et al. found similar low coupling constants but arrived at the opposite conclusion. They stated that the low coupling constants are typical for an axial-equatorial/equatorial-equatorial arrangement and argued that all the spectroscopic data reported agreed with the assignment of a pseudo equatorial arrangement of the C3-methyl group. It is unclear why they arrive at this conclusion as they do not mention Karplus or even discuss the dihedral angles further.

8.1.2 Dynamics of the methylpiperazine ring

There is obvious coalescence at ~3.3 ppm in figure 7.1. The development of this signal over a temperature range can be seen in figure 7.2.

Ciprofloxacin (Cipro) has been investigated by T. Skauge [3]. The structure of Cipro resembles that of Oflo, but a piperazine ring replaces the methylpiperazine, a cyclopropyl as R1 and a hydrogen attached to the carbon postitoned at X8 replaces the benzoxacine group using the nomenclature in figure 3.1 a). The ^{1}H NMR spectrum of Cipro exhibits two identical signals from the 3´/5´ and 2´/6´ protons with no coalescence neither at elevated nor decreased temperatures, leading to the conclusion that the properties of O1 and/or the methyl group on piperazine are vital (*some of this information arise from personal communication with Skauge, and not the referenced thesis*).

The distance between the two signals from the 2´/6´ protons at 271 K is almost the same as at 283 K and it is reasonable to assume that the minimum temperature is found. At high temperatures equal signals from the 2´/6´ and 3´/5´ protons are expected, as seen in Cipro. This is not achieved at 330 K, the highest temperature obtained, indicating that the high temperature limit is not found. Acquirement of spectra at higher temperatures was attempted, but failed due to loss of lock signal and long periods of waiting for the instrument to heat up. The high temperature limit is vital in calculations of the rate constants and thus, these rate constants must be considered uncertain. The results are, however, close enough to be advisory, as calculations of dynamics of this kind contain a high degree of uncertainty anyway. More scans are required to achieve accurate results. The 2´/6´ and 3´/5´ protons are expected to couple, so the equation used to calculate k_c is strictly not valid as it only applies to systems not coupled to each other. Still it is supposed to give a relatively good approximation.

The coalescence may actually arise from either hindering of ring rotation, hindering of ring inversion or slow ring inversion or perhaps a combination of these.

Although the delta H, delta S, delta G and Ea given are highly uncertain, they might tell something about the system. Large, positive delta S values are consistent with less ordered transition states, like ligand dissociation or bond breaking. Delta S is positive and relatively high, indicating that the coalescence is due to bonding. Hydrogen bonding could be expected as both oxygen and fluorine are electronegative hydrogen binders.

Delta G for ring inversion of N-methylpiperazine is reported to be 52 kJ/mol in gaseous conditions not expected to vary much in solution[33]. The coherence temperature was ~250K in the reference, but a lower field (499.92MHz) was used, and the higher the observing frequency, the higher the coalescence temperature. Oflo has a boat-chair inversion when inversion is hindered in the C2´/C6´ and the inversion investigated is a chair-chair inversion. Boat-chair inversion is expected to be less favourable giving higher delta H and delta G. This is in coherence with the results in this thesis. Thus delta G for hindering of rotation is not known and hindering of rotation can therefore not be excluded on this ground. On the other hand, delta H is reported to be 51.9 kJ/mol, almost half of the delta H found here. This may be consistent with a boat-chair inversion.

Considering that the boat-chair inversion is less probable than a chair-chair inversion, boat-chair inversion is only likely if the 2´/6´ hydrogens are directly involved in the hydrogen bonds expected in fluorine and oxygen. This is not expected as the 2´ and 6´ protons are attached to carbons. Also, if one considers the scalar couplings to the 3´/5´ peak there seems to be equal couplings above coalescence and two different couplings after coalescence. This is consistent with the 2´ and the 6´ protons having different chemical environments below coalescence, indicating hindering of rotation.

From this it seems that the coalescence arises from a hindering of the rotation of the methylpiperazine ring, but no certain conclusion can be made without further investigations.

A ^{1}H NMR spectrum of Oflo with pH 4.92 was also acquired (*see appendix A*). This spectrum was acquired at 293.9K (*actual temperature*), but it seems clearly below coalescence. Integration of the peaks shows that the quartet at 3.3 ppm contains two protons and the whole group of peaks ranging from 3.55 to 3.70 ppm contains six protons.
The splitting of the peaks in this spectrum can be explained as follows:
The quartet at 3.30 ppm arises from 3´/5´ protons. There is fast inversion in C3´ and C5´ and the two 3´/5´ protons are identical. There is no fast inversion in C2´ and C6´ making the 2´/6´ different. The 3´/5´ protons are therefore splitted from the two different 2´/6´protons and from the proton now situated at N4´ leading to a quartet. There are in fact two quartets, but the other is more difficult to observe. The 2´/6´ protons have a geminal coupling and are therefore splitted in a dublet. The 3´/5´ protons split this doublet once more in a doublet. The easiest of these two dublets to observe is the one most downfield.
This indicates two things: The assignment of the 2´/6´proton and 3´/5´ proton signals is not correct and the 3´/5´ proton signals are splitted as a result of slow inversion. No findings in the 6.99 pH spectra support this. The splitting pattern in the spectra acquired with pH 6.99 is better explained if the triplet arises from 3´/5´ protons splitted from the different 2´/6´ protons. Clearly further investigations are needed. 2D spectra acquired at lowered temperatures can reveal whether the two peaks at 3.00 ppm and 3.30 ppm couple to one or two carbons. If the peaks couple to only one carbon the coalescence must arise from hindering of rotation and if they couple to two

carbons the coalescence must arise from inversion.

8.1.3 Stacking measurements

Two or more Oflo molecules stacking together are expected to move much slower in the solution than one molecule alone resulting in a considerable decrease in the diffusion constant.The diffusion constants in table 7.4 lead to the conclusion that Oflo is not stacking in the concentration range 1 - 6 mM, i.e. there is no change in the stacking conditions. Conclusions cannot be drawn on whether stacking occurs at lower concentrations. Unfortunately no measurements at lower concentrations were performed. This should be conducted to confirm the results in this thesis, especially since the self-diffusion constant of Oflo is used to calculate the association constants.

Lecomte et al.[34] investigated Pefloxacin, a fluoroquinolone with structure similar to Oflo, but the benzoxacine ring is replaced by an ethyl-group as R1 using the nomenclature in figure 3.1 a). They concluded that Pefloxacin is monomeric at 10^{-4} mol L^{-1} (*pH 7.4*) and the stacking was highly dependent on pH. From figure 7.4 it appears that the diffusion constant is lowered above pH 7, which could be explained by the high dependency on pH. Diffusion measurements at different pH is out of the scope of this thesis and since only one of the samples used has a pH higher than 7 it is impossible to investigate this aspect. Experiments focusing on stacking conditions at different pH should therefore be performed at a later stage.

From figure 7.4 it appears that the diffusion constant is dependent on concentration in the 1 - 6 mM range. No conclusions can be drawn on whether this applies to the concentration levels used to titrate GGCC. The dependency is small however, considering the uncertainty is calculated to be $\pm$ 0.06 m^2/s. The diffusion constants calculated in this thesis are regarded independent of concentration within the limits of the titration. Oflo is also regarded as monomeric in the stacking measurements. No association constants could be calculated without these assumptions.

8.2 The DNA-oligomer GGCC

8.2.1 Assignment of the NMR spectra of GGCC

This assignment is based on a previous assignment performed by Vinje et al. and parts of it have been published[32]. The coherence between the NOESY spectra obtained in this thesis and in the reference is substatial, leading to the conclusion that the GGCC oligomer is in fact in the duplex state and has a normal B-DNA geometry. The appearence of imino peaks in the 1D spectrum and imino crosspeaks in the NOESY spectrum supports the assumption of a double helix state. The magnitude of the NOESY crosspeaks indicates B-DNA geometry.

Crosspeaks between A10 and T9 and between T1 and A2 are missing in the NOESY spectrum (*figure 7.9*). This comes as no surprise as they are the base pairs positioned at the ends of the oligomer. adenine-thymine pairs at the ends often give open ends as they only exhibit two hydrogen bonds.

It is apparent from the aromatic region that paramagnetic impurities are present (*figure 7.6*). Paramagnetic impurities especially bind to GC base pairs and the G4 and G5 signals are clearly broadened and damped. This could be expected as purification of paramagnetic impurities was not conducted. It was however at the time not considered to have any impact on the final results. The oligomer is rather large compared to any impurities. The diffusion constant is therefore not expected to differ and diffusion constants can be measured using any single resonance signal from the spectrum rendering the G or C signals disposable for diffusion measurements. The paramagnetic impurities may have had an impact on the interaction between Oflo and GGCC. This is further discussed in chapter 8.5

The pH of the sample was not measured. A phosphate buffer was used, but no measurements were performed to secure that enough buffer was applied. The final pH of the sample at end of the titration was 6.54. Given that the pH of the stock-solution Oflo was 6.99 and a total of 110 microL of this sample was impeded in the GGCC sample (*450 microL initial volum*), this predicts a starting pH somewhere above 6, which should be sufficient. Thus, pH is not expected to affect the results.

8.2.2 Measurements of the self-diffusion constant of GGCC

The diffusion part of the XWinNMR program does not take into account tau when bipolar pulses are used, complicating the calculations and they must therefore be conducted manually. The calculations are performed using the same data as XWinNMR, the uncertainty is thus not affected.

The sample with the lowest concentration of GGCC results in a poor Simfit plot (*see Appendix A*). Even so, the diffusion constant is only $0.023 * 10^{-10}$ higher than the diffusion constant obtained for pure GGCC. The uncertainty of the self-diffusion constants will be high in this concentrati-

on range as the signals are weak. Acquiring more scans could have improved this. All measurements were acquired using the same number of scans. Not changing the number of scans made the experimental time shorter, but it also gave information on what concentration range the diffusion constants may be acquired at approximately without too high uncertainty. The borderline of certain results appears to be precisely at the concentration levels used in this thesis. This should apply to all diffusion constant measurements.

From the small deviations in the diffusion constant of GGCC in the titration series it is clear that the diffusion constant of GGCC can be taken as constant. This was expected, as diffusion constants are more influenced by molecular size and geometry than structure. Without this assumption it would not be possible to calculate the association constants from the diffusion constants.

The diffusion constant calculated is in coherence with previously calculated self-diffusion constants for DNA[30, 35] and supports the suggested double helix conformation of the oligomer.

8.3 Oflo and GGCC titration

8.3.1 Oflo concentration

Calculations of initial concentration of Oflo in the GGCC sample increase the uncertainty. Precise calculations of how much it should be increased are impossible, the uncertainty of ± 0.09 mM from the stock-solution is therefore kept. The Oflo sample of concentration 0.07 mM falls within the uncertainty of 0.09 mM and is considered not dependable.

The point at (0.66 , 311314224) is removed from all the plots, as this point was clearly deviating from the regression line.

The splitting of the N4´-methyl signal from Oflo was not expected. There are at least two possible explanations; it could either result from Oflo interacting with GGCC or it could result from an additional proton at N4´. The N4´ nitrogen is protonated at lowered pH. This proton may not appear in the ^{1}H spectrum but is expected to split the methyl signal. The pKa_1 value for Oflo is 6.02. The N4´-methyl (b) signal is strong and increasing. Since pH of the sample increases as Oflo stock-solution is added, the protonation of N4´ should decrease. Splitting of the N4´-methyl signal resulting from protonation of N4´ is expected to give two signals with equal intensity while the two signals observed clearly has different intensities and even different development of the intensities as Oflo is imbedded in the GGCC solution. A spectrum of Oflo acquired at lowered pH confirms this (*see appendix A*). Even at pH 4.92 the N4´-methyl signal is not splitted, i.e. the splitting is unobservable. One can therefore conclude that the two signals must arise from interactions between Oflo and GGCC.

Given the conclusion that the N4´-methyl signal is splitted from interactions between Oflo and GGCC, the development of the two peaks are worth investigating. From the plots in figure 7.13 it can be seen that the two signals develop differently. The N4´-methyl (a) signal is growing slowly in the first three spectra and then more rapidly. This growth from the fourth spectrum appears to slow down in the four last spectra. The N4´-methyl (b) signal behave quite differently. In the first three spectra the intensities increase rapidly, then flattens out and then in the last five spectra increase again. From investigations of the ^{1}H NMR spectra one conclude that intercalation of Oflo in to GGCC is taking place at ratios Oflo:GGCC higher than 1 (*see chapter 8.3.2*). The N4´-methyl signal is distinctly splitted already at Oflo:GGCC ratio 0.15, so other binding modes than intercalation are bound to be present. The splitting of the N4´-methyl signal is thus expected to result from either minor/major groove binding or surface binding.

One question still remains; which of the two signals from N4´-methyl results from the interaction and which represents non-interacting Oflo?

Diffusion measurements performed on the N4´-methyl (a) signal indicated that some, but not all

N4´-methyl groups giving rise to this signal are involved in some sort of interactions. If all were involved the diffusion constant would be equal to that of pure GGCC and if non were involved it would be equal to that of pure Oflo. Diffusion measurements were attempted on the N4´-methyl (b) signal, but the uncertainty of the results is high due to the low intensities and the overlap between the two N4´-methyl peaks and only the three last spectra in the titration could be measured. The diffusion constant measured from the N4´-methyl (b) signal appears to result in a diffusion constant similar to pure GGCC (*results not shown*). The diffusion constants from N4´-methyl (b) are highly uncertain and not dependable, but together with the diffusion measurements from the N4´-methyl (a) displaying a diffusion constant not similar to neither pure Oflo nor pure GGCC, leads to the conclusion that the N4´-methyl (b) signal is the signal from Oflo having N4´-methyl groups interacting strongest with GGCC; binding in minor or major groove. Given the poor coherence between fraction of Oflo intercalating calculated from the C3-methyl signal and the N4´-methyl (b) signal, the N4´-methyl signal appears less likely to be splitted from the intercalation.

An interesting feature is that the N4´-methyl (b) signal is flattening out at the same Oflo:GGCC ratio where intercalation is expected, indicating that the intercalation and the minor/major groove binding is somehow linked.

8.3.2 Titration of GGCC with Oflo

Unfortunately no NOESY spectra were recorded during the titration, but some information can be gained from the ^{1}H NMR spectra and the two NOESY spectra obtained. After the mishappening at the laboratory 390 microL of the sample was recovered. This volume was further diluted to 450 microL giving an initial GGCC concentration of 0.48 mM.

Both 1D and 2D spectra immediately show a clear interaction between Oflo and GGCC. Some signals are broadened, some disappear and some decrease or increase.

There is, of course, a possibility that the DNA no longer exists in the double helix state. Imino crosspeaks are completely lost in the NOESY spectrum supporting this. But the T3 and T9 imino signals in the ^{1}H NMR spectra are never completely lost. Also, GGCC has a rather constant diffusion constant being $1.33 \pm 0.07 * 10^{-10}$ m^2s^{-1} for pure GGCC and $1.4 \pm 0.2 * 10^{-10}$ m^2s^{-1} in the final spectrum. Reports have shown that it is roughly a ratio of 0.65 between double stranded:single stranded DNA diffusion constants[34], giving a diffusion constant of approximately $2 * 10^{-10}$ m^2s^{-1} for single stranded GGCC. The ratio Oflo:GGCC in the final titration is 2.67 meaning that even if all of the Oflo in the solution are bound to GGCC, only 2.67 Oflo molecules would be bound to each GGCC; this cannot account for such a low diffusion constant unless GGCC is, in fact, in the double helix state.

The loss of NOESY crosspeaks strongly indicates intercalative mode of interaction. The broadening of the guanine signals and the disappearing crosspeaks between the guanines and between

the guanines and the thymine and adenine in the NOESY spectrum further indicate intercalation between the two guanines. The loss of proton signals from the guanines in the 1D spectra may also indicate interactions in this site. The crosspeaks are symmetrically missing around the two guanines in table 7.11 supporting intercalation between the guanine base pairs.

An intercalative mode is also supported by the drift in the chemical shifts of T1 and T9, as seen in figure 7.19. The two signals T1 and T9 are drifting at Oflo:GGCC ratios above 1. The C3-methyl signal is splitted in this same concentration range, leading to two conclusions; the intercalation does not take place until the Oflo:GGCC ratio is around 1 and the splitting of the C3-methyl signal is caused by intercalation.
The C3-methyl signal was investigated and the fraction of Oflo represented by the lowest peak, as well as the association constants being calculated. The high association constants calculated from this peak supports the theory that this splitting results from intercalation. The C3-methyl signal appears at 1.48 ppm for pure Oflo and from the two signals from N4´-methyl it is concluded that the upfield signal is the signal from the interaction. The upfield signal, that is C3-methyl (b) is thus the signal shifted from intercalation interactions. The C3-methyl signal is a doublet and is almost not appearing in the diffusion spectra; therefore no diffusion measurements have been performed on these signals.

Table 7.13 shows downfield shifts of the signals resulting from H1', H2' and H2" on the sugar to which A2 is attached. T9 is not shifted in the same amount, indicating that the minor/major groove interaction takes place somewhere in the region T1A2T3-A8T9A10. It is more probable that the interaction occurs between A2/T9 and T3/A8 since the outer base pairs are less stable. This theory is also supported by the strong drift of the H2" on the sugar to which T3 is attached.

8.4 Association constants

Association constants have been calculated from three different sources. The three entirely different results as to percentage interaction Oflo:GGCC indicates the presence of three different mechanisms of action. This is further discussed in the next chapter.

The association constants are confirming the assumptions that the split of C3-methyl arise from intercalation and the split of N4´-methyl from minor/major groove binding, since intercalation are expected to give rise to higher association constants.

8.5 Models of interaction between quinolones and DNA

8.5.1 Proposal of a model of interaction between Oflo and GGCC

Tables 7.15, 7.16 and 7.17 indicates overlap of measurements. If there are three binding modes, the fraction interacting Oflo would be nearly 100%, not being very likely from the diffusion constant measured on the N4´-methyl (a) signal. The most reliable results are then the splitting of the two signals from C3-methyl and N4´-methyl. These two splittings are not considered arising from the same interaction. The two N4´-methyl peaks are visible from the very first spectrum, whereas the two C3-methyl doublets are not observed until an Oflo:GGCC ratio of approximately 1:1. This indicates that the N4´-methyl signal is splitted due to a binding in the minor/major groove or surface binding, while the splitting of the C3-methyl comes from an intercalation interaction. The diffusion measurements were performed on the N4´-methyl (a) signal not considered to result from minor/major groove- or surface interactions and thus considered to display intercalating Oflo. Table 7.15 shows the fraction intercalating Oflo calculated from the diffusion constant whereas the fraction intercalating Oflo calculated from the splitting of the C3-methyl signal is shown in table 7.16. The C3-methyl calculations display a larger fraction Oflo intercalating at all Oflo:GGCC ratios. The diffusion constant has a high uncertainty, especially at lowered concentrations. The diffusion measurements were performed on a splitted peak with heavy overlap, and were therefore not imbedded in this model.

The development of the N4´-methyl (b) peak maps the minor/major groove binding mode. Before reaching a 1:1 ratio Oflo:GGCC the peak grows faster than after this ratio and at the ratio hardly grows at all, indicating a rather constant minor/major groove interaction, except when the intercalation mode is beginning.

The development of the C3-methyl (b) peak shows a rather constant intercalation mode. The intercalation starts at a high rate and decays constantly, expected to level out when all intercalation sites are occupied. Two intercalation sites are expected on each DNA, between the guanines in each strand (*this is not proved in this thesis as the concentration levels of Oflo is not high enough, but the postulation of more than one intercalation site is supported by the fact that in the final spectrum 1.13 Oflo per GGCC is calculated to interact*).

This leads to the following model:
Below 1:1 ratio Oflo:GGCC:
Even at very diluted concentrations Oflo binds in the minor or major groove of the oligomer. This is the only interaction between Oflo and GGCC at these concentration levels. The minor/major groove interaction occurs somewhere in the T1A2T3-A8T9A10 region of the oligomer.

At 1:1 ratio Oflo:GGCC:
Oflo intercalates in the oligomer between the guanine pairs. The minor/major groove binding is

affected by the intercalation reaction and is merely acting as a reaction pathway at this ratio.

Above 1:1 ratio Oflo:GGCC:
Both intercalation and minor/major groove interactions appear. There is more than one intercalation site in each oligomer. The two interaction mechanisms are not seemingly competing, but the major/minor groove binding continues at a slower rate after the intercalation starts, indicating that they are in some way depending on each other.

8.5.2 Other possible models of interaction.
The results do not give enough information to arrive at an undisputable model, but there are enough indices to propose a model for the interaction between Oflo and GGCC. The model must thus be considered indicating, but not finally proved.

The interaction proposed disregards the diffusion constant measurements. If, on the other hand they are not to be disregarded, there are not two but three mechanisms of interaction. The percentage interacting Oflo calculated from the diffusion constant may be true meaning that minor or major groove binding is splitting the N4´-methyl signal and the other (*minor/major*) are not, or the minor/major interaction is splitting the signal whilst a surface binding mode is not. In the first case Oflo binds in both minor and major groove from very diluted concentrations and it is possible to monitor the development of both. From figure 7.13 it is then possible to see that the groove binding that splits the signal is somewhat dependent on the intercalation and the groove binding giving signal at the same frequency as non-interacting Oflo is not. At Oflo:GGCC ratio 1.03 approximately all of the Oflo present is then involved in interactions with GGCC. This is supported by the diffusion constant measurements on the peaks at 3.5 ppm and 8.4 ppm (*results not shown*).

No crosspeaks between Oflo and GGCC are found in the NOESY spectrum. This is somewhat strange if Oflo is interacting with GGCC through both intercalation sites, minor/major groove binding and perhaps even surface binding.

Oflo is in fact a racemic mixture, complicating the models of interaction. The S-isomer is reported to be 3 - 4 times more reactive against DNA than the R-isomer[9]. The split of either the N4´-methyl or the C3-methyl signal may arise from the two diastereomers being distinct while binding. Since the C3-methyl group is situated at the chiral centre, its signal may be shifted due to this effect. The two isomers are expected (*but not confirmed*) to be present in equal amounts. Table 7.16 are then, if all S-isomers are interacting with DNA, displaying the percentages of S-isomers versus R-isomers, though not indicating where or how Oflo is interacting and this is read out from the split of the N4´-methyl signal. There are still two different interaction mechanisms; minor/major groove binding and intercalation. Both mechanisms are functioning even at very diluted concentrations.
This model is less likely since the T1 and T9 signals in figure 7.19 does not indicate intercalation

until Oflo:GGCC ratio 1. Also the association constants for the intercalation are expected to be higher than for the minor/major groove interactions. This is not the case in this model. Even though this model cannot be disregarded as no proves can be put forward to eliminate it, it seems less likely than the model already proposed.

8.5.3 The proposed model in comparison to models from the literature

8.5.3.1 The Shen model

Shen et al. proposed that DNA-gyrase produced single stranded fragments where quinolones could interact. They also proposed that the intercalations of the quinolones are a cooperative process with stacking interactions making stable complexes with four quinolones in each DNA helix. No other interaction modes between quinolone and DNA were proposed.

The ratio Oflo:GGCC is not high enough to predict whether four quinolones may interact in one DNA, but there is no sign of a cooperative intercalation. All intercalation sites in one DNA would then have been filled up before intercalation in another DNA. The NOESY spectrum indicates that all of, or at least most of the DNA present is intercalated. No crosspeaks from non-intercalated GGCC is observed even when investigating the baseline. Also, the results in this thesis indicate several interaction modes. The presence of minor/major groove interactions is contradictory to that proposed by Shen et al..

8.5.3.2 The Maxwell model

Maxwell et al. proposed that quinolones could not interact with Gyrase or DNA alone, but could only interact with the DNA-Gyrase complex. They proposed that two quinolones was intercalating in a "DNA-bubble" created by the Gyrase approximately four or five base pairs away. They also performed experiments with Ca^{2+} indicating that drug induced cleavage is only occurring when the appropriate DNA base sequence exists at the active site.

The results in this thesis clearly show that quinolone may interact with DNA without the presence of DNA-gyrase. Without the Gyrase no "DNA-bubble" is formed, but the proposal of two quinolones intercalating some base pairs away could be in coherence with the results of this thesis. No experiments on metal ions were performed in this thesis and thus no conclusions may be drawn on whether presence of Ca^{2+} is necessary for DNA cleavage.

8.5.3.3 The Nordén model

Nordén et al. proposed a model where the intercalation is not a traditional one, but where the DNA is deformed at the binding site. They concluded with only one binding site and excluded both minor groove interactions and surface binding interactions. They found that quinolones could interact with DNA without the presence of Gyrase or metal-ions.
The results in this thesis clearly show that quinolones may interact with DNA without the presence of DNA-Gyrase or metal ions. The proposed model in this thesis indicates minor or major

groove interactions, but no crosspeaks are found supporting this conclusion. No evidence is found found indicating that DNA is not deformed. On the contrary, it may in fact appear that the DNA is deformed after intercalation as most of the crosspeaks between base pairs are lost and internal crosspeaks in base pairs are either lost or shifted heavily. The results of this thesis cannot counter-prove the Nordén model in any way, nor can it support all its findings.

8.5.3.4 Other models

A great deal of the models are based on the presence of metal ions. These models cannot be totally disregarded, as paramagnetic impurities were not removed from the sample. There is no way of telling whether the results in this thesis are a result of paramagnetic metal-ions making quinolone-DNA interactions possible. Since the nature of the paramagnetic impurities and the concentration of the impurities are not known it is not possible to discuss this problem in detail.

Baily et al. reported that intercalation of the quinolone was sequence dependent, preferably intercalating between a guanine and a cytosine. The results in this thesis show that more than one quinolone may intercalate in the DNA sequence. There exist indications that the intercalation is between the two guanines rather than guanine and cytosine, but intercalation between guanine and cytosine cannot be excluded. The results of this thesis are therefore not thought to support the findings of Baily et al..

8.6 Suggestions for further work

The properties of Ofloxacin should be further investigated. This thesis fails to conclude whether the coalescence arises from hindering of ring rotation or ring inversion. One way to investigate this might be to run HSQC and HMQC NMR experiments on lowered temperatures to assign the 2´/6´ protons to the C2´ and C6´. Molecular dynamics could also be investigated by molecular modelling to find which of the two possible causes for the coalescence is energetically favourable.

Though Oflo is an extensively used antimicrobial, few reports have been made on the chemical properties of the molecule using NMR. Mucci et al. is a fair exception. The pKa-values should be confirmed and the microspecies found, this would be a valuable experiment. Also, Oflo being a racemic mixture, has two isomers that should be investigated separately as they are reported to behave rather differently. It is nearly impossible to distinguish the two in an NMR spectrum. Separation is necessary in order to tell whether only one or both isomers have the same interaction modes. DECODES (Diffusion encoded spectroscopy)[36] could be attempted, but wether this technique applies to isomers are uncertain.

The interaction between Oflo and GGCC was difficult to investigate, due to the complete loss of crosspeaks between the two. There is no doubt though, that interactions occur. To investigate the interaction further it would be preferable to use a non-palindromic DNA-sequence. The GGCC-oligomer is heavily distorted around the GGCC base pairs and there are no actual means to tell whether the intercalation is between the guanines or between the neighbouring guaning and cytosine. The choice of a non-palindromic sequence with only one GG site could also answer the question of how many intercalation sites are present and how many Ofloxacin molecules could intercalate at one site.

The use of ^{19}F NMR diffusion measurements could also solve the problem of not knowing how big a fraction of the Oflo is actually interacting. The experiments in this thesis clearly shows that Oflo and GGCC have mostly overlapping proton signals, the only exception being N4´-methyl which is not trustworthy from splittings and low concentration levels. The concentration levels should be raised.

The recommendation must thus be to repeat the Oflo-GGCC titration. The next time one should use a non-palindromic DNA oligomer preferably with one GG site and one ATA site to check for intercalation and minor/major groove interactions and perform the experiments on both Oflo isomers separate. NOESY spectra should be recorded in all titrations.
The experiments should also be repeated with the metal ions present to monitor if any difference in the interacting mode occur.

Conclusions

- The self-diffusion constant of Ofloxacin is 4.36 (±0.06) * 10^{-10} m^2/s in the 1 - 6 mM concentration range

- There is no change in the stacking conditions for Ofloxacin in the concentration range 1 - 6 mM.

- The self-diffusion constant of the DNA-oligomer GGCC is 1.34 (±0.07) * 10^{-10} m^2/s

- Ofloxacin interacts with double-stranded DNA.

- Ofloxacin and GGCC interact through intercalation and at least one more interaction mechanism.

Appendices

A1. Plots from results

A1.1 Simfit and Regression plot for calculation of diffusion constant of GGCC using peak at 7.12 ppm

Table A1.1 Information obtained to calculate diffusion constant for pure GGCC using the peak at 7.12 ppm

Gradient strength	Intensities (absolut)	Normalised intensities	Y Ln (I/I_0)	X (see eq. 5 - 10)
0	--*			
2.252	32236	0.9039	0.1011	48550708
4.503	35664	1.0000	0.0000	194116605
6.755	28512	0.7995	0.2238	436827026
9.007	27796	0.7794	0.2492	776638863
11.26	25696	0.7205	0.3278	1213767695
13.51	24356	0.6829	0.3814	1747308104
15.76	22472	0.6301	0.4619	2377777534
18.01	20664	0.5794	0.5457	3105175985
20.27	18380	0.5154	0.6629	3933383490
22.52	16468	0.4618	0.7727	4855070778
24.77	14524	0.4072	0.8983	5873687087
27.02	13100	0.3673	1.0015	6989232416
29.27	10612	0.2976	1.2122	8201706767
31.52	8504	0.2384	1.4336	9511110138
33.78	7148	0.2004	1.6073	10923909251
36.03	6132	0.1719	1.7606	12427601459
38.28	5300	0.1486	1.9064	14028222688
40.53	3712	0.1041	2.2626	15725772937
42.78	3424	0.0960	2.3433	17520252207
45.03	2316	0.0649	2.7343	19411660498

** The spectrum was rendered by ringing and intensities could not be read out.*

Table A1.2 Settings for instrumental parameters

Little delta	Big delta	Tau	Gamma	Max Gradient
2.3 milliseconds	65 milliseconds	500 microsecond	4357 Hz/Gauss	70 Gauss/cm

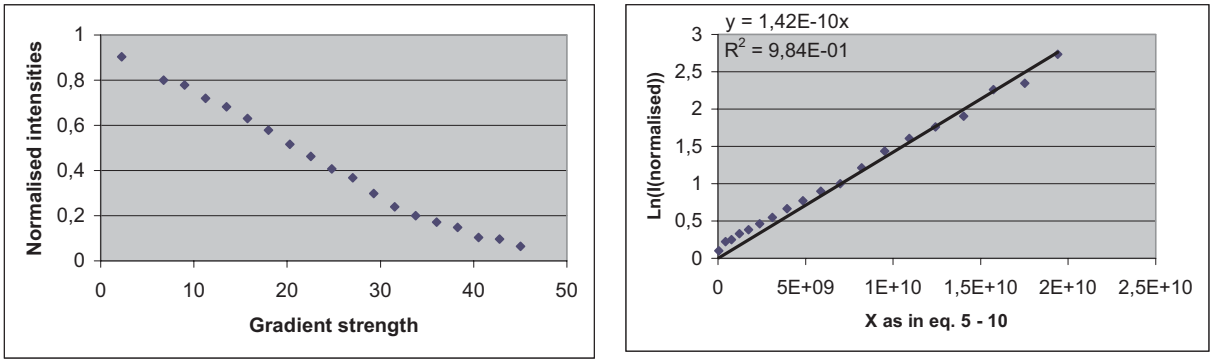

Figure A1.1 Simfit and Regression plot for diffusion measurements of GGCC for peak at 7.12 ppm. The point at Gradient strength 2.252 is not included in the plots.

A1.2 Simfit and Regression plot for calculation of diffusion constant of GGCC using peak at 7.81 ppm

Table A1.3 Information obtained to calculate diffusion constant for pure GGCC using the peak at 7.81 ppm

Gradient strength	**Intensities (absolut)**	**Normalised intensities**	**Y Ln (I/I_0)**	**X (see eq. 5 - 10)**
0	--*			
2.252	37936	1	0	
4.503	32624	0.8600	0.1509	491539530
6.755	36508	0.9624	0.0384	436827026
9.007	36540	0.9632	0.0375	776638862
11.26	34480	0.9089	0.0955	1213767695
13.51	32160	0.8477	0.1652	1747308104
15.76	29312	0.7727	0.2579	2377777534
18.01	26836	0.7074	0.3462	3105175985
20.27	24528	0.6466	0.4361	3933383490
22.52	21008	0.5538	0.5910	4855070778
24.77	18436	0.4860	0.7216	5873687087
27.02	16672	0.4395	0.8222	6989232416
29.27	13080	0.3448	1.0648	8201706767
31.52	11976	0.3157	1.1530	9511110138
33.78	9224	0.2431	1.4141	10923909251
36.03	8072	0.2128	1.5475	12427601459
38.28	6592	0.1738	1.7500	14028222688
40.53	5264	0.1388	1.9750	15725772937
42.78	4276	0.1127	2.1829	17520252207
45.03	3176	0.0837	2.4803	19411660498

* *The spectrum was rendered by ringing and intensities could not be read out.*

Table A1.4 Settings for instrumental parameters

Little delta	**Big delta**	**Tau**	**Gamma**	**Max Gradient**
2.3 milliseconds	65 milliseconds	500 microsecond	4357 Hz/Gauss	70 Gauss/cm

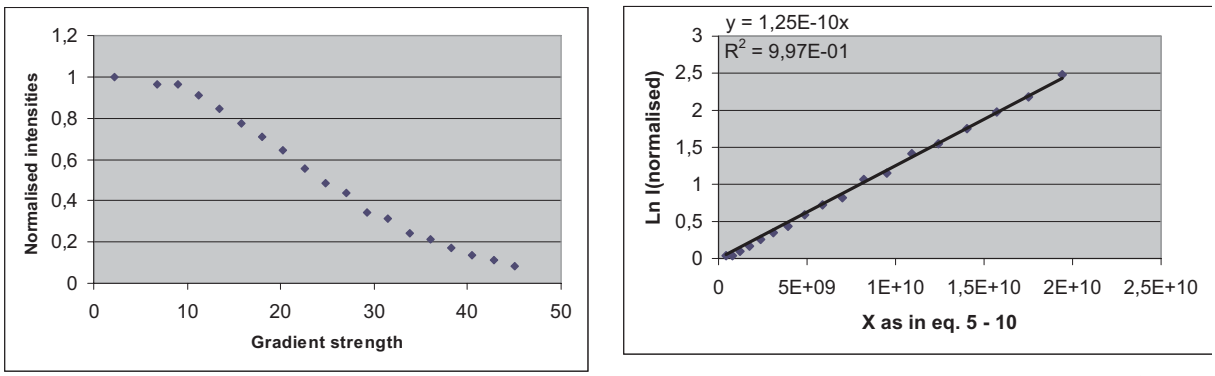

Figure A1.2 Simfit and Regression plot for diffusion measurements of GGCC for peak at 7.12 ppm. The point at Gradient strength 4.503 is not included in the plots.

A1.3 Simfit and Regression plot for calculation of diffusion constant of GGCC using peak at 8.18 ppm

Table A1.5 Information obtained to calculate diffusion constant for pure GGCC using the peak at 8.18 ppm

Gradient strength	**Intensities (absolut)**	**Normalised intensities**	**Y Ln (I/I_0)**	**X (see eq. 5 - 10)**
0	--*			
2.252	18044	1	0	48550708
4.503	15820	0.8767	0.1315	194116605
6.755	17772	0.9849	0.0152	436827026
9.007	16664	0.9235	0.0796	776638863
11.26	15048	0.8340	0.1816	1213767695
13.51	14640	0.8114	0.2091	1747308104
15.76	13316	0.7380	0.3038	2377777534
18.01	12036	0.6670	0.4049	3105175985
20.27	11004	0.6098	0.4946	3933383490
22.52	10048	0.5569	0.5854	4855070778
24.77	8928	0.4948	0.7036	5873687087
27.02	7104	0.3937	0.9322	6989232416
29.27	6364	0.3527	1.0422	8201706767
31.52	5344	0.2962	1.2168	9511110138
33.78	4724	0.2618	1.3402	10923909251
36.03	3632	0.2013	1.6030	12427601459
38.28	2760	0.1530	1.8776	14028222688
40.53	1816	0.1006	2.2962	15725772937
42.78	1992	0.1104	2.2037	17520252207
45.03	1452	0.0805	2.5199	19411660498

* *The spectrum was rendered by ringing and intensities could not be read out.*

Table A1.6 Settings for instrumental parameters

Little delta	**Big delta**	**Tau**	**Gamma**	**Max Gradient**
2.3 milliseconds	65 milliseconds	500 microsecond	4357 Hz/Gauss	70 Gauss/cm

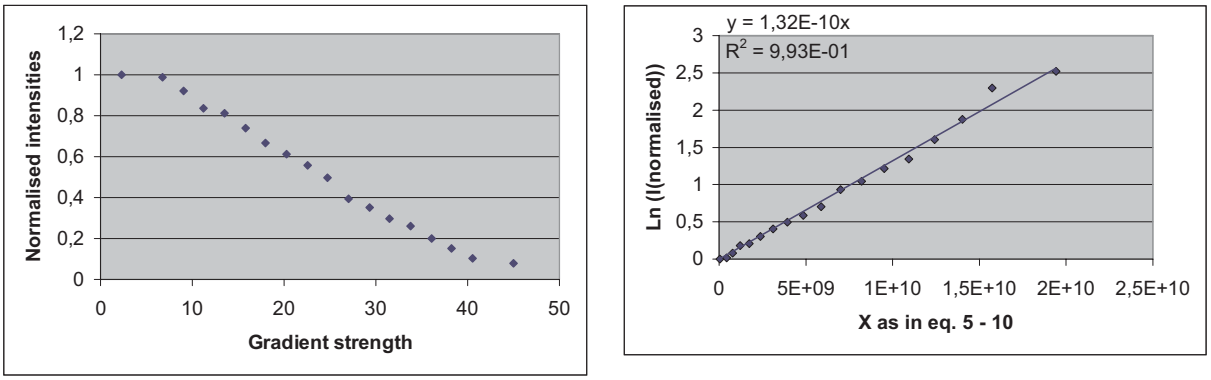

Figure A1.3 Simfit and Regression plot for diffusion measurements of GGCC for peak at 7.12 ppm. The point at gradient strengths 4.503 and 42.78 is not included in the plots.

A1.4 Simfit and Regression plot for calculation of diffusion constant of GGCC using peak at 8.28 ppm

Table A1.7 Information obtained to calculate diffusion constant for pure GGCC using the peak at 8.28 ppm

Gradient strength	**Intensities (absolut)**	**Normalised intensities**	**Y Ln (I/I_0)**	**X (see eq. 5 - 10)**
0	--*			
2.252	11924	1	0	48550708
4.503	10748	0.9014	0.1038	194116605
6.755	10272	0.8615	0.1491	436827026
9.007	11048	0.9265	0.0763	776638863
11.26	9716	0.8148	0.2048	1213767695
13.51	9460	0.7934	0.2315	1747308104
15.76	8580	0.7196	0.3291	2377777534
18.01	7572	0.6350	0.4541	3105175985
20.27	7008	0.5877	0.5315	3933383490
22.52	6344	0.5320	0.6310	4855070778
24.77	5396	0.4525	0.7929	5873687087
27.02	4516	0.3787	0.9709	6989232416
29.27	3640	0.3053	1.1866	8201706767
31.52	3360	0.2818	1.2666	9511110138
33.78	2644	0.2217	1.5062	10923909251
36.03	1656	0.1389	1.9741	12427601459
38.28	1836	0.1540	1.8710	14028222688
40.53	1500	0.1258	2.0731	15725772937
42.78	1280	0.1073	2.2317	17520252207
45.03	836	0.0701	2.6577	19411660498

* *The spectrum was rendered by ringing and intensities could not be read out.*

Table A1.8 Settings for instrumental parameters

Little delta	**Big delta**	**Tau**	**Gamma**	**Max Gradient**
2.3 milliseconds	65 milliseconds	500 microsecond	4357 Hz/Gauss	70 Gauss/cm

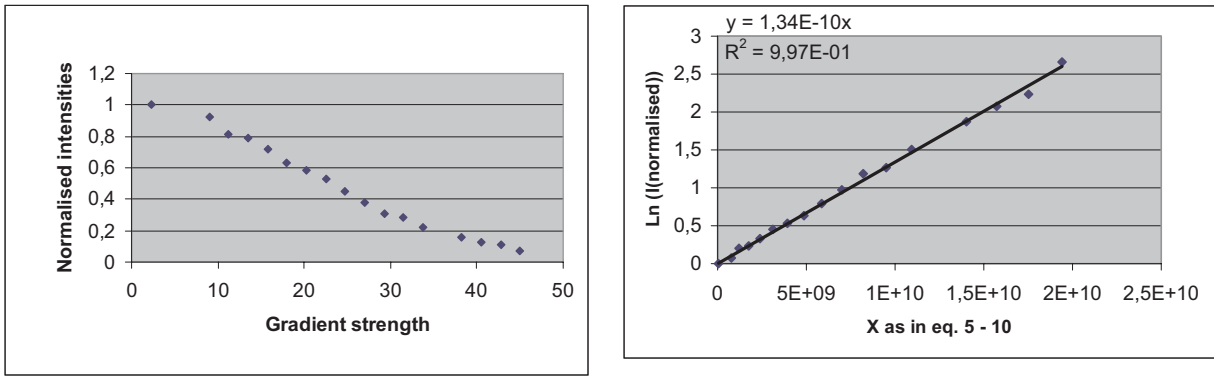

Figure A1.4 Simfit and Regression plot for diffusion measurements of GGCC for peak at 8.28 ppm. The points at gradient strengths 4.503, 6.755 and 36.03 is not included in the plots.

A1.5 Simfit and Regression plot for calculation of diffusion constant of GGCC in Oflo-GGCC mixture at Oflo:GGCC ratio 0.52 using peak at 7.12 ppm

Table A1.9 Information obtained to calculate diffusion constant for GGCC in Oflo-GGCC mixture at Oflo:GGCC ratio 0.52 using the peak at 7.12 ppm

Gradient strength	**Intensities (absolut)**	**Normalised intensities**	**Y Ln (I/I_0)**	**X (see eq. 5 - 10)**
2.252	11155	0.9750	0.0253	43629766
4.278	10423	0.9111	0.0931	157444565
6.305	11441	1.0000	0.0000	341992274
8.331	10831	0.9467	0.0548	597090804
10.36	10223	0.8936	0.1125	923348449
12.38	9311	0.8138	0.2060	1318522067
14.41	9040	0.7901	0.2356	1786380934
16.44	9529	0.8329	0.1828	2325143384
18.46	8322	0.7274	0.3182	2931632358
20.49	7119	0.6223	0.4744	3611852697
22.52	6768	0.5915	0.5251	4362976619
24.54	6711	0.5866	0.5334	5180780949
26.57	4831	0.4223	0.8621	6073362759
28.60	4911	0.4292	0.8458	7036848152
30.62	3507	0.3066	1.1823	8065967838
32.65	3802	0.3323	1.1016	9170911120
34.68	3138	0.2742	1.2937	10346757985
36.70	2140	0.1870	1.6765	11587193026
38.73	2314	0.2023	1.5980	12904497779
40.76	1596	0.1395	1.9698	14292706116
42.78	1268	0.1108	2.1998	15744456514

Table A1.8 Settings for instrumental parameters

Little delta	**Big delta**	**Tau**	**Gamma**	**Max Gradient**
2.5 milliseconds	50 milliseconds	500 microsecond	4357 Hz/Gauss	70 Gauss/cm

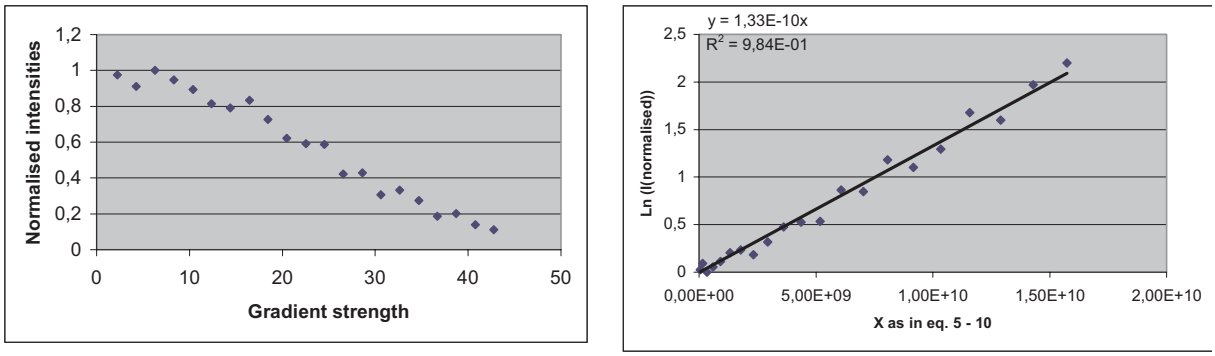

Figure A1.5 Simfit and Regression plot for diffusion measurements of GGCC in Oflo-GGCC mixture with Oflo:GGCC ratio 0.52 using peak at 7.12 ppm. All points are included in the plots.

A1.6 Simfit and Regression plot for calculation of diffusion constant of GGCC in Oflo-GGCC mixture at Oflo:GGCC ratio 0.52 using peak at 7.81 ppm

Table A1.9 Information obtained to calculate diffusion constant for GGCC in Oflo-GGCC mixture at Oflo:GGCC ratio 0.52 using the peak at 7.81 ppm

Gradient strength	**Intensities (absolut)**	**Normalised intensities**	**Y Ln (I/I_0)**	**X (see eq. 5 - 10)**
2.252	9895	1.0000	0.0000	43629766
4.278	9015	0.9110	0.0932	157444565
6.305	8916	0.9011	0.1041	341992274
8.331	9354	0.9454	0.0562	597090804
10.36	8965	0.9060	0.0987	923348449
12.38	8452	0.8542	0.1576	1318522067
14.41	8518	0.8608	0.1499	1786380934
16.44	7966	0.8050	0.2169	2325143384
18.46	7498	0.7578	0.2773	2931632358
20.49	6313	0.6379	0.4495	3611852697
22.52	6454	0.6523	0.4273	4362976619
24.54	5313	0.5369	0.6220	5180780949
26.57	4937	0.4989	0.6954	6073362759
28.60	4313	0.4358	0.8305	7036848152
30.62	3936	0.3978	0.9218	8065967838
32.65	3567	0.3605	1.0202	9170911120
34.68	3389	0.3425	1.0716	10346757985
36.70	2238	0.2262	1.4864	11587193026
38.73	2194	0.2218	1.5062	12904497779
40.76	1545	0.1562	1.8568	14292706116
42.78	1469	0.1485	1.9073	15744456514

Table A1.8 Settings for instrumental parameters

Little delta	**Big delta**	**Tau**	**Gamma**	**Max Gradient**
2.5 milliseconds	50 milliseconds	500 microsecond	4357 Hz/Gauss	70 Gauss/cm

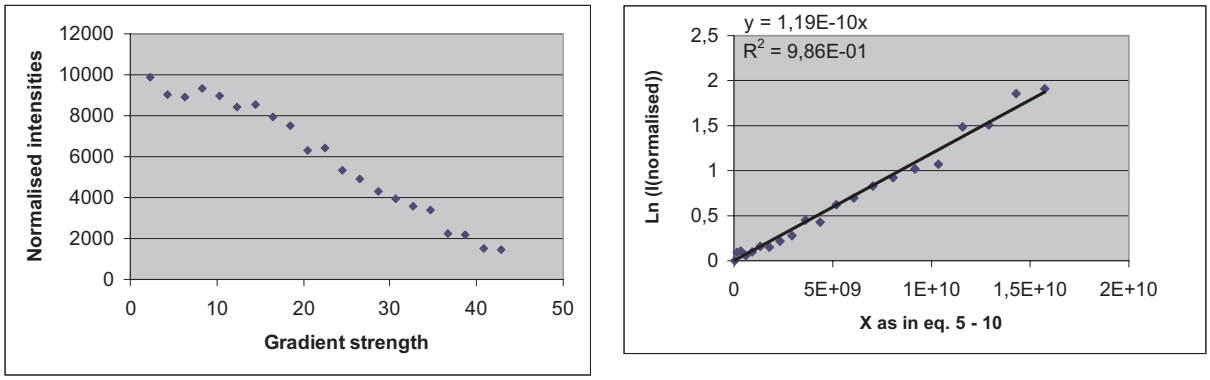

Figure A1.6 Simfit and Regression plot for diffusion measurements of GGCC in Oflo-GGCC mixture with Oflo:GGCC ratio 0.52 using peak at 7.81 ppm. All points are included in the plots.

A1.7 Simfit and Regression plot for calculation of diffusion constant of GGCC in Oflo-GGCC mixture at Oflo:GGCC ratio 0.52 using peak at 8.18 ppm

Table A1.11 Information obtained to calculate diffusion constant for GGCC in Oflo-GGCC mixture at Oflo:GGCC ratio 0.52 using the peak at 8.18 ppm

Gradient strength	**Intensities (absolut)**	**Normalised intensities**	**Y Ln (I/I_0)**	**X (see eq. 5 - 10)**
2.252	5205	0.8708	0.1383	43629766
4.278	5977	1.0000	0.0000	157444565
6.305	5402	0.9039	0.1011	341992274
8.331	5156	0.8626	0.1478	597090804
10.36	4702	0.7867	0.2399	923348449
12.38	4514	0.7552	0.2808	1318522067
14.41	4462	0.7466	0.2923	1786380934
16.44	4170	0.6978	0.3599	2325143384
18.46	3646	0.6100	0.4943	2931632358
20.49	3207	0.5366	0.6225	3611852697
22.52	3512	0.5875	0.5318	4362976619
24.54	2492	0.4170	0.8747	5180780949
26.57	2411	0.4033	0.9080	6073362759
28.60	2478	0.4146	0.8806	7036848152
30.62	1879	0.3144	1.1571	8065967838
32.65	1948	0.3260	1.1209	9170911120
34.68	1386	0.2319	1.4614	10346757985
36.70	1088	0.1820	1.7039	11587193026
38.73	698	0.1167	2.1481	12904497779
40.76	1103	0.1846	1.6896	14292706116
42.78	398	0.0666	2.7095	15744456514

Table A1.12 Settings for instrumental parameters

Little delta	**Big delta**	**Tau**	**Gamma**	**Max Gradient**
2.5 milliseconds	50 milliseconds	500 microsecond	4357 Hz/Gauss	70 Gauss/cm

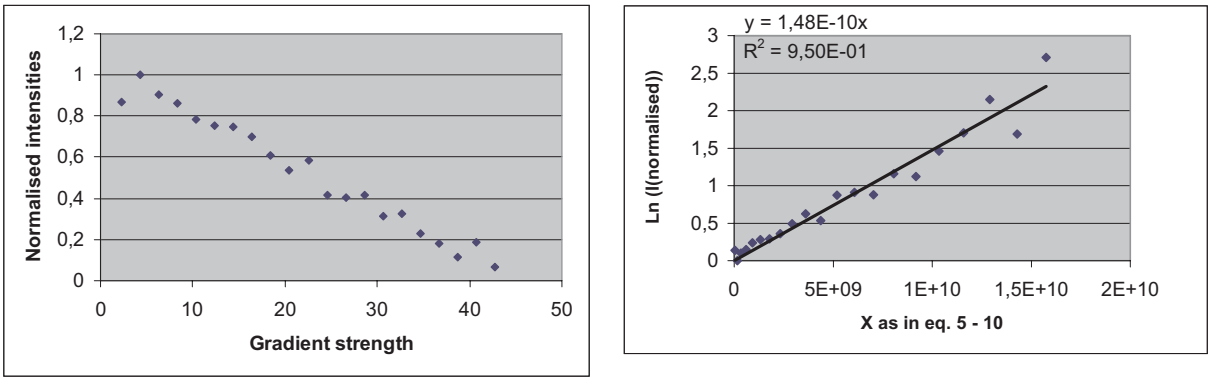

Figure A1.7 Simfit and Regression plot for diffusion measurements of GGCC in Oflo-GGCC mixture with Oflo:GGCC ratio 0.52 using peak at 8.18 ppm. All points are included in the plots.

A1.8 Simfit and Regression plot for calculation of diffusion constant of GGCC in Oflo-GGCC mixture at Oflo:GGCC ratio 0.52 using peak at 8.28 ppm

Table A1.13 Information obtained to calculate diffusion constant for GGCC in Oflo-GGCC mixture at Oflo:GGCC ratio 0.52 using the peak at 8.28 ppm

Gradient strength	**Intensities (absolut)**	**Normalised intensities**	**Y Ln (I/I_0)**	**X (see eq. 5 - 10)**
2.252	3595	0.8357	0.1795	43629766
4.278	3354	0.7797	0.2489	157444565
6.305	3234	0.7518	0.2852	341992274
8.331	4301	1.0000	0.0000	597090804
10.36	3680	0.8556	0.1559	923348449
12.38	2955	0.6870	0.3755	1318522067
14.41	2929	0.6809	0.3843	1786380934
16.44	3319	0.7717	0.2592	2325143384
18.46	2677	0.6223	0.4743	2931632358
20.49	2562	0.5956	0.5182	3611852697
22.52	2955	0.6870	0.3755	4362976619
24.54	1988	0.4623	0.7716	5180780949
26.57	1721	0.4001	0.9160	6073362759
28.60	1201	0.2791	1.2761	7036848152
30.62	1146	0.2663	1.3230	8065967838
32.65	1307	0.3038	1.1915	9170911120
34.68	811	0.1885	1.6689	10346757985
36.70	1121	0.2607	1.3445	11587193026
38.73	877	0.2039	1.5902	12904497779
40.76	644	0.1497	1.8991	14292706116
42.78	486	0.1130	2.1803	15744456514

Table A1.14 Settings for instrumental parameters

Little delta	**Big delta**	**Tau**	**Gamma**	**Max Gradient**
2.5 milliseconds	50 milliseconds	500 microsecond	4357 Hz/Gauss	70 Gauss/cm

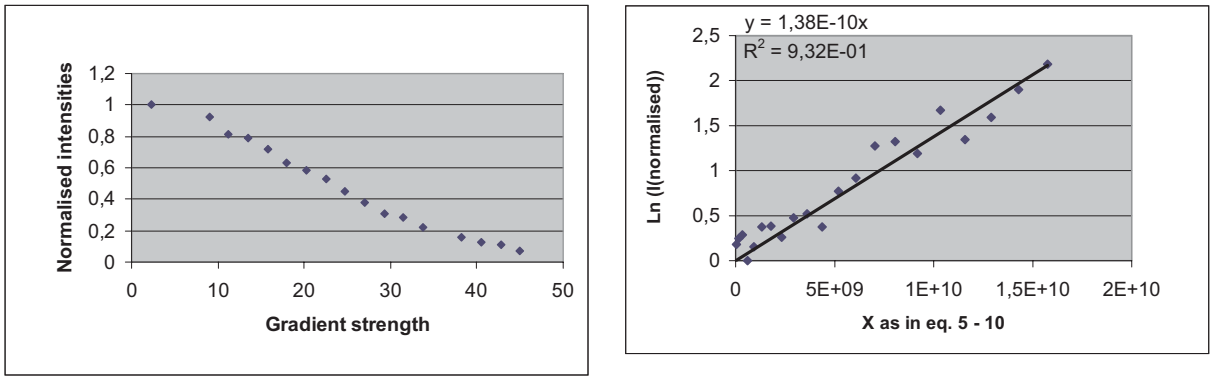

Figure A1.8 Simfit and Regression plot for diffusion measurements of GGCC in Oflo-GGCC mixture with Oflo:GGCC ratio 0.52 using peak at 8.28 ppm. All points are included in the plots.

A1.9 Simfit and Regression plot for calculation of diffusion constant of GGCC in Oflo-GGCC mixture at Oflo:GGCC ratio 2.67 using peak at 7.12 ppm

Table A1.15 Information obtained to calculate diffusion constant for GGCC in Oflo-GGCC mixture at Oflo:GGCC ratio 2.67 using the peak at 7.12 ppm

Gradient strength	**Intensities (absolut)**	**Normalised intensities**	**Y Ln (I/I_0)**	**X (see eq. 5 - 10)**
2.252	7501	0.7831	0.2444	43629766
4.278	8272	0.8636	0.1466	157444565
6.305	3783	0.3950	0.9280	341992274
8.331	9578	1.0000	0.0000	597090804
10.36	8783	0.9170	0.0866	923348449
12.38	7333	0.7656	0.2671	1318522067
14.41	6951	0.7258	0.3205	1786380934
16.44	6849	0.7151	0.3354	2325143384
18.46	7195	0.7513	0.2860	2931632358
20.49	5894	0.6154	0.4854	3611852697
22.52	5273	0.5506	0.5968	4362976619
24.54	5264	0.5496	0.5986	5180780949
26.57	3242	0.3385	1.0832	6073362759
28.60	2880	0.3007	1.2015	7036848152
30.62	4081	0.4260	0.8532	8065967838
32.65	2883	0.3010	1.2005	9170911120
34.68	2843	0.2968	1.2146	10346757985
36.70	1196	0.1249	2.0805	11587193026
38.73	2431	0.2538	1.3712	12904497779
40.76	611	0.0638	2.7524	14292706116
42.78	1499	0.1565	1.8545	15744456514

Table A1.16 Settings for instrumental parameters

Little delta	**Big delta**	**Tau**	**Gamma**	**Max Gradient**
2.5 milliseconds	50 milliseconds	500 microsecond	4357 Hz/Gauss	70 Gauss/cm

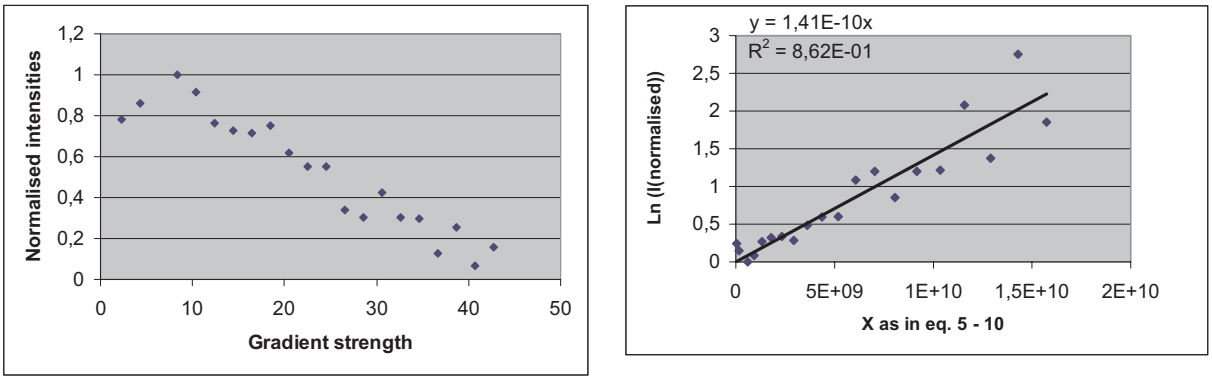

Figure A1.9 Simfit and Regression plot for diffusion measurements of GGCC in Oflo-GGCC mixture with Oflo:GGCC ratio 2.67 using peak at 7.12 ppm. Point at gradient strength 6.305 are not included in the plots.

A1.10 Simfit and Regression plot for calculation of diffusion constant of GGCC in Oflo-GGCC mixture at Oflo:GGCC ratio 2.67 using peak at 7.81 ppm

Table A1.17 Information obtained to calculate diffusion constant for GGCC in Oflo-GGCC mixture at Oflo:GGCC ratio 2.67 using the peak at 7.81 ppm

Gradient strength	**Intensities (absolut)**	**Normalised intensities**	**Y Ln (I/I_0)**	**X (see eq. 5 - 10)**
2.252	6140	1.0000	0.0000	43629766
4.278	4695	0.7646	0.2684	157444565
6.305	4124	0.6717	0.3980	341992274
8.331	4581	0.7460	0.2930	597090804
10.36	4217	0.6869	0.3756	923348449
12.38	4148	0.6756	0.3922	1318522067
14.41	4279	0.6970	0.3610	1786380934
16.44	3100	0.5049	0.6833	2325143384
18.46	3529	0.5747	0.5539	2931632358
20.49	3399	0.5535	0.5914	3611852697
22.52	3002	0.4890	0.7155	4362976619
24.54	2550	0.4153	0.8786	5180780949
26.57	2330	0.3795	0.9690	6073362759
28.60	2082	0.3391	1.0815	7036848152
30.62	1881	0.3064	1.1830	8065967838
32.65	1909	0.3110	1.1681	9170911120
34.68	1877	0.3058	1.1850	10346757985
36.70	1226	0.1996	1.6112	11587193026
38.73	1029	0.1677	1.7858	12904497779
40.76	732	0.1192	2.1269	14292706116
42.78	634	0.1032	2.2711	15744456514

Table A1.18 Settings for instrumental parameters

Little delta	**Big delta**	**Tau**	**Gamma**	**Max Gradient**
2.5 milliseconds	50 milliseconds	500 microsecond	4357 Hz/Gauss	70 Gauss/cm

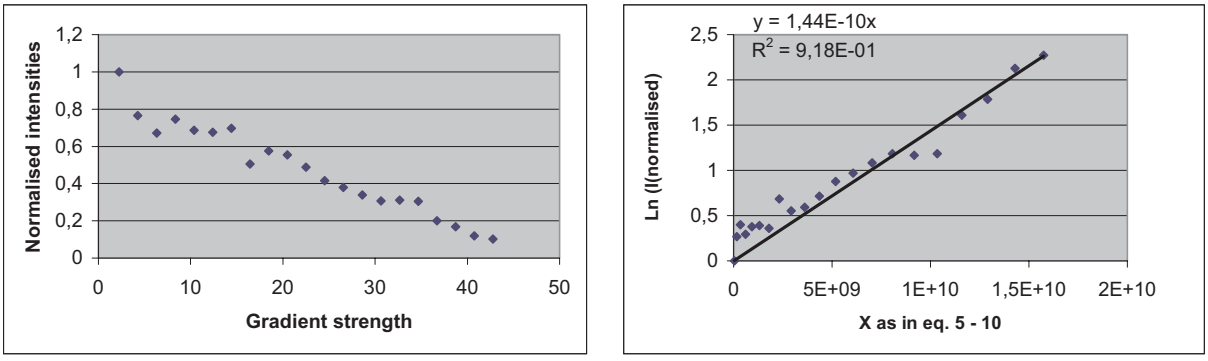

Figure A1.10 Simfit and Regression plot for diffusion measurements of GGCC in Oflo-GGCC mixture with Oflo:GGCC ratio 2.67 using peak at 7.81 ppm. All points are included in the plots.

A1.11 Simfit and Regression plot for calculation of diffusion constant of GGCC in Oflo-GGCC mixture at Oflo:GGCC ratio 2.67 using peak at 8.18 ppm

Table A1.19 Information obtained to calculate diffusion constant for GGCC in Oflo-GGCC mixture at Oflo:GGCC ratio 2.67 using the peak at 8.18 ppm

Gradient strength	**Intensities (absolut)**	**Normalised intensities**	**Y Ln (I/I_0)**	**X (see eq. 5 - 10)**
2.252	1231	0.4467	0.8058	43629766
4.278	2516	0.9133	0.0907	157444565
6.305	1235	0.4481	0.8027	341992274
8.331	2555	0.9273	0.0755	597090804
10.36	2755	1.0000	0.0000	923348449
12.38	2579	0.9359	0.0662	1318522067
14.41	2429	0.8815	0.1261	1786380934
16.44	1697	0.6159	0.4847	2325143384
18.46	1853	0.6726	0.3966	2931632358
20.49	2300	0.8346	0.1808	3611852697
22.52	1011	0.3669	1.0028	4362976619
24.54	1939	0.7040	0.3510	5180780949
26.57	1535	0.5570	0.5853	6073362759
28.60	1382	0.5016	0.6899	7036848152
30.62	799	0.2900	1.2380	8065967838
32.65	1166	0.4233	0.8598	9170911120
34.68	771	0.2798	1.2737	10346757985
36.70	686	0.2491	1.3900	11587193026
38.73	1003	0.3642	1.0102	12904497779
40.76	965	0.3503	1.0490	14292706116
42.78	477	0.1731	1.7536	15744456514

Table A1.20 Settings for instrumental parameters

Little delta	**Big delta**	**Tau**	**Gamma**	**Max Gradient**
2.5 milliseconds	50 milliseconds	500 microsecond	4357 Hz/Gauss	70 Gauss/cm

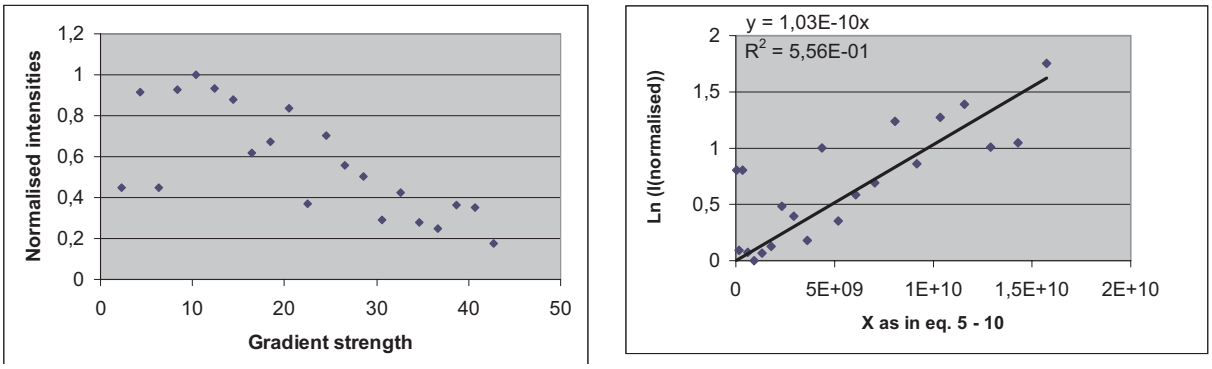

Figure A1.11 Simfit and Regression plot for diffusion measurements of GGCC in Oflo-GGCC mixture with Oflo:GGCC ratio 2.67 using peak at 8.18 ppm. All points are included in the plots.

A1.12 Simfit and Regression plot for calculation of diffusion constant of GGCC in Oflo-GGCC mixture at Oflo:GGCC ratio 2.67 using peak at 8.28 ppm

Table A1.21 Information obtained to calculate diffusion constant for GGCC in Oflo-GGCC mixture at Oflo:GGCC ratio 2.67 using the peak at 8.28 ppm

Gradient strength	**Intensities (absolut)**	**Normalised intensities**	**Y Ln (I/I_0)**	**X (see eq. 5 - 10)**
2.252	3487	0.8213	0.1968	43629766
4.278	3053	0.7191	0.3298	157444565
6.305	4246	1.0000	0.0000	341992274
8.331	2840	0.6689	0.4022	597090804
10.36	2456	0.5784	0.5474	923348449
12.38	2404	0.5663	0.5687	1318522067
14.41	2554	0.6016	0.5082	1786380934
16.44	2609	0.6146	0.4868	2325143384
18.46	1575	0.3710	0.9916	2931632358
20.49	1859	0.4378	0.8261	3611852697
22.52	1806	0.4254	0.8547	4362976619
24.54	1722	0.4055	0.9027	5180780949
26.57	1537	0.3620	1.0160	6073362759
28.60	1054	0.2483	1.3932	7036848152
30.62	1235	0.2908	1.2351	8065967838
32.65	780	0.1837	1.6943	9170911120
34.68	754	0.1776	1.7280	10346757985
36.70	612	0.1441	1.9374	11587193026
38.73	536	0.1262	2.0702	12904497779
40.76	510	0.1202	2.1189	14292706116
42.78	816	0.1922	1.6492	15744456514

Table A1.22 Settings for instrumental parameters

Little delta	**Big delta**	**Tau**	**Gamma**	**Max Gradient**
2.5 milliseconds	50 milliseconds	500 microsecond	4357 Hz/Gauss	70 Gauss/cm

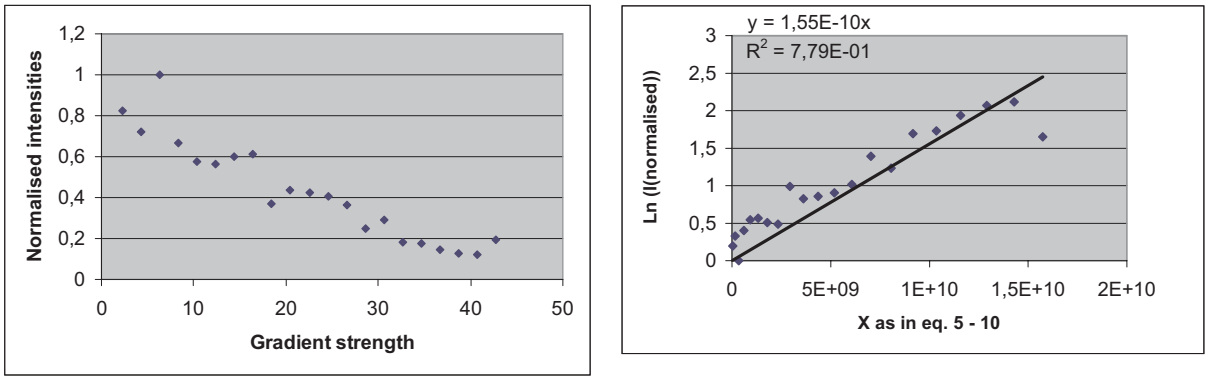

Figure A1.12 Simfit and Regression plot for diffusion measurements of GGCC in Oflo-GGCC mixture with Oflo:GGCC ratio 2.67 using peak at 8.28 ppm. All points are included in the plots.

A2. Spectra from results

A2.1 Spectrum obtained of Oflo in D_2O

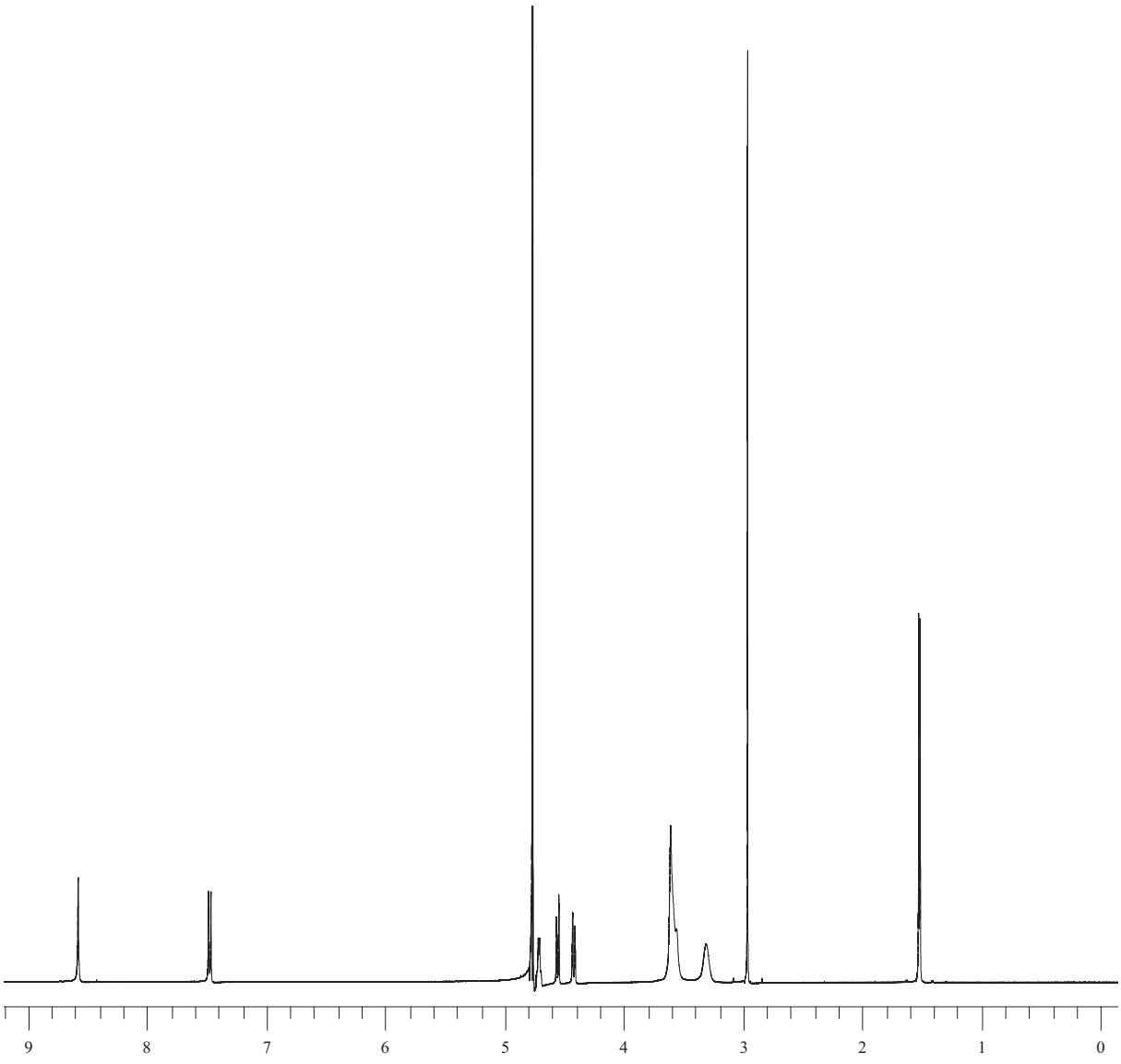

Figure A2.1 7 mM Ofloxacin with pH 5.5 obtained using D_2O as solvent without water suppression

A2.2 Spectrum obtained of ~5 mM Oflo in water (10% D_2O) with pH 4.92 and presaturation of the water signal

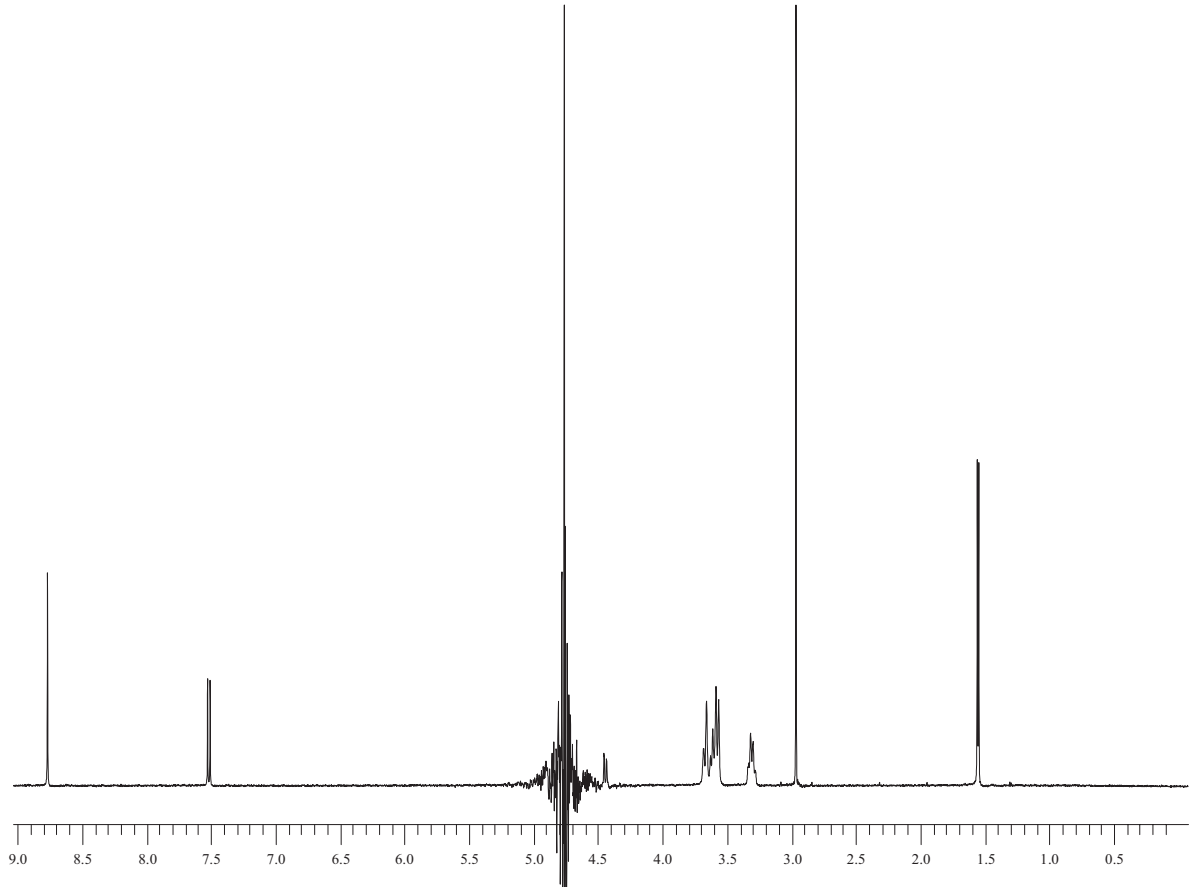

Figure A2.2 ~5mM Ofloxacin in water (10% D_2O) with pH 4.92 obtained at 293.9 K (actual temperature) with presaturation of the water signal.

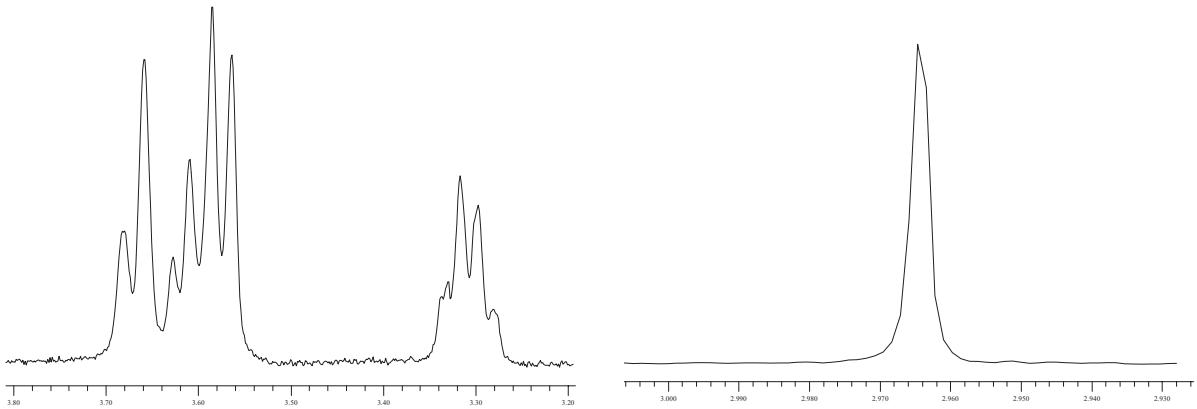

Figure A2.3 Expansions of the piperazine ring protons and the N4´-methyl protons from the spectrum above.

A2.3 Spectrum obtained for 0.07 mM Ofloxacin in 0.48 mM GGCC resulting in a 0.15 ratio Oflo:GGCC

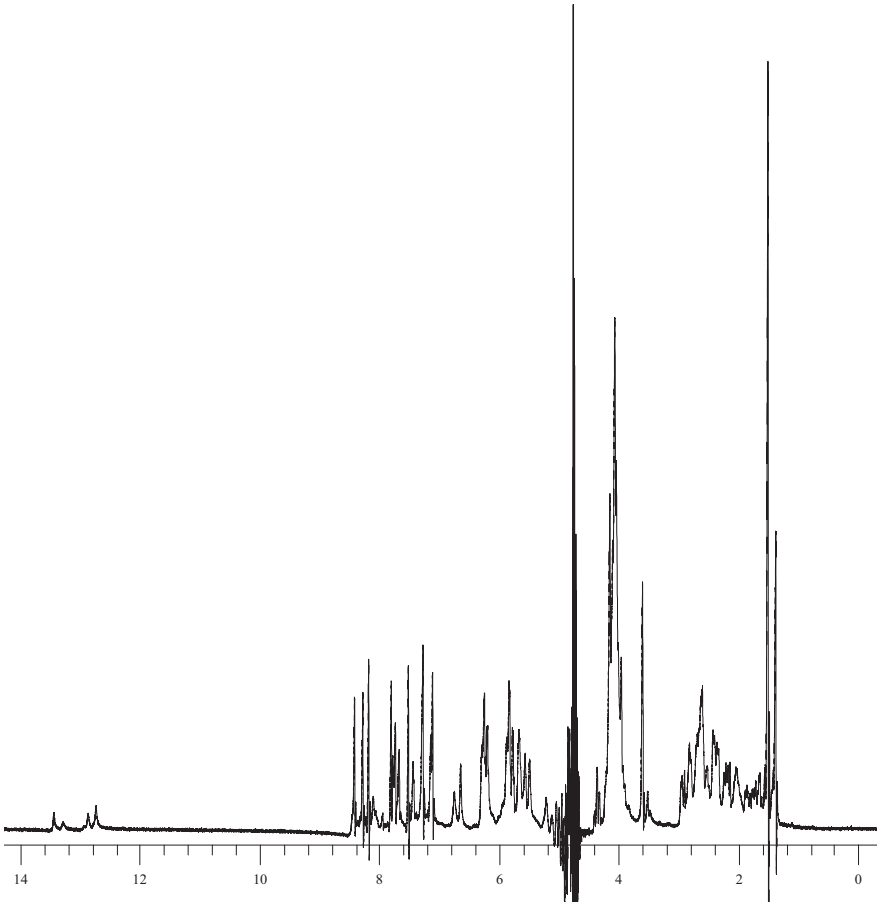

Figure A2.4 ^{1}H NMR spectrum of ratio Oflo:GGCC 0.15.

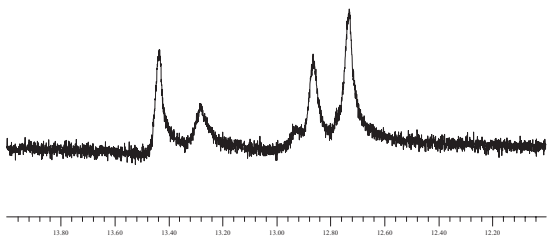

Figure A2.5 Expansion of the imino region from figure A2.4.

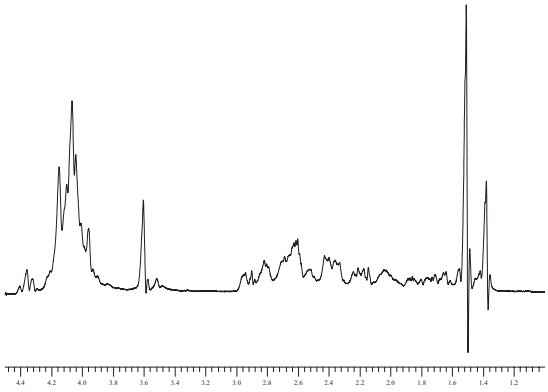

Figure A2.6 Expansion of the 1.0 - 4.5 ppm region from figure A2.4.

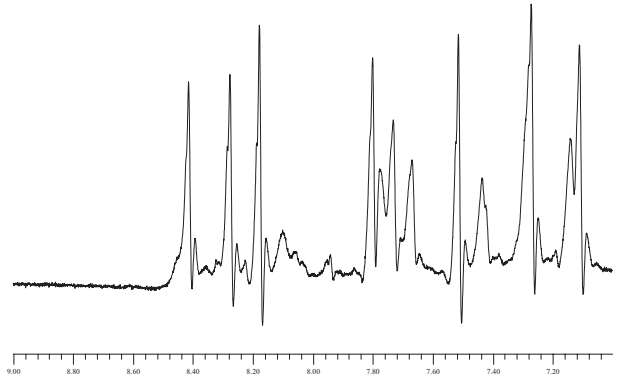

Figure A2.7 Expansion of the aromatic region from figure A2.4.

A2.4 Spectrum obtained for 0.13 mM Ofloxacin in 0.47 mM GGCC resulting in a 0.27 ratio Oflo:GGCC

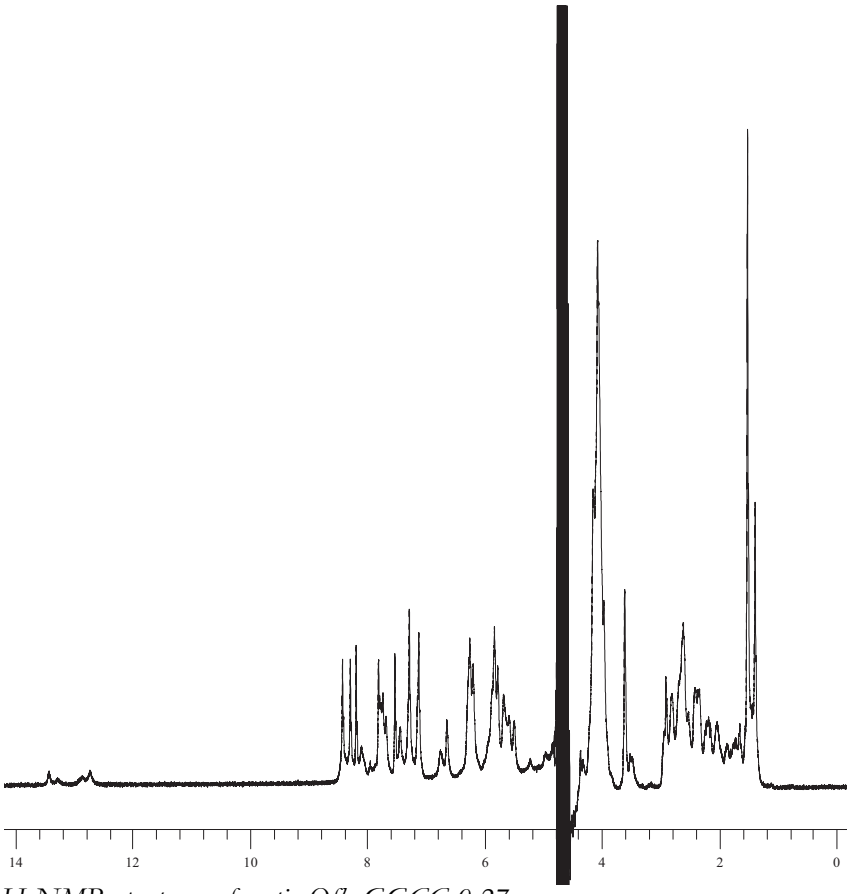

Figure A2.8 ^{1}H NMR spectrum of ratio Oflo:GGCC 0.27.

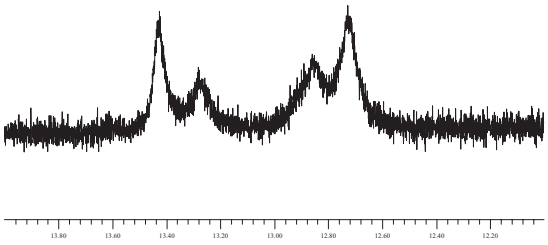

Figure A2.9 Expansion of the imino region of figure A2.8.

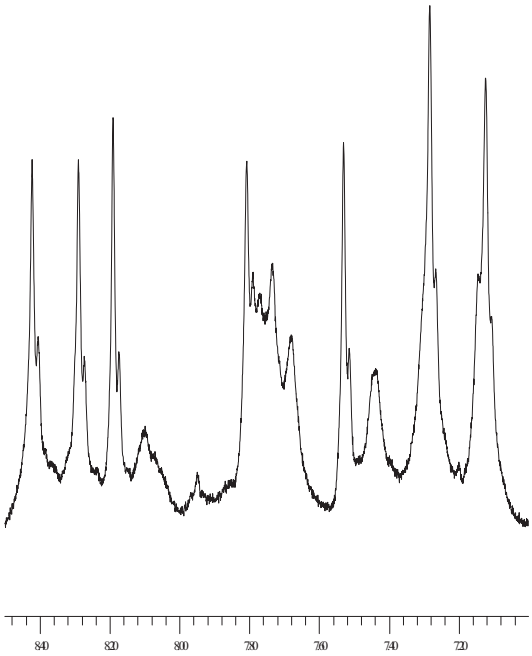

Figure A2.10 Expansion of the aromatic region of figure A2.8.

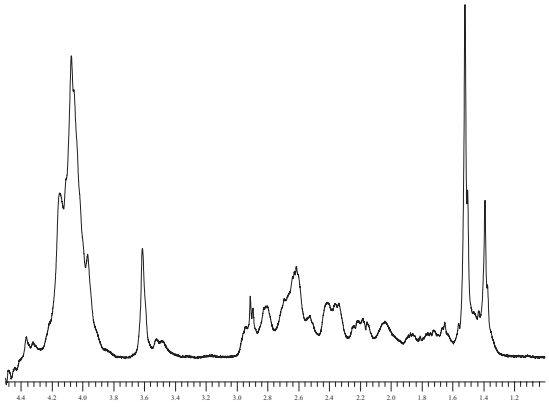

Figure A2.11 Expansion of the 1.0 - 4.5 ppm region of figure A2.8

A2.5 Spectrum obtained for 0.24 mM Ofloxacin in 0.46 mM GGCC resulting in a 0.52 ratio Oflo:GGCC

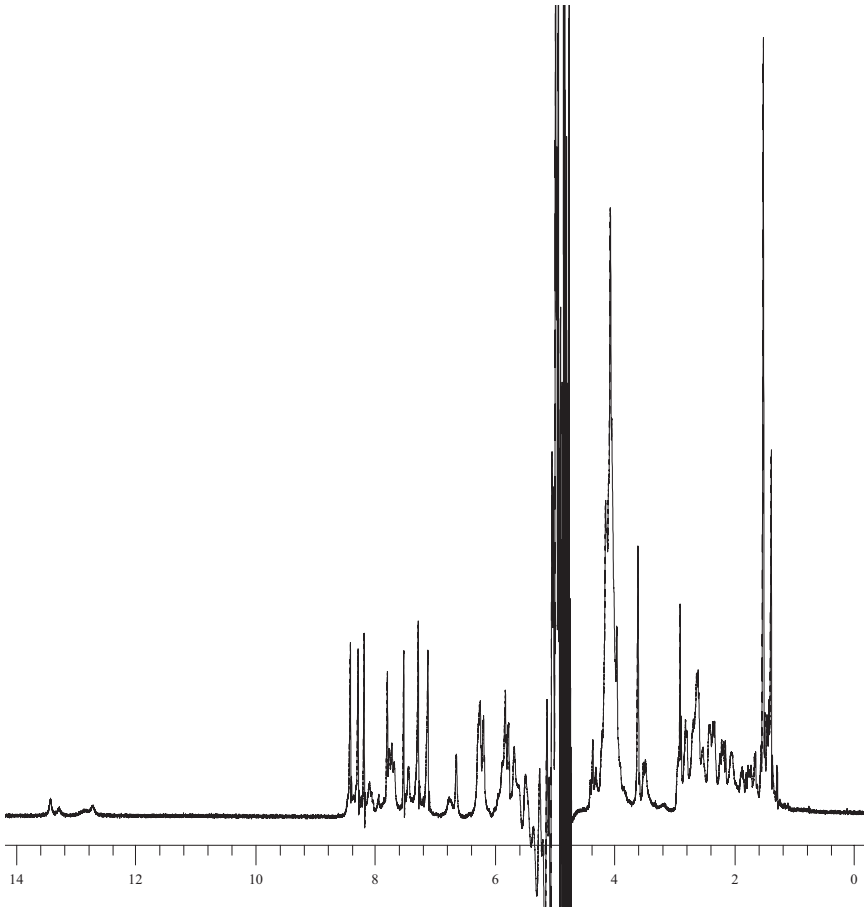

Figure A2.12 S¹H NMR spectrum of ratio Oflo:GGCC 0.52.

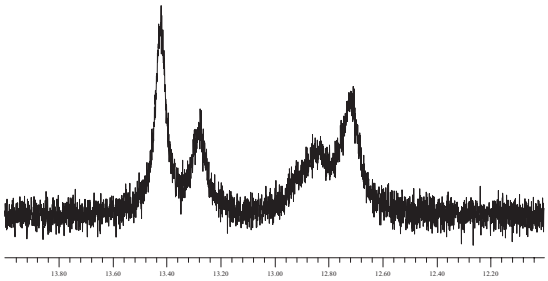

Figure A2.13 Expansion of imino region

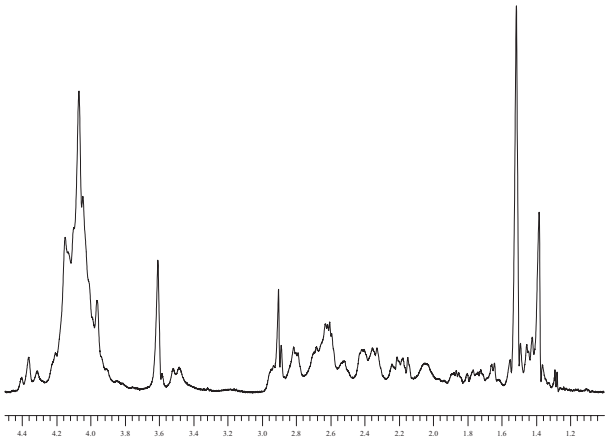

Figure A2.14 Expansion of 1.0 - 4.5 ppm region of figure A2.12

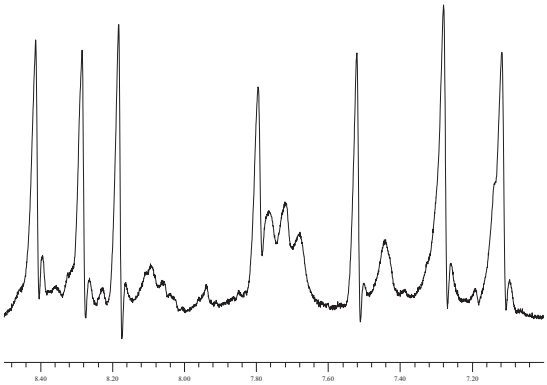

Figure A2.15 Expansion of aromatic region

A2.6 Spectrum obtained for 0.35 mM Ofloxacin in 0.45 mM GGCC resulting in a 0.77 ratio Oflo:GGCC

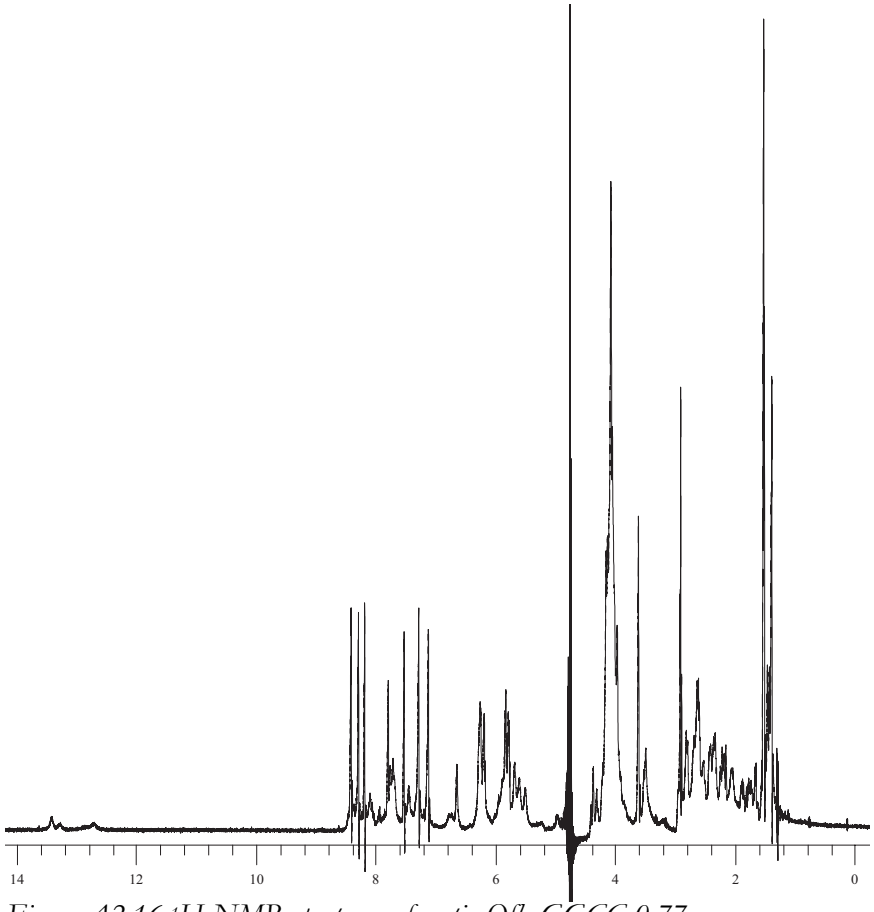

Figure A2.16 ^{1}H NMR spectrum of ratio Oflo:GGCC 0.77

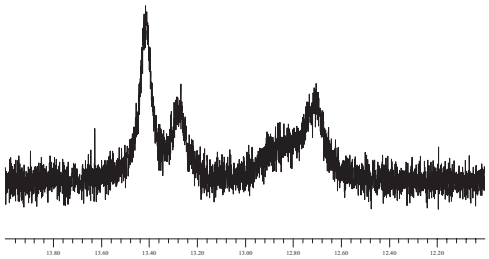

Figure A2.17 Expansion of imino region

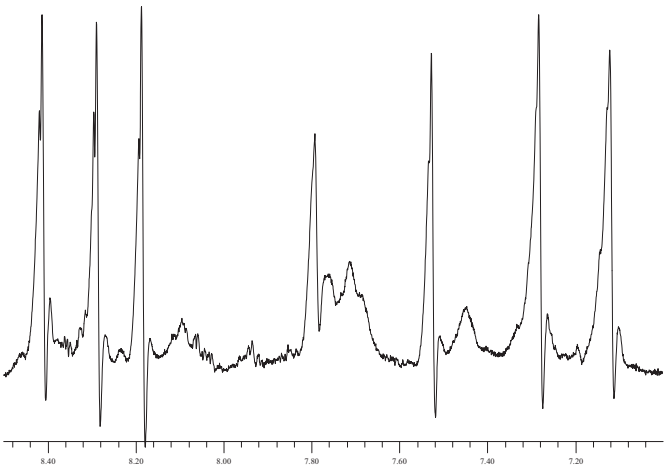

Figure A2.18 Expansion aromatic region

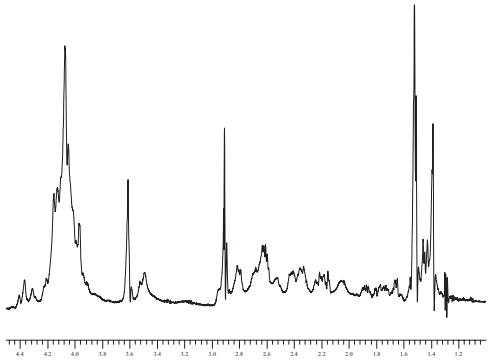

Figure A2.19 Expansion of 1.0 - 4.5 ppm region

A2.7 Spectrum obtained for 0.45 mM Ofloxacin in 0.44 mM GGCC resulting in a 1.03 ratio Oflo:GGCC

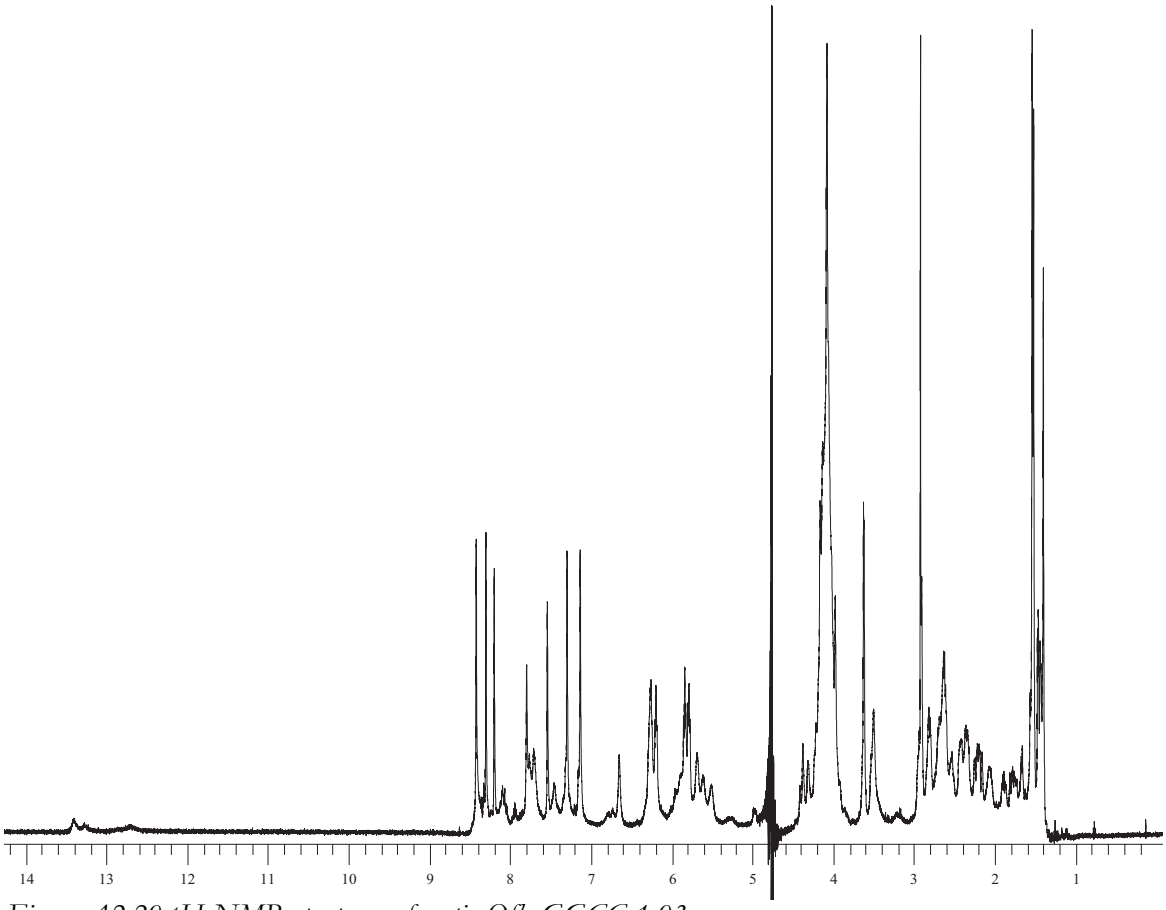

Figure A2.20 ^{1}H NMR spectrum of ratio Oflo:GGCC 1.03

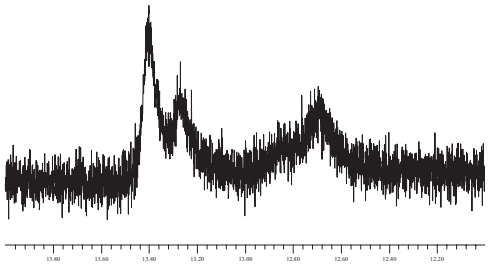

Figure A2.21 Expansion of imino region

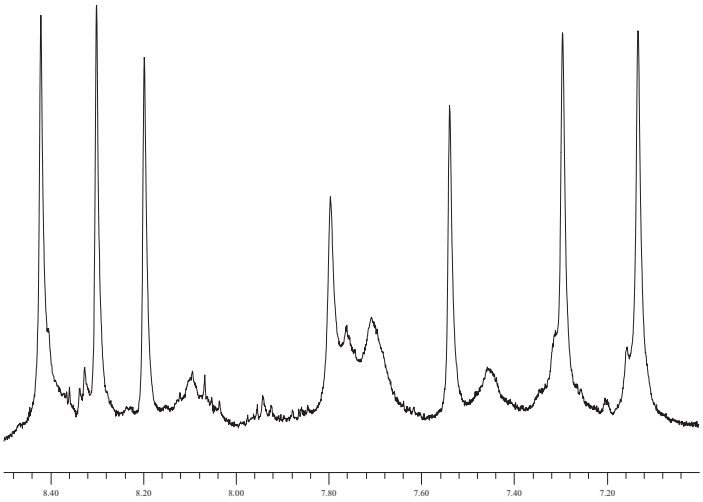

Figure A2.22 Expansion of aromatic region

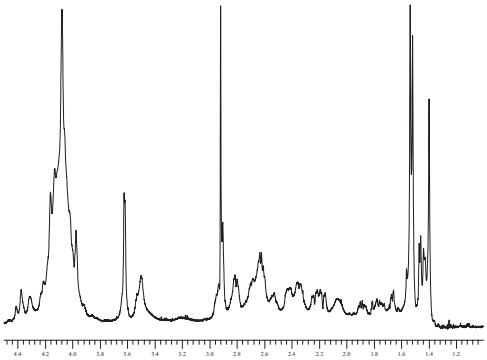

Figure A2.23 Expansion of 1.0 - 4.5 ppm region

A2.8 Spectrum obtained for 0.56 mM Ofloxacin in 0.43 mM GGCC resulting in a 1.29 ratio Oflo:GGCC

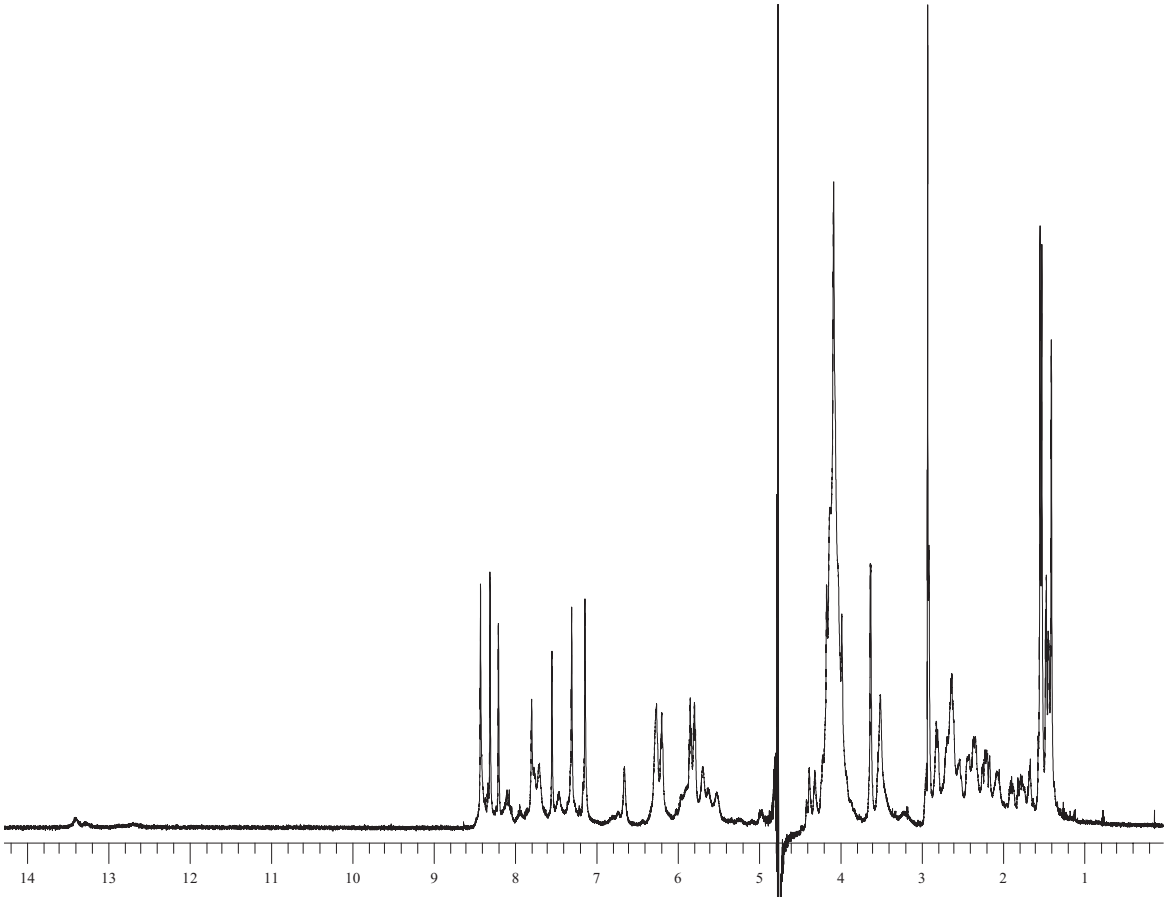

Figure A2.24 ^{1}H NMR spectrum of ratio Oflo:GGCC 1.29.

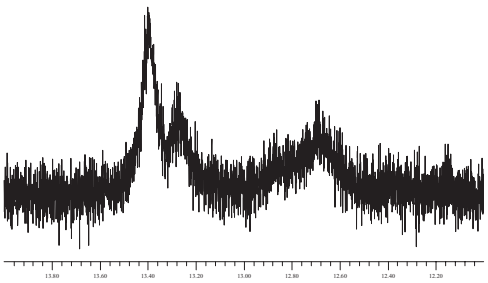

Figure A2.25 Expansion of imino region

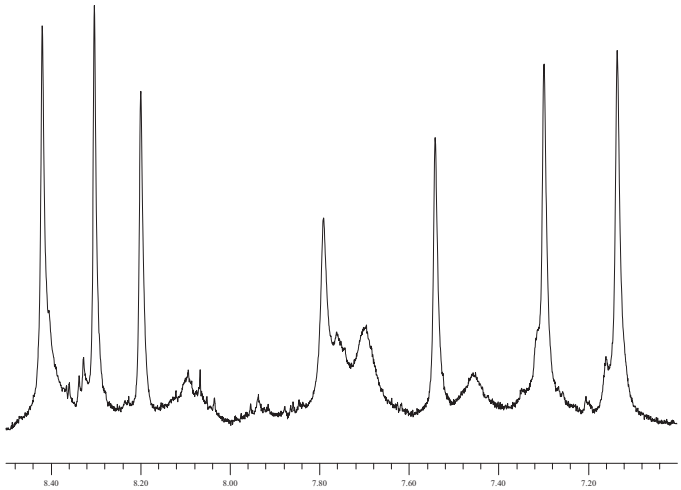

Figure A2.26 Expansion of aromatic region

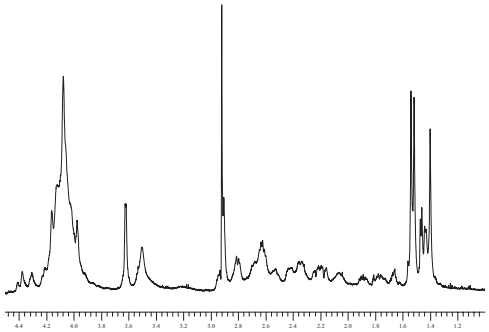

Figure A2.27 Expansion of 1.0 - 4.5 ppm region

A2.9 Spectrum obtained for 0.67 mM Ofloxacin in 0.42 mM GGCC resulting in a 1.56 ratio Oflo:GGCC

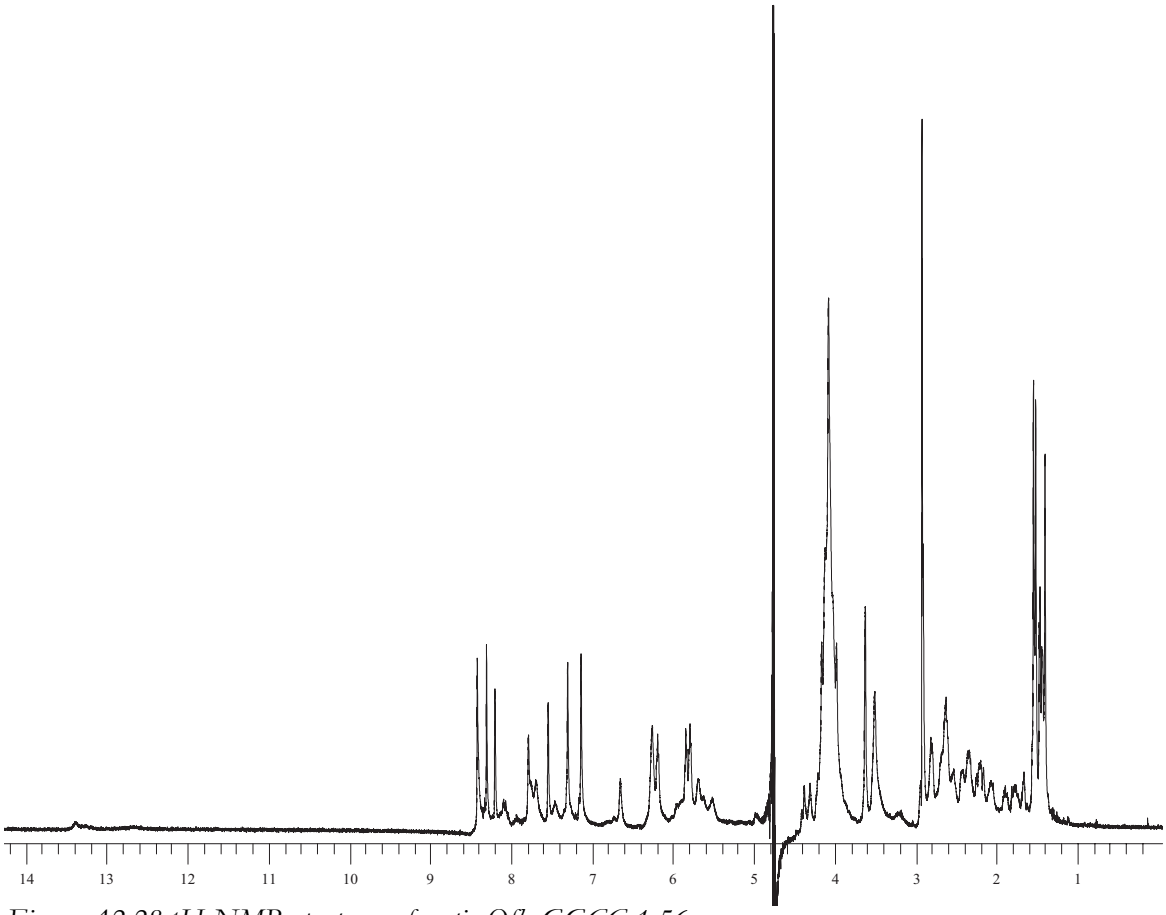

Figure A2.28 ^{1}H NMR spectrum of ratio Oflo:GGCC 1.56

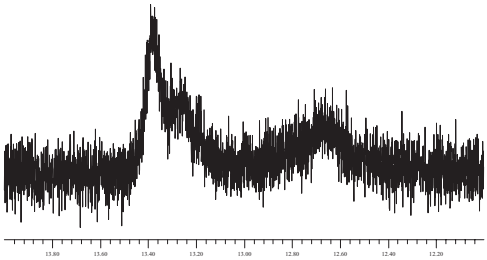

Figure A2.29 Expansion of imino region

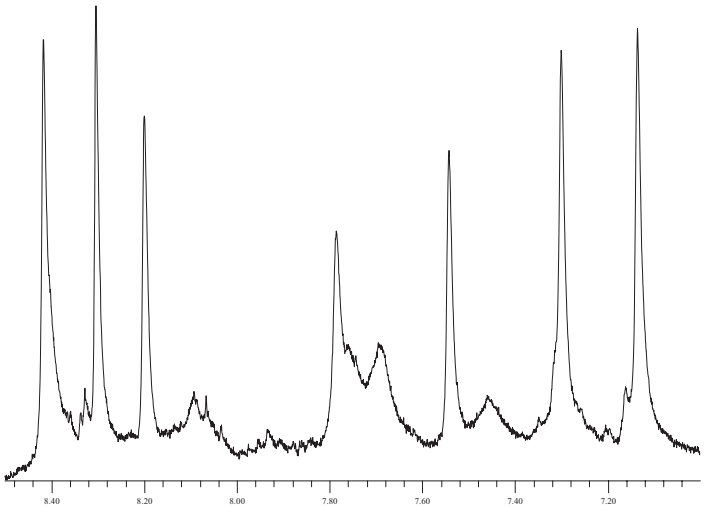

Figure A2.30 Expansion of aromatic region

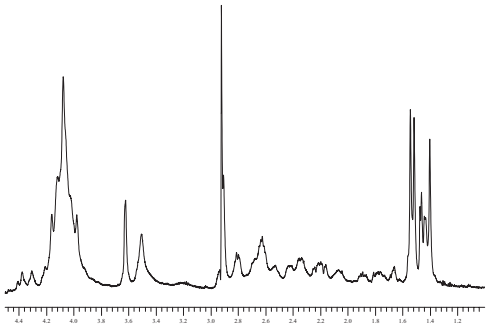

Figure A2.31 Expansion of 1.0 - 4.5 ppm region

A2.10 Spectrum obtained for 0.77 mM Ofloxacin in 0.42 mM GGCC resulting in a 1.83 ratio Oflo:GGCC

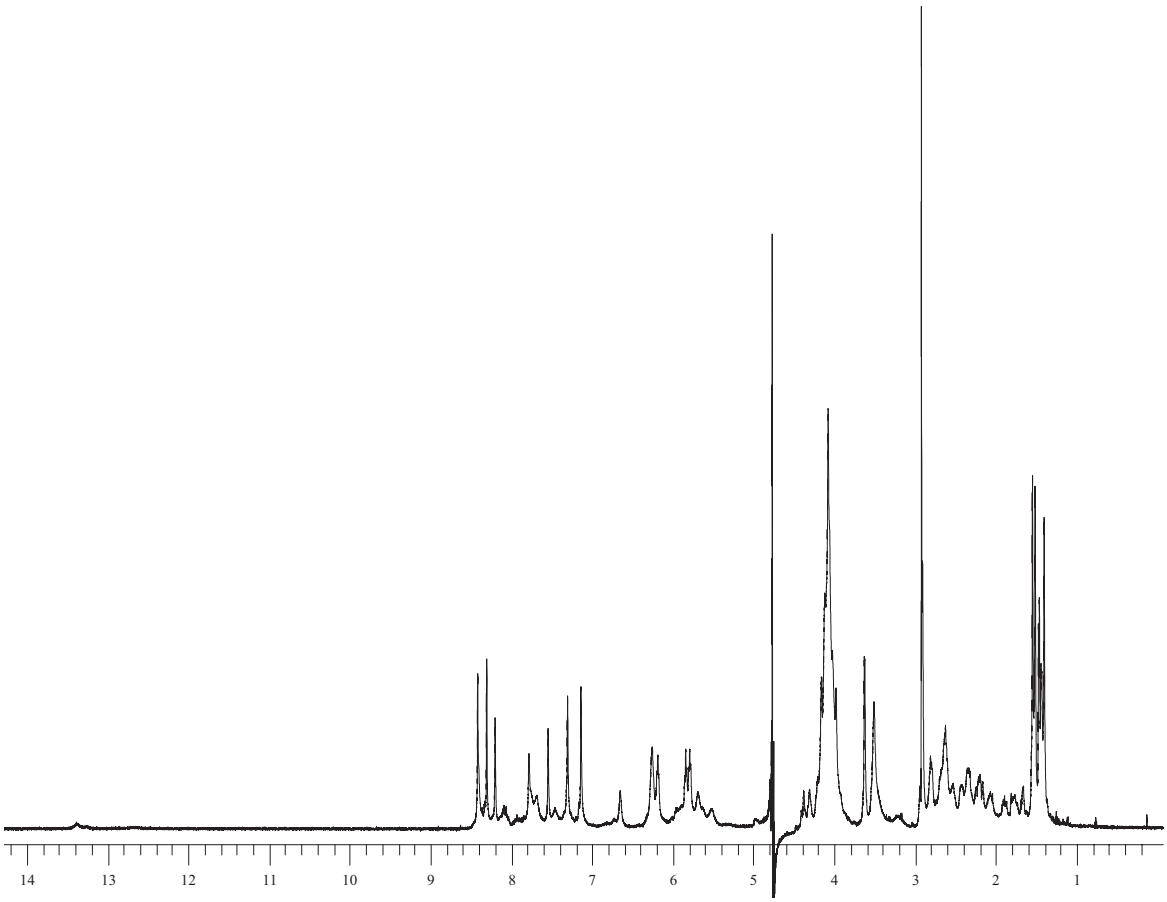

Figure A2.32 ^{1}H NMR spectrum of ratio Oflo:GGCC 1.83.

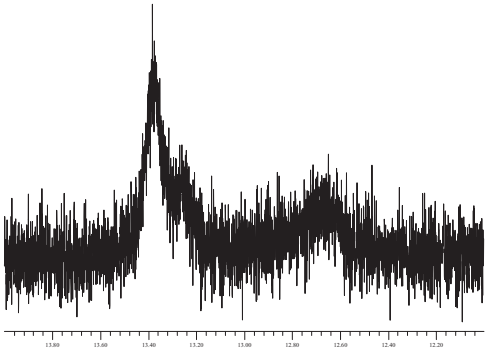

Figure A2.33 Expansion of imino region

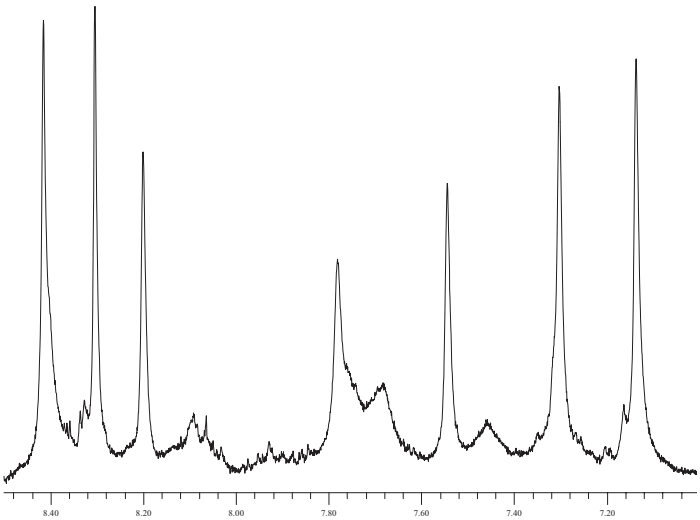

Figure A2.34 Expansion of aromatic region

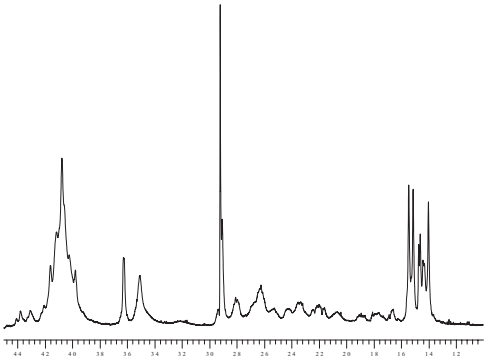

Figure A2.35 Expansion of 1.0 - 4.5 ppm region

A2.11 Spectrum obtained for 0.86 mM Ofloxacin in 0.41 mM GGCC resulting in a 2.11 ratio Oflo:GGCC

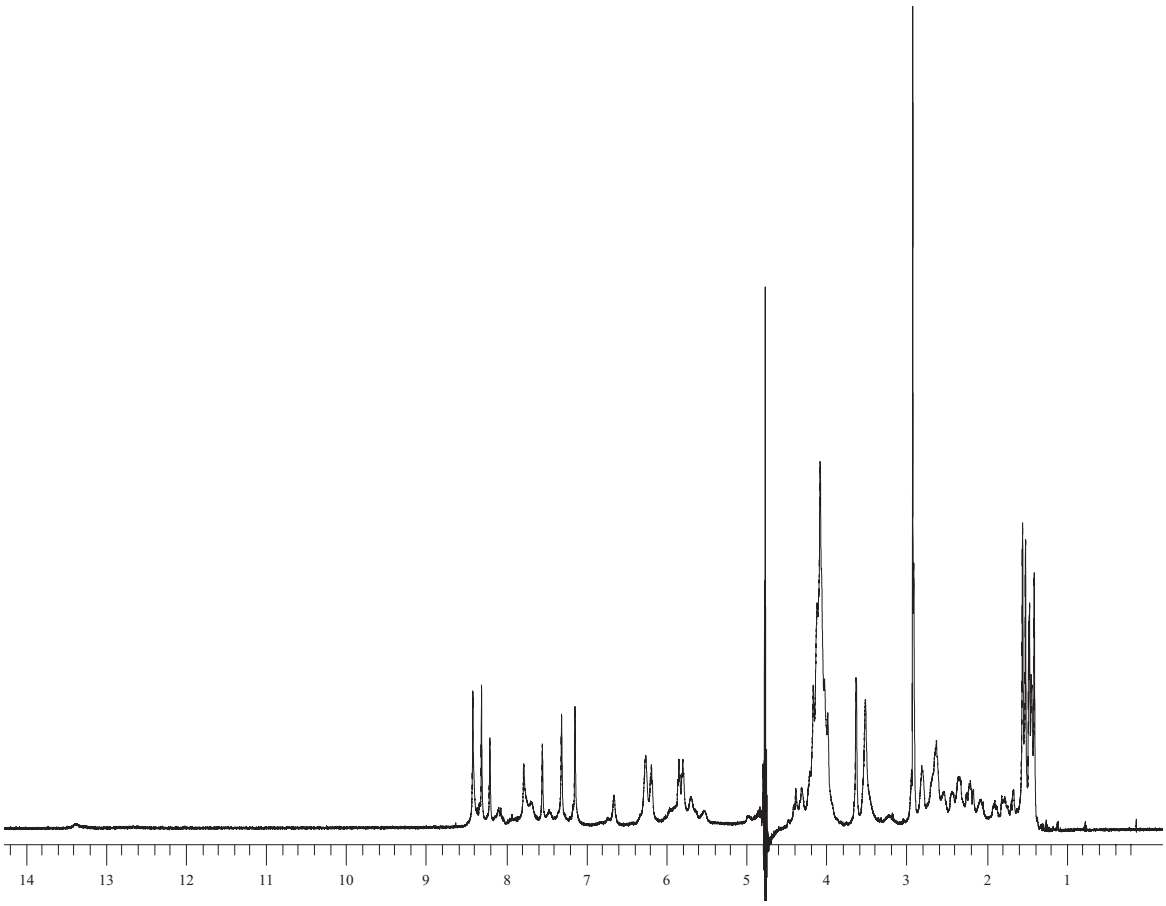

Figure A2.36 ^{1}H NMR spectrum of ratio Oflo:GGCC 2.11

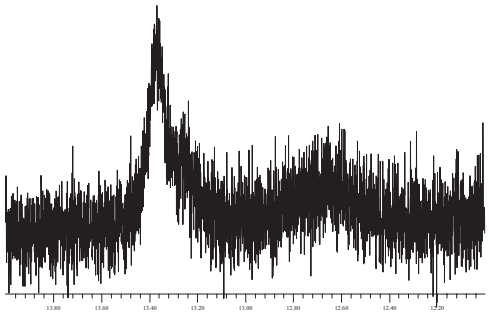

Figure A2.37 Expansion of imino region

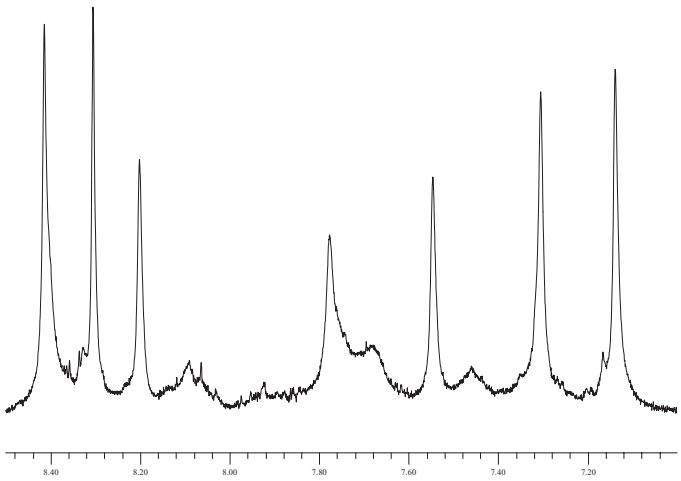

Figure A2.38 Expansion of aromatic region

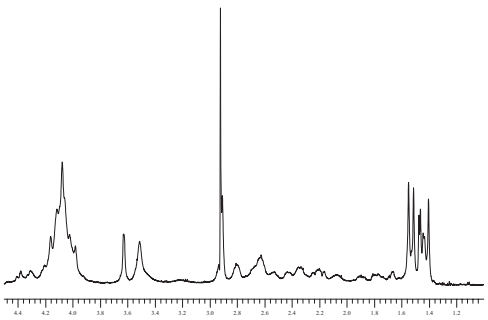

Figure A2.39 Expansion of 1.0 - 4.5 ppm region

A2.12 Spectrum obtained for 0.95 mM Ofloxacin in 0.40 mM GGCC resulting in a 2.39 ratio Oflo:GGCC

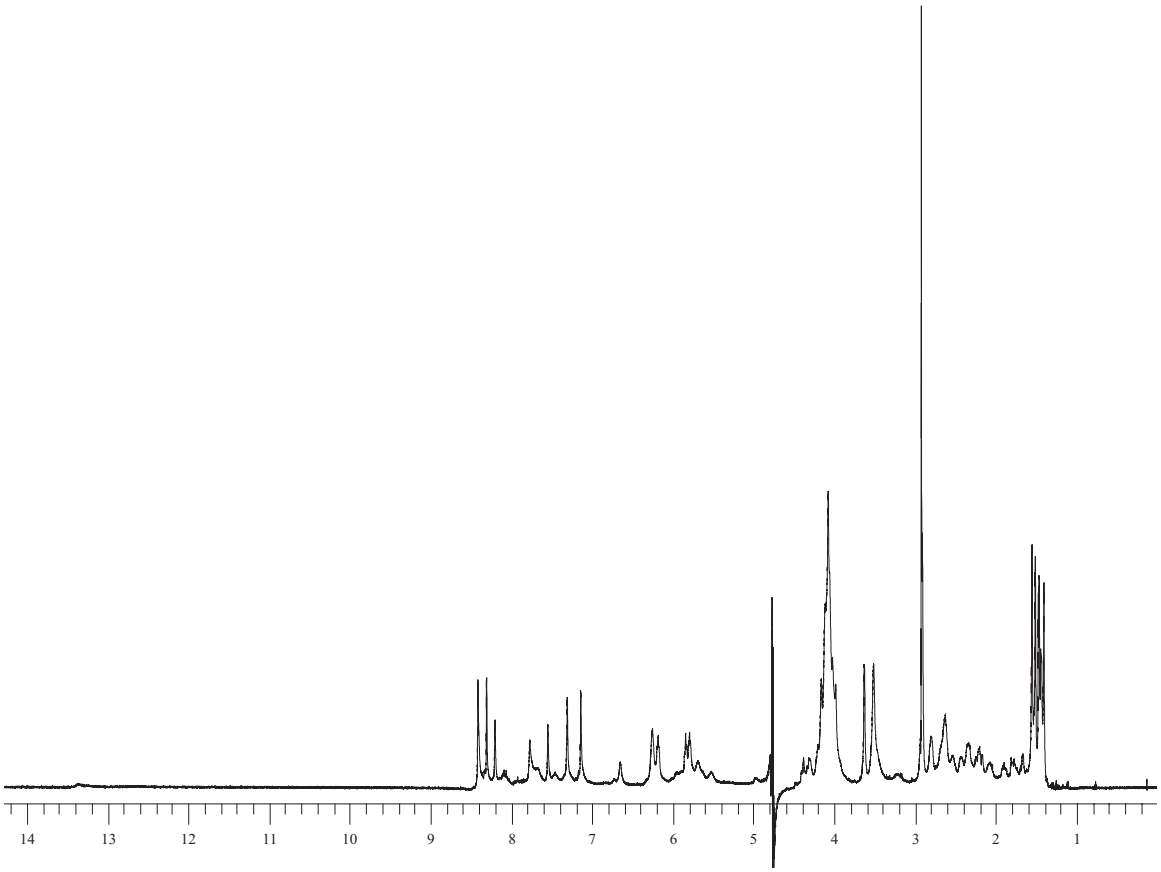

Figure A2.40 ^{1}H NMR spectrum of ratio Oflo:GGCC 2.39

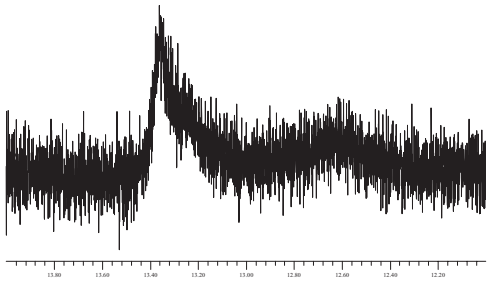

Figure A2.41 Expansion of imino region

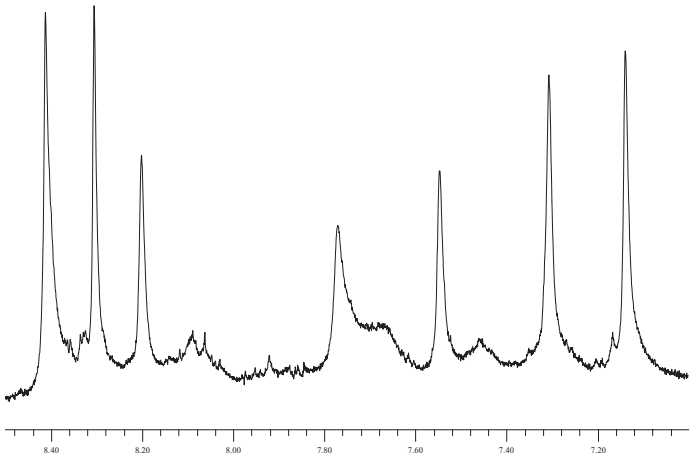

Figure A2.42 Expansion of aromatic region

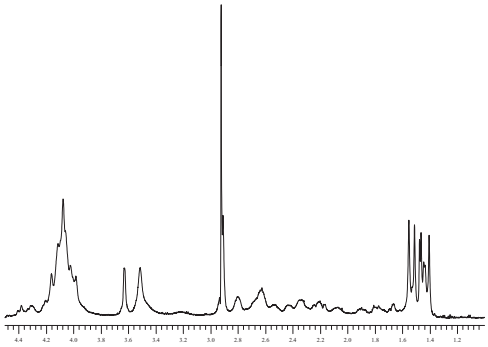

Figure A2.43 Expansion of 1.0 - 4.5 ppm region

A2.13 Spectrum obtained for 1.05 mM Ofloxacin in 0.39J mM GGCC resulting in a 2.67 ratio Oflo:GGCC

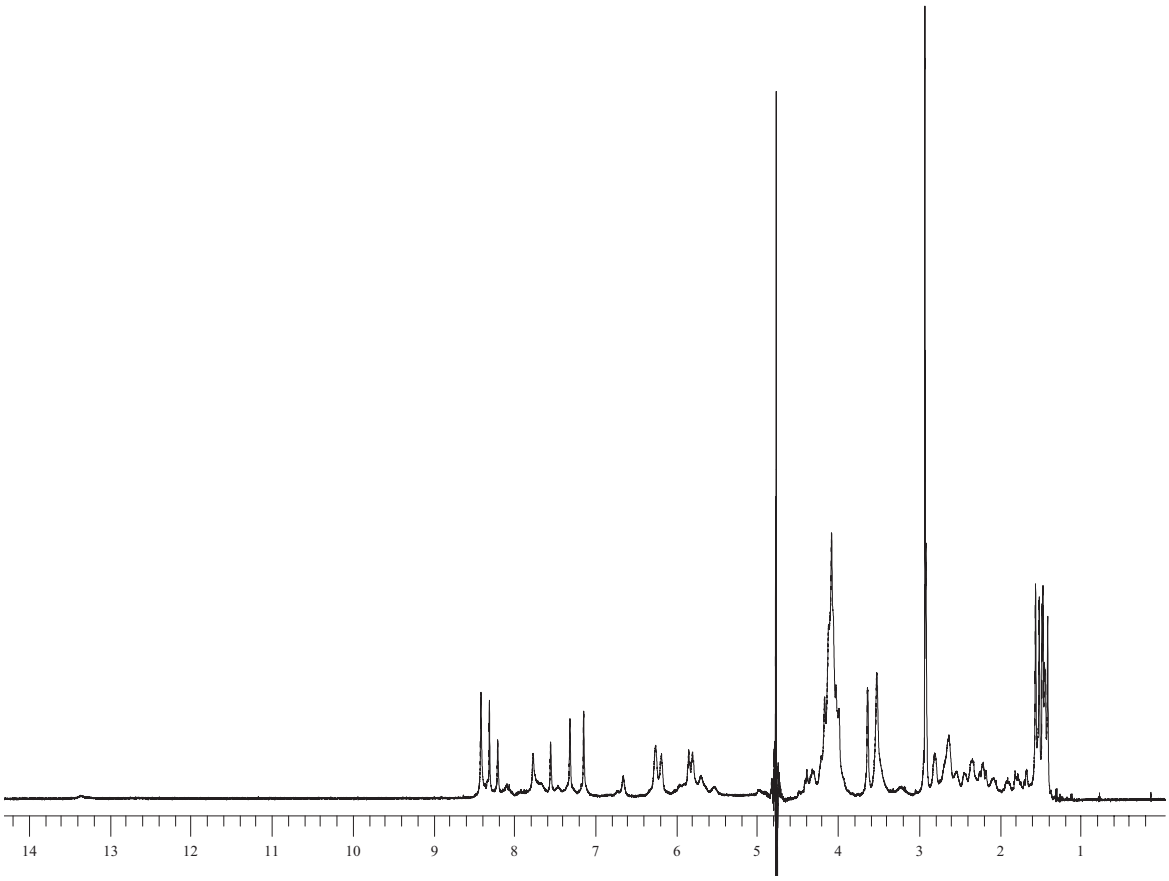

Figure A2.44 ^{1}H NMR spectrum of ratio Oflo:GGCC 2.67

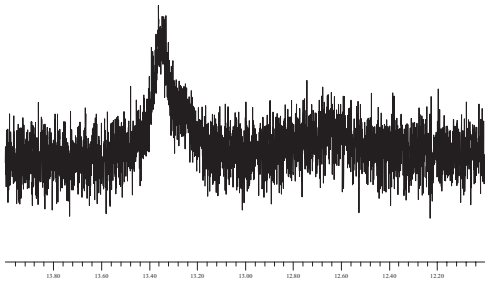

Figure A2.45 Expansion of imino region

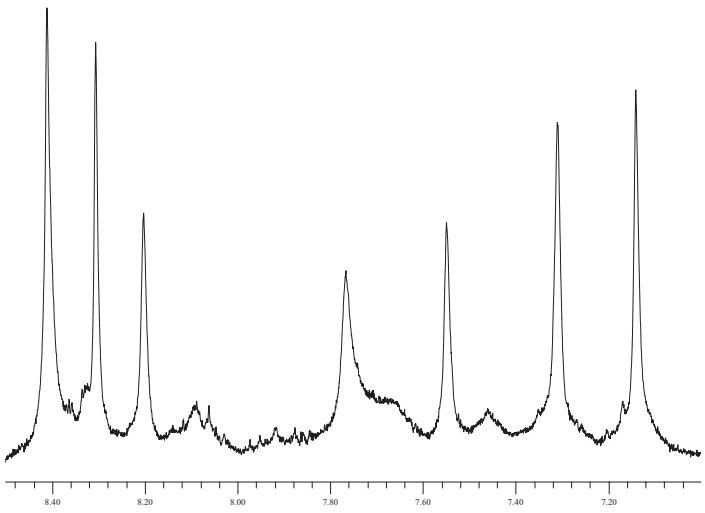

Figure A2.46 Expansion of aromatic region

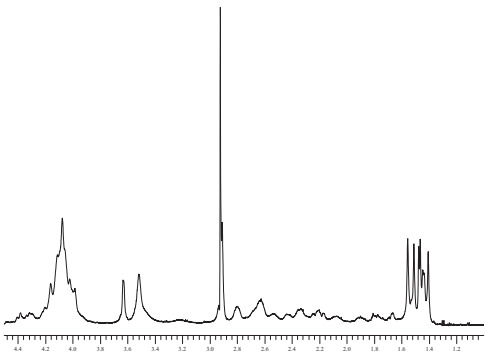

Figure A2.47 Expansion of 1.0 - 4.5 ppm region

B. Pulseprogrammes

B.1 1D ^{1}H spectrum without water suppression

```
;zg
;avance-version
;1D sequence


#include <Avance.incl>


1 ze
2 d1
  p1 ph1
  go=2 ph31
  wr #0
exit

ph1=0 2 2 0 1 3 3 1
ph31=0 2 2 0 1 3 3 1



;pl1 : f1 channel - power level for pulse (default)
;p1 : f1 channel -  high power pulse
;d1 : relaxation delay; 1-5 * T1
```

B.2 1D ^{1}H spectrum with presaturation of water

```
;zgpr
;avance-version
;1D sequence with f1 presaturation


#include <Avance.incl>



"d12=20u"

"d13=3u"


1 ze
2 d12 pl9:f1
  d1 cw:f1
  d13 do:f1
  d12 pl1:f1
  p1 ph1
  go=2 ph31
  wr #0
exit

ph1=0 2 2 0 1 3 3 1
ph31=0 2 2 0 1 3 3 1


;pl1 : f1 channel - power level for pulse (default)
;pl9 : f1 channel - power level for presaturation
;p1 : f1 channel -  90 degree high power pulse
;d1 : relaxation delay; 1-5 * T1
;d12: delay for power switching                  [20 usec]
;d13: short delay                                [3 usec]
```

B.3 1D ^{1}H NMR spectrum with w5 water suppression

```
;dpfgsew5
;avance-version
;1D sequence
;water suppression using w5 pulse sequence with gradients
;and excitation sculpting
;
;
;  M. Liu, X. Mao, C. Ye, H. Huang, J.K. Nicholson and J.C. Lindon,
;  J. Magn. Reson., 132, 125-129 (1998)
;
;  T.-L. Hwang & A.J. Shaka, J. Magn. Reson.,
;  Series A 112, 275-279 (1995).
;
;


#include <Avance.incl>
#include <Grad.incl>


1 ze
2 d1 pl1:f1
  p1 ph1
  50u UNBLKGRAD
  GRADIENT(cnst21)
  d16 pl18:f1
  p28*0.0867 ph3
  d19*2
  p28*0.2056 ph3
  d19*2
  p28*0.4133 ph3
  d19*2
  p28*0.7778 ph3
  d19*2
  p28*1.4911 ph3
  d19*2
  p28*1.4911 ph4
  d19*2
  p28*0.7778 ph4
  d19*2
  p28*0.4133 ph4
  d19*2
  p28*0.2056 ph4
  d19*2
  p0*0.0867 ph4
  50u
```

```
  GRADIENT(cnst22)
  d16
  50u
  GRADIENT(cnst23)
  d16
  p28*0.0867 ph3
  d19*2
  p28*0.2056 ph3
  d19*2
  p28*0.4133 ph3
  d19*2
  p28*0.7778 ph3
  d19*2
  p28*1.4911 ph3
  d19*2
  p28*1.4911 ph4
  d19*2
  p28*0.7778 ph4
  d19*2
  p28*0.4133 ph4
  d19*2
  p28*0.2056 ph4
  d19*2
  p0*0.0867 ph4
  46u
  GRADIENT(cnst24)
  d16
  4u BLKGRAD
  go=2 ph31
  wr #0
exit


ph1=0 2
ph3=0
ph4=2
ph31=0 2


;pl1 : f1 channel - power level for pulse (default)
;pl18: f1 channel - power level for w5-pulse
;p0 : f1 channel -  90 degree pulse at pl18
;                   use for fine adjustment
;p1 : f1 channel -  90 degree high power pulse
;p16: homospoil/gradient pulse
;p28: f1 channel -  90 degree pulse at pl18
;d1 : relaxation delay; 1-5 * T1
;d16: delay for homospoil/gradient recovery
```

```
;d19: delay for binomial water suppression
;     d19 = (1/(2*d)), d = distance of next null (in Hz)
;NS: 8 * n
;DS: 4

;use gradient program (GRDPROG) : 4sine

;use gradient ratio:       cnst21 : cnst22 : cnst23 : cnst24
;                              40 :     40 :      7 :      7
```

B.4 Spin echo diffusion measurement with w5 water suppression

```
;segsw5
;avance-version
;2D sequence for diffusion measurement using standard PGSE
;
;water suppression using w5 pulse sequence with gradients
;M. Piotto, V. Saudek & V. Sklenar, J. Biomol. NMR 2, 661 - 666 (1992)
;M. Liu, X. Mao, C. Ye, H. Huang, J.K. Nicholson and J.C. Lindon,
;J. Magn. Reson., 132, 125-129 (1998)


#include <Avance.incl>
#include <Grad.incl>


"ds=l20"


1  ze
2  d1 pl1:f1 BLKGRAD
3  50u UNBLKGRAD
   p1 ph1
   GRADIENT(cnst21)
   d16 pl18:f1
   p28*0.0867 ph3
   d19*2
   p28*0.2056 ph3
   d19*2
   p28*0.4133 ph3
   d19*2
   p28*0.7778 ph3
   d19*2
   p28*1.4911 ph3
   d19*2
   p28*1.4911 ph4
   d19*2
   p28*0.7778 ph4
   d19*2
   p28*0.4133 ph4
   d19*2
   p28*0.2056 ph4
```

```
  d19*2
  p0*0.0867 ph4
  46u
  GRADIENT(cnst21)
  d16
  4u BLKGRAD
  go=2 ph31
  d1 wr #0 if #0 zd
  lo to 3 times td1
exit


ph1=0 0 1 1 2 2 3 3
ph3=1 3 2 0 3 1 0 2
ph4=3 1 0 2 1 3 2 0
ph31=0 0 1 1 2 2 3 3


;pl1 : f1 channel - power level for pulse (default)
;pl18: f1 channel - power level for 3-9-19-pulse (watergate)
;p0 : f1 channel -  90 degree pulse at pl18
;                  use for fine adjustment
;p1 : f1 channel -  high power pulse
;p16: gradient pulse (little DELTA)
;p28: f1 channel -  90 degree pulse at pl18
;d1 : relaxation delay; 1-5 * T1
;d16: delay for gradient recovery
;d19: delay for binomial water suppression
;    d19 = (1/(2*d)), d = distance of next null (in Hz)
;l20: dummy scans (ds)
;NS: 2 * n
;DS: l20
;td1: number of experiments
;MC2: use xf2 and ilt for processing


;use gradient program (GRDPROG) : Se

;use AU-program dosy or dosyq to calculate gradient-file dramp
```

B.5 Stimulated spin echo diffusion measurement with 3-9-19 water suppression

```
;ledbp19gs2s.nf
;avance-version
;2D sequence for diffusion measurement using stimulated
;   echo and LED
;using bipolar gradient pulses for diffusion
;using 2 spoil gradients
;D. Wu, A. Chen & C.S. Johnson Jr.,
;   J. Magn. Reson. A 115, 260-264 (1995).
;
;
;water suppression using 3-9-19 pulse sequence with gradients
;M. Piotto, V. Saudek & V. Sklenar, J. Biomol. NMR 2, 661 - 666 (1992)
;V. Sklenar, M. Piotto, R. Leppik & V. Saudek, J. Magn. Reson.,
;   Series A 102, 241 -245 (1993)


#include <Avance.incl>
#include <Grad.incl>



"p2=p1*2"


"d30=d21-p19-d16-4u"
"d31=d20-p1*2-d19*10-p28*4.539-p0*0.231-p16*2-d16*3-p19"


1 ze
2 d1 BLKGRAD
3 50u UNBLKGRAD
  p1 ph1
  GRADIENT(cnst21)
  d16 pl18:f1
  p28*0.231 ph11
  d19*2
  p28*0.692 ph11
  d19*2
  p28*1.462 ph11
  d19*2
```

```
  p28*1.462 ph12
  d19*2
  p28*0.692 ph12
  d19*2
  p0*0.231 ph12
  GRADIENT(-cnst21)
  d16 pl1:f1
  p1 ph2
  GRADIENT2(cnst22)
  d16
  d31
  p1 ph3
  GRADIENT(cnst21)
  d16
  p2 ph1
  GRADIENT(-cnst21)
  d16
  p1 ph4
  GRADIENT2(cnst23)
  d16
  d30
  4u BLKGRAD
  p1 ph5
  go=2 ph31
  d1 wr #0 if #0 zd
  lo to 3 times td1
exit


ph1 = 0
ph11= 0
ph12= 2
ph2 = 0 0 2 2
ph3 = 0 0 0 0 2 2 2 2 1 1 1 1 3 3 3 3
ph4 = 0 2 0 2 2 0 2 0 1 3 1 3 3 1 3 1
ph5 = 0 0 0 0 2 2 2 2 1 1 1 1 3 3 3 3
ph31= 0 2 2 0 2 0 0 2 3 1 1 3 1 3 3 1


;pl1 : f1 channel - power level for pulse (default)
;pl18: f1 channel - power level for 3-9-19-pulse (watergate)
```

```
;p0 : f1 channel -  90 degree pulse at pl18
;                   use for fine adjustment
;p1  : f1 channel -  90 degree high power pulse
;p2  : f1 channel - 180 degree high power pulse
;p16: gradient pulse (little DELTA)
;p19: gradient pulse 2 (spoil gradient)
;p17: gradient pulse 3 (Watergate)
;p28: f1 channel -  90 degree pulse at pl18
;d1  : relaxation delay; 1-5 * T1
;d16: delay for gradient recovery
;d20: diffusion time (big DELTA)
;d21: eddy current delay (Te)                [5 ms]
;d30: d21 - p19 - d16 - 4u
;d31: d20 - p1*2 - d19*10 - p28*4.539 - p0*0.231 - p16*2 - d16*3 - p19
;l20: dummy scans (ds)
;NS: 8 * n
;DS: l20
;td1: number of experiments
;MC2: use xf2 and ilt for processing


;use gradient program (GRDPROG) :       Ledbp2s

;use gradient ratio:    cnst22 : cnst23
;                       -13.17 : -17.13

;use AU-program dosy or dosyq to calculate gradient-file dramp
```

B.6 2D NOESY with w5 water suppression

```
;noesydpfgsew5
;avance-version
;2D homonuclear correlation via dipolar coupling
;dipolar coupling may be due to noe or chemical exchange.
;phase sensitive using States-TPPI method
;water suppression using w5 pulse sequence with gradients
;and excitation sculpting
;
;
;  M. Liu, X. Mao, C. Ye, H. Huang, J.K. Nicholson and J.C. Lindon,
;  J. Magn. Reson., 132, 125-129 (1998)
;
;  T.-L. Hwang & A.J. Shaka, J. Magn. Reson.,
;  Series A 112, 275-279 (1995).
;
;

#include <Avance.incl>
#include <Grad.incl>


;;"d0=3u"
;;"d11=30m"
;;"d12=20u"

"d0=in0/2-p1*4/3.14159265"

"l3=(td1/2)"


1 ze
2 d1
3 d11
4 d12 pl1:f1
  p1 ph1
  d0
  p1 ph2
  d8
  p1 ph3
  d12 pl18:f1
```

50u UNBLKGRAD
GRADIENT(cnst21)
d16
p28*0.0867 ph4
d19*2
p28*0.2056 ph4
d19*2
p28*0.4133 ph4
d19*2
p28*0.7778 ph4
d19*2
p28*1.4911 ph4
d19*2
p28*1.4911 ph5
d19*2
p28*0.7778 ph5
d19*2
p28*0.4133 ph5
d19*2
p28*0.2056 ph5
d19*2
p0*0.0867 ph5
50u
GRADIENT(cnst22)
d16
50u
GRADIENT(cnst23)
d16
p28*0.0867 ph4
d19*2
p28*0.2056 ph4
d19*2
p28*0.4133 ph4
d19*2
p28*0.7778 ph4
d19*2
p28*1.4911 ph4
d19*2
p28*1.4911 ph5
d19*2
p28*0.7778 ph5

```
  d19*2
  p28*0.4133 ph5
  d19*2
  p28*0.2056 ph5
  d19*2
  p0*0.0867 ph5
  46u
  GRADIENT(cnst24)
  d16
  4u BLKGRAD
  go=2 ph31
  d1 wr #0 if #0 ip1 zd
  lo to 3 times 2
  d11 id0
  lo to 4 times l3
exit


ph1=0 2
ph2=0 0 0 0 0 0 0 0 2 2 2 2 2 2 2 2
ph3=0 0 2 2 1 1 3 3
ph4=0
ph5=2
ph31=0 2 2 0 1 3 3 1 2 0 0 2 3 1 1 3


;pl1 : f1 channel - power level for pulse (default)
;pl18: f1 channel - power level for 3-9-19-pulse (watergate)
;p0 : f1 channel -  90 degree pulse at pl18
;                   use for fine adjustment
;p1 : f1 channel -  90 degree high power pulse
;p2 : f1 channel - 180 degree high power pulse
;p16: homospoil/gradient pulse
;p28: f1 channel -  90 degree pulse at pl18
;d0 : incremented delay (2D)                  [3 usec]
;d1 : relaxation delay; 1-5 * T1
;d8 : mixing time
;d11: delay for disk I/O                      [30 msec]
;d12: delay for power switching               [20 usec]
;d16: delay for homospoil/gradient recovery
;d19: delay for binomial water suppression
```

```
;     d19 = (1/(2*d)), d = distance of next null (in Hz)
;L3: loop for phase sensitive 2D using States-TPPI method: l3 = td1/2
;in0: 1/(1 * SW) = 2 * DW
;nd0: 1
;NS: 8 * n
;DS: 16
;td1: number of experiments
;MC2: States-TPPI

;use gradient program (GRDPROG) : 4sine

;use gradient ratio:       cnst21 : cnst22 : cnst23 : cnst24
;                              40 :     40 :      7 :      7
```

C. Adjustable NMR parameters

Pulse program
The program running the pulse sequense.
Pulse programs are outlined in Appendix B.

ns
Number of scans in the experiment.

p1
Duration of the pulse

o1p
Defines the midle of the spectrum, usually situated at the water signal.

rg
Resiever gain, a multiplication of the signal from the resiever coil before entering the digital converter.

d1
Waiting time between the aquisition and the next pulse.

td
Time domain, number of datapoints from the FID sampled

sw
Spectral width in ppm

pl18
Radio frequency pulse power attenuation for the gradient pulses in the w5 water suppression sequense

p0
Pulse duration for the gradients in the w5 water suppression sequense

p28
Pulse duration for the gradients in the w5 water suppression sequense

d19
Delay for binominal water suppression

te
Temperature kept by the temperature control unit

ds
Number of dummy scans in the experiment

aq
Aquisition time, set automatically from td and swh

dw
Dwell time, the intervals between the points making up the FID.

de
Pre-scan delay

p19
Delay for the binominal water suppression in the 3-9-19 pulse sequense

d8
Mixing time

si
Spectral size

WDW
Window function, "qsine" means a squared sine bell function

SSB
Fase of the window function, "2" turnes WDW to a cosine function

lb
Line broadening

ME_Mod
Linear prediction can be turned on using LPfc

LPBIN
Number of data points in predicted FIDs

MC2
Detection scheme

d16
Delay. Used to calculate big delta in a spin-echo pulse-sequense

p16
Little delta in both spin-echo and stimulated spin-echo pulse-sequences
Also used to calculate big delta in a spin-echo pulse-sequence

d20
Big delta in a stimulated spin-echo pulse-sequence

d21
Delay

References

1 Daune M., Molecular Biophysics -Structures in motion, 1999; Oxford University Press

2 www.m-w.com/mw/art/dna.html

3 Skauge, T. Antibacterial agent-DNA interactions, 2001; Cand.Scient thesis, University of Bergen

4 Lesher, G.Y., Forelich, E.D., Gruet, M.D., Bailey, J.H., Brundage, R.P. J.Med.Pharm.Chem., 1962;**5**:1063-1068

5 Azcurra, A.I., Yudi, L.M., Baruzzi, A.M. J.Electroanal.Chem., 1999;**461**:194-200

6 http://www.ortho-mcneil.com/products/pi/pdfs/floxtab.pdf

7 Chidangil, S., Shukla, M.K., Mishra, P.C. J.Mod.Model, 1998;**4**:250-258

8 Djurdjevic, P.T., Jelikic-Stankov, M. J.Pharm.Biomed.Anal., 1999;**19**:501-510

9 Lee, E-J., Yeo, J-A., Jung, K., Hwangbo, H.J., Lee, G-J., Kim, S.K. Arch.Biochem.Biophys., 2001;**395**:21-24

10 Hwangbo, H.J., Yun, B.H., Cha, J.S., Kwon, D.Y., Kim, S.K. Eur.J.Pharma.Sci., 2003;**18**:197-203

11 Mucci, A., Malmusi, L., Vandelli, M.A., Fresta, M., Schenetti, L. Med.Chem.Res., 1996:353-363

12 Couturier, M., Bahassi, E.M., Melderen, L.V. Trends in Microbiol., 1998; **6**:269-275

13 Morrison, A., Cozzarelli, N.R. Cell, 1979;**17**:175-184

14 Shen, L.L., Pernet, A.G. Proc.Natl.Acad.Sci.USA, 1985;**82**:307-311

15 Shen, L.L., Mitscher, L.A., Sharma, P.N., O´Donnell, T.J., Chu, D.W.T., Cooper, C.S., Rosen, T., Pernet, A.G. Biochem., 1989;**28**:3886-3894

16 Shen, L.L., Baranowski, J., Pernet, A.G. Biochem., 1989;**28**:3879-3885

17 Shen, L.L., Baranowski, J., Wai, T., Chu, D.T.W., Pernet, A.G. Quinolones, 1989:159-170

18 Shen, L.L. Biochem.Pharma. 1989;**38**;12:2042-2044

19 Willmott, c.J., Maxwell, A. Antimicrob.Agents.Chemother., 1993;**37**:126-127

20 Critchlow, S.E., Maxwell, A. Biochem., 1996;**35**:7387-7393

21 Kampranis, S.C., Maxwell, A. J.Biol.Chem., 1998;273;**35**:22615-22626

22 Son, G.S., Yeo, J-A., Kim, M-S., Kim, S.K., Holmén, A., Åkerman, B., Nordén, B. J.Am.Chem.Soc., 1998;**120**:6451-6457

23 Palù, G., Valisena, S., Ciarrocchi, G., Gatto, B., Palumbo, M. Proc.Natl.Acad.Sci.USA, 1992;**89**:9671-9675

24 Fan, J.Y., sun, D., Yu, H.T., Kerwin, S.M., Hurley, L.H. J.Med.Chem., 1995;**38**:408-424

25 Bailly, C., Colson, P., Houssier, C. Biochem.Biophys.Res.Comm., 1998;**243**:844-848

26 Frøystein, N.Å., K304 Practical NMR Spectroscopy, handed out as curriculum in a course with the same name, 2001

27 Antalek, B., Con. Mag. Res., 2002;**14**(4):225-258

28 Stilbs, P., Prog. NMR spec., 1987;**19**:1-45

29 Kärger, J., Pfeifer, H., Heink, W., Adv. Mag. Reson., 1988;**12**:1-89

30 Johnson, C.S.Jr., Prog. Nuc. Mag. Res. Spec., 1999;**34**:203-256

31 Hodge, P., Monvisade, P., Morris, G.A., Preece, I., Royal Soc. of Chem., 2001:239-240

32 Vinje, J., Parkinson, J.A., Sadler, P.J., Brown, T., Sletten, E., Chem. Eur. J., 2003;**9**(7):1620-1630

33 Tafazzoli, M., Suarez, C., True, N.S., LeMaster, C.B., LeMaster, C.L., J. Mol. Struc., 1994;**317**:137-145

34 Lecomte, S., Tabary, X., Moreau, N.J., Chenon, M-T., Magn. Reson. Chem., 1996;**34**:458-466

35 Lapham, J., Rife, J.P., Moore, P.B., Crothers, D.M., J. Biol. NMR., 1997;**10**:255-262

36 Anderson, R.C., Lin, M., Shapiro, J., Am. Chem. Soc., 1999;**1**:69-72